COSMIC RAYS:

THEIR COMPOSITION, ENVIRONMENT, NUCLEAR INTERACTIONS AND RADIOBIOLOGICAL and ELECTRONIC EFFECTS

A THESIS

SUBMITTED TO THE FACULTY OF ATLANTA UNIVERSITY

IN PARTIAL FULFILLMENT OF THE REQUIREMENTS FOR

THE DEGREE OF MASTER OF SCIENCE

BY

OCTAVIA LAUREN BLOUNT

DEPARTMENT OF PHYSICS

ATLANTA, GEORGIA

JULY 1989

ABSTRACT

PHYSICS

BLOUNT, OCTAVIA L. B.A. LINCOLN UNIVERSITY, 1987

COSMIC RAYS: THEIR COMPOSITION, ENVIRONMENT, NUCLEAR INTERACTIONS AND RADIOBIOLOGICAL and ELECTRONIC EFFECTS

Advisor: Dr. Rein Silberberg

Thesis dated July, 1989

Cosmic rays consist of atomic nuclei ranging from H to U. They are the most energetic particles in nature, with energies 10^6 eV to 10^{21} eV. They are of Galactic origin and are probably produced by supernova shock waves that accelerate stellar flare particles. The composition of cosmic rays at the sources resembles that of normal stars like the sun; (with modifying factors due to the first ionization potential effects and nucleosynthesis processes in Wolf-Rayet stars). The propagation equation, with the calculated cross sections of Silberberg and Tsao, yields a mean path length traversed in interstellar gas of $\langle x \rangle \simeq 5$ g/cm^2 near energies of 4 GeV per nucleon, with a confinement time of 10^7 years (determined by the extent of survival of the long-lived radio-active nuclide Be^{10}). Calculations combined with the latest experimental data on cosmic-ray relative abundances show that the cosmic-ray path lengths have an exponential

distribution. Improvements in the cross section calculations of Silberberg and Tsao, from Z = 14 to 19, were made. Comparisons of HETC (high energy transport code) and experimental data for nuclear recoil energy spectra uncovered a systematic error in HETC; a new correction factor of exp(.03*E) is proposed. Protection from cosmic radiation is handled through shielding. The Earth's magnetic field and atmosphere serve as a good shielding mechanism; but radiation hazards are significant outside the Earth's atmosphere. A new mean quality factor, <Q> = 14, was derived for neutrons by integrating over their energy spectrum. Examples of radiation protection are presented, using the new quality factor, to aid in the prevention of biological damage to human tissue. And damage to electronic components (single event upsets) is explored.

DEDICATION

I would like to dedicate this Masters Thesis to the memory of my mother Gwendolyn Armenta Blount. My mother always taught me to persevere regardless of the odds. I entered Lincoln University in 1983 to obtain an education that would enable me to get a good job and take care of my mother. When my mother left this world in 1984, I believe she left me her energy so that I could get on with my life and continue my education without mourning her passing for a extended period of time. My mother was a strong advocate of education and for this reason I plan to continue my education to the Ph.D. level.

ACKNOWLEDGEMENTS

I was truly blessed the day I received a letter from a Dr. Rein Silberberg asking me to come to the Naval Research Laboratory to aid in his research on cosmic rays. I am forever grateful and indebted to Dr. Silberberg for depositing his knowledge in this area of research on me, for being patient with me as I explored and learned this new area, and for aiding in every way possible to see that this research was completed. My research was performed as a fellow under the appointment to the American Society for Engineering Education (ASEE) administered by the Office of Naval Research (ONR). I would like to thank Dr. C.H. Tsao of NRL for helping with and explaining all the computer programs used in this thesis, for his incentive for me to work through problems on my own, and for his aid with the MASS11 word processor which put this thesis in its final form. I would like to thank Dr. Alfred Msezane, the Physics Department Head, for his permission for allowing me to do my research at NRL, for his guidance in my school studies, and for being a friend when I needed one. I would also like to thank Mrs. Hattie Bell, the faculty of the physics department, and students for their encouragement and support. I would like to thank my aunt, Elizabeth Blount L.P.N., for the use of her computer, which allowed me to type at home and spend more time researching while at NRL. I would like to thank Ms. Anna Beckett for supplying me with housing during my stay in Washington. And I would like to thank Mrs. Jessica Hileman, the ONR coordinator at NRL, for arranging my appointment at the laboratory. I would also like to thank the Cosmic-Ray and Gamma-Ray Branch of NRL for their help, their encouragement, and for welcoming me in their family.

TABLE OF CONTENTS

LIST OF TABLES

LIST OF FIGURES

LIST OF ABBREVIATIONS

SN	Supernova(e)
NCRP	National Council on Radiation Protection and Measurements
ICRP	International Council on Radiological Protection
HETC	High Energy Transport Code
UPROP	Universal Propagation Equation
L	Light Nuclei (Li,Be,B)
M	Medium Nuclei (C,N,O,F)
GCR	Galactic Cosmic Rays
LIS	Local Interstellar Space
CRS	Cosmic Ray Source
FIP	First Ionization Potential
A.U	Astronomical Units
S&T	Silberberg and Tsao
SEU	Single Event Upsets

LET	Linear Energy Transfer
CREME	Cosmic Ray Effects on Microelectronics
WR	Wolf-Rayet
ISM	Interstellar Medium

I. INTRODUCTION

The topics of research in cosmic-ray physics vary among the many physicists engaged in this field of study because it encompasses many separate research areas: high energy astrophysics, elementary particle physics, nuclear physics, plasma physics, nucleosynthesis in stars and many other areas of physics and astronomy. This research ranges from basic investigations regarding the origin(s) of cosmic rays, cosmic-ray interactions and transformations in the interstellar medium (ISM), to their useful applications in radiation biology.

Cosmic rays were first discovered on one of many manned balloon flights of Victor Hess. The flight that gave physics a new area of research was on August 7, 1912. This flight, which reached an altitude of about 5 km, was particularly successful; at this altitude, the ionization rate was several times higher than the rate measured at sea level [1]. By the late 1930's, it had been shown that the radiation arriving at the top of Earth's atmosphere was mainly positively charged and was of high energy as shown by its great penetrating power [2]. The charge was deduced from the East-West asymmetry of lower energy cosmic-rays, as they enter into the region of the geomagnetic field.

On energetic grounds alone, the likeliest sites of cosmic-ray acceleration within the Galaxy appear to be supernovae(SN), and their expanding remnants with strong hydromagnetic shock waves. In a supernova explosion, some 10^{51} or 10^{52} ergs are released within a short time [3], much of which remains in the supernova remnant. The pulsating neutron star in many supernova remnants supplies energy

for thousands of years. The accepted source of the nuclidic material that is "promoted" to cosmic-ray energies is matter ejected by stars, which in turn has been formed by nucleosynthesis in previous generation stars, especially those that become supernovae. The Big Bang Theory of nucleosynthesis only accounts for the nuclides from hydrogen to lithium-7. Because of the low density involved in this process, and the gaps of stable or long-lived nuclides at mass numbers 5 and 8, it is harder to synthesize the heavier elements. The heavier elements ($Z \geq 6$) have a better chance of being formed in stars where the density is much higher, since the collision of three helium nuclei in close succession is needed to form carbon. This is one of the processes of stellar nucleosynthesis.

As these particles propagate from the sites of origin, through the interstellar medium, to distances where they are measured near the Earth, they undergo many nuclear interactions (Fig. A). Interactions give information on the source abundances that can be compared to general abundance of elements in nature, (e.g. in the stars), on secondary production of nuclides by spallation and on the individual energy spectra of hydrogen to iron, which are affected by the combined effects of cosmic-ray leakage from the Galaxy and nuclear interactions.

The propagation and interactions of cosmic rays from sources to Earth is an important source of astronomical information on topics like the interstellar magnetic fields and the interstellar medium. There exists, so far, no definitive explanation of the origin of cosmic rays, but equations by Silberberg and Tsao [4]

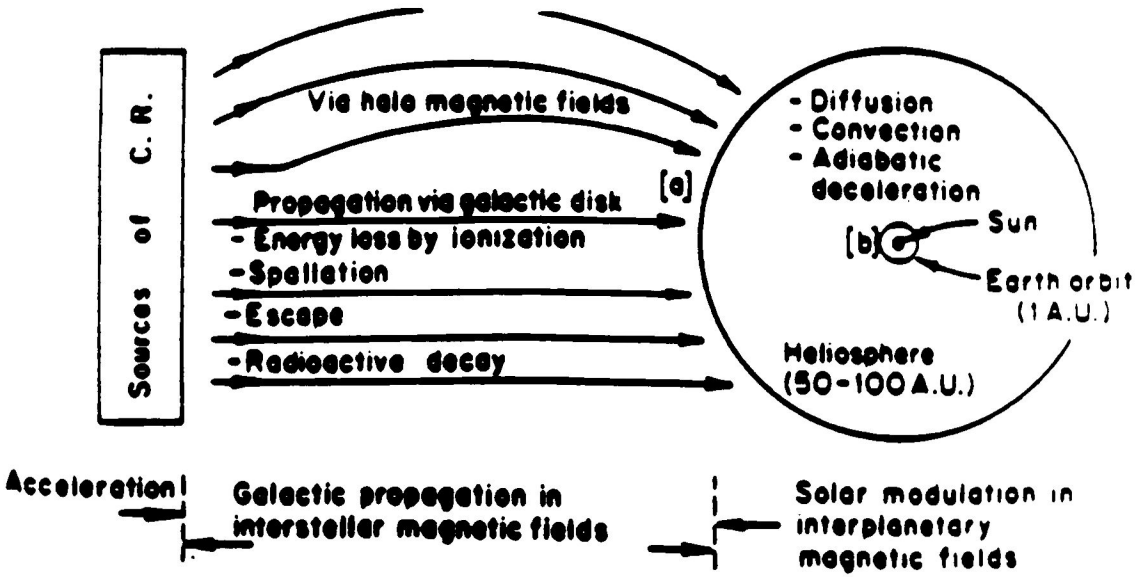

Fig. A Cosmic Ray Interactions During Propagation

to explain many cosmic ray interactions en route to earth enable interested physicists to extrapolate the cosmic-ray source composition at the sites of origin and their energy spectra. To evaluate the effects of cosmic rays in biological tissue and electronic components, mathematical formulations of nuclear cross sections, nuclear recoils, ionization losses, and radiation transport calculations need to be carried out. This thesis will present computerized calculations of each of these processes. These equations are of great importance not only to physicists, but also to the general public.

In papers by Decampli et al.[5] and James Adams Jr. et al. [6] radiation exposure has been investigated for biological damage to humans and for upsets in micro-electronic components. Different exposure limits have been set by the National Council on Radiation Protection (NCRP) for the general public, for radiation workers, and for a few astronaut volunteers. With the aid of cosmic-ray flux measurements, cross section and propagation equations by Silberberg and Tsao, the nuclidic abundance data of Cameron [7], and experiments by radiobiologists, persons who are at risk of excess doses of radiation on long duration flights in space or frequent flights in the upper atmosphere can be properly protected. By comparing experimental data with theoretical predictions, systematic errors are found and established equations are improved to better explain cosmic ray interactions. Radiation shielding and component sensitivity requirements for avoiding upsets in electronic components on aircraft

and space satellites at various altitudes have been more precisely defined through improved nuclear recoil calculations.

In this thesis, the latest versions of equations are utilized along with transport code calculations like HETC and UPROP [8] to provide information on the most recent discoveries in cosmic-ray research: their origin, propagation to Earth, radiation protection above and near the top of the Earth's atmosphere, and useful applications. However, cosmic ray investigations for basic astrophysical research will probably continue for a very long time.

II. COSMIC RADIATION

What are cosmic rays

a. historic overview

Webster's definition of cosmic rays is,

> A stream of atomic nuclei of heterogeneous character that enter the earth's atmosphere from outer space at speeds approaching that of light and bombard atmospheric atoms to produce mesons as well as secondary particles possessing some of the original energy. [9]

With this definition come many questions. Where do these nuclei originate? What are their modes of propagation? What types and how many interactions do they encounter? Specifically, what nuclides are produced? What is the energy of the particles arriving at Earth? And how damaging are they once they reach Earth?

As inscribed on a plaque on the wall of the Secretariat room in the Ettore Majorana Centre in Erice, Italy:

> Here in the Erice maze
> Cosmic rays are the craze
> and this because a guy named Hess
> ballooning up found more not less. [2]

This inscription summarizes the observation that the rate of ionization increases with increasing altitude. For instance, in manned balloon flight experiments made in 1914, when an altitude of 9 km was reached [3] the ionization proved to be much greater than at sea level.

Because of their great penetrating power, cosmic rays were first assumed to be a form of gamma rays. By the 1930's it was shown that charged particles dominated in the primary cosmic rays [10]. This

was discovered by studying the intensity of cosmic rays as a function of magnetic latitude (charged particles, with a component perpendicular to the magnetic field, are deflected). As a result, the flux of the primary cosmic rays, that reaches the Earth's atmosphere, depends on the geomagnetic latitude, being higher near the magnetic poles.

Primary cosmic rays were proved to be, not only charged, but for the most part protons. Such a conclusion was drawn from the results of the East-West asymmetry. This effect showed that the flux of particles from the west was larger. Positively charged particles tend to arrive preferentially from the west because the cutoff energy (or magnetic rigidity) for particles arriving from the west is lower than that from the east (e.g. the cutoff energy of positively and singly charged particles at the geomagnetic equator is 10 GeV from west and 60 GeV from east). The rigidity is defined as momentum divided by charge. Rigidity is inversely proportional to the radius of curvature of a particle in a magnetic field.

The next milestone in cosmic ray research occurred in 1948 with the discovery of helium and heavier elements ($Z \leq 28$) . In the mid 1960's came the discovery of ultra-heavy cosmic rays with atomic numbers from Z=29 through the rest of the periodic table, up to and including uranium [2].

Experiments of the 1960's also resulted in the discovery of the primary electron and positron components. The protons of the primary radiation interact strongly with the nuclei of the atmosphere. In these interactions a variety of particles are produced,

the most important, for this present historical overview, being those shown in figure 1. Cosmic rays were used to study elementary particles and their interactions at high energies (from measurements on balloons, and later on rockets and satellites: near Earth): positrons, muons, pions, K-mesons, and some hyperons were discovered in cosmic rays. (From 1929 to 1955 or 1956 elementary particle research was the main aspect of cosmic-ray physics.) Elementary particles in cosmic rays are further discussed in Appendix D.

Cosmic radiation encompasses nuclear particles and electrons of astrophysical origin over a wide energy range, extending from energies that just exceed those of the flare particles ($\simeq 10^6$ eV) to the highest energy particles observed, up to 10^{21} eV. Dealing with that wide a range in energy, one should not be surprised that the origin of this radiation and its behavior is likely to involve a variety of different physical phenomena.

b.origin and acceleration

During the past seventy years, many proposed hypotheses on the origin of cosmic rays broke down when they were tested against the most recent experimental and observational data. According to observational data, energetic particles are definitely produced by the sun, in our Galaxy during the outburst of supernovae, and in the higher energy cosmic/gamma-ray sources, like pulsars and binary stellar systems that have a compact object like a neuron star.

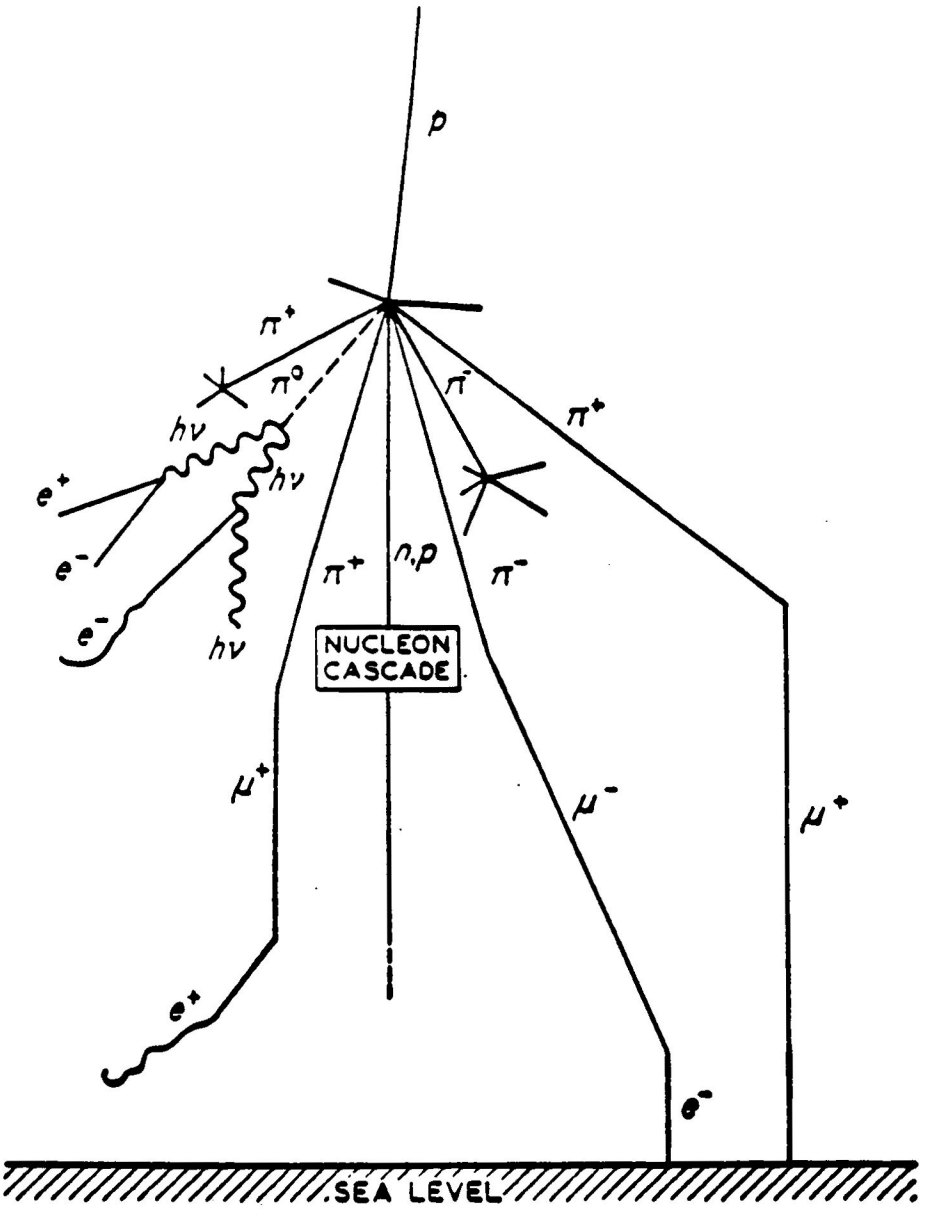

Fig. 1 Nuclear Interactions In The Atmosphere

The fairly large number of theories on the origin of cosmic rays can be classified according to the location of the source of primary cosmic rays that reach the Earth. Four types of theories can be distinguished in this approach. Alfven and Unsold [11,12] suggested solar origin with acceleration of solar flare particles by interplanetary magnetic fields due to the solar plasma. In the theories of solar origin of cosmic rays, their basic source is the sun and the cosmic rays accumulate in the circumsolar region. This theory was discarded for two reasons: (a) interplanetary fields cannot accelerate particles to the ultra-high energies seen in extensive air showers and (b) gamma rays from the Galaxy (produces by cosmic-ray interactions) have an intensity that implies the same cosmic-ray density in distant regions (at 1-10 Kpc) in the Galaxy as in the solar system.

According to the Galactic theory, which is strongly favored, the cosmic rays reaching the Earth are accelerated within our Galaxy. The question concerning a cosmic ray source is: which regions of the Galaxy are the sources where acceleration takes place? It is therefore best to start with a discussion of the models of the distribution of cosmic rays in the Galaxy and the question of the energy balance. There are two different galactic models: (a) a model in which the cosmic rays more or less evenly fill the whole volume of the Galaxy including the halo and (b) a model in which the cosmic rays are confined to a considerable degree in the galactic disk, in the spiral arms or its individual regions (Fig. 2). Arguments, both data of a radio-astronomical nature and dynamic considerations and

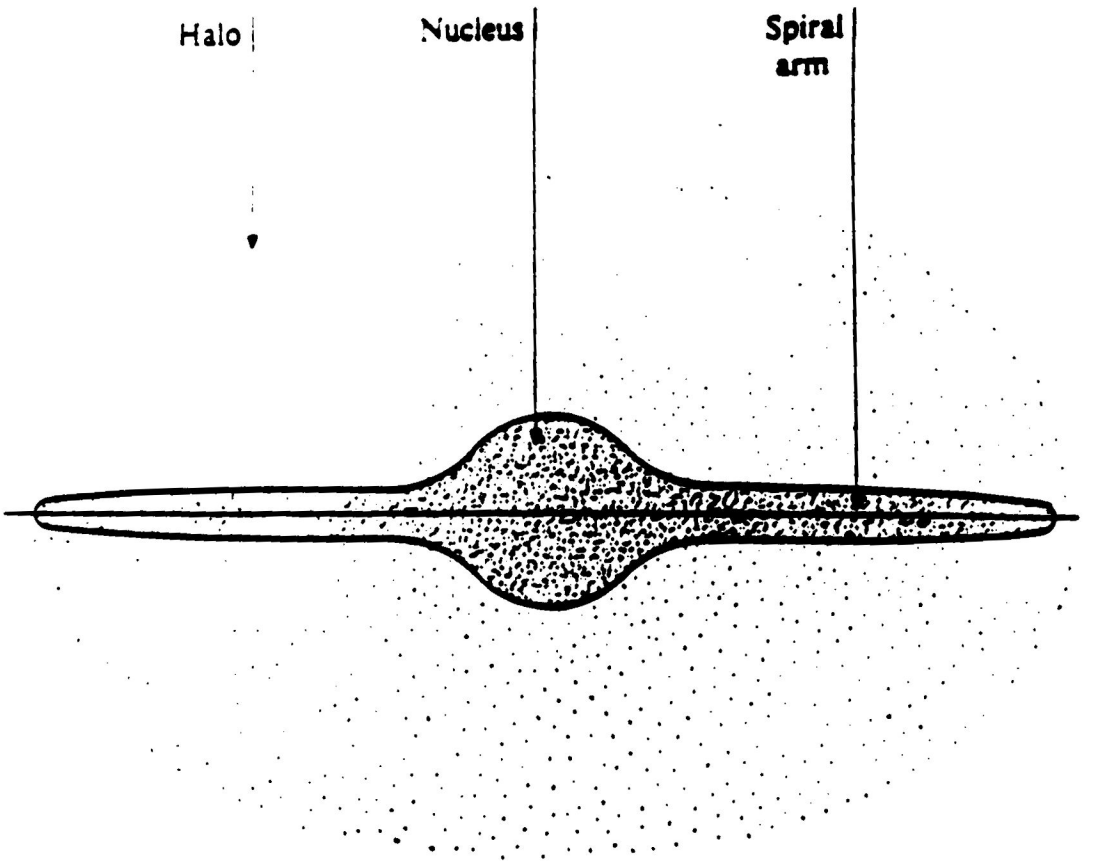

Fig. 2 Schematic Diagram of the Galaxy

intensity distribution of cosmic gamma rays in the Galaxy support model (a). However, the Galactic confinement time of 10^7 years and the density of region traversed (0.2 atoms/cm^3) imply a limited circulation of particles back from the halo. (The density in the halo is only $\simeq$ 0.01 atoms/cm^3 i.e., much lower than that of the medium traversed by cosmic-ray nuclei we observe.)

As stated previously, cosmic rays have energies ranging from 10^6 eV up to 10^{21} eV. The total energy input of cosmic rays is high. The energy density of cosmic rays in the Galaxy is 1 eV/cm^3. From this energy density, the 10^7 year galactic confinement time of cosmic rays (deduced from the partial survival of the long-lived radio-active nuclide Be^{10}), and the galactic volume of cosmic-ray confinement (10^{67} cm^3) one obtains an annual galactic input into cosmic rays of 10^{60} eV/year, or 10^{48} ergs/year. It is not easy to provide so much energy, hence considerations connected with taking the energy balance into account are very important. The most plausible sources of energy for acceleration of cosmic rays are the supernovae [13], each of which generates about 10^{51} ergs of non-neutrino kinetic energy (most of the energy in a supernova is emitted as weakly interacting neutrinos). If the rate of supernovae in the Galaxy is 1 in 30 years (including those in obscured regions like clouds), the rate of energy production is $3X10^{49}$ ergs/year, which is quite sufficient for the cosmic-ray energy requirement of 10^{48} ergs/year.

Cosmic-ray particles have energies of about $1X10^9$ eV on the average, but as mentioned previously and exhibited in the graph of the

integral energy spectrum [Fig. 16] the energy range extends to 10^{21} eV. The cosmic-ray elemental abundances (dicussed later) imply initial injection conditions at energies of 1 eV. While it is not yet known how the energy gain by a factor of $1X10^{9}$ occurs, it probably occurs in three stages.

We shall now consider the energy gain from the stellar surface (photospheric) energies of 1 eV. The coronae of stars and the sun, and stellar winds have energies of about 10^{3} eV/atom. The sun's mass is $2X10^{33}$ g, i.e. it contains about $1X10^{57}$ hydrogen nuclei (assume about $1X10^{53}$ are in the photosphere and $1X10^{-10}$ of it, i.e. about $1X10^{43}$ in the low density corona and outflowing wind). As plasma waves, including acoustic waves, move into less dense regions, their energy gets distributed among fewer particles, i.e. the energy per particle increases. Only a fraction of $1X10^{-7}$ of the energy of the photosphere needs to be distributed among the coronal particles to heat them up by a factor of $1X10^{3}$.

Now the second boost, from $1X10^{3}$ to $1X10^{6}$ eV, can occur in stellar flares. Here the mechanism is release of magnetic energy. Sunspots have magnetic fields close to $1X10^{3}$ gauss with an energy density of $3X10^{3}$ erg/cm^{3} and with a volume of $1X10^{29}$ cm^{3}. Thus the total magnetic energy is $3X10^{32}$ ergs. Possibly 1% of it, about $3X10^{30}$ ergs, can go into acceleration of solar and stellar flares. Magnetic fields are powerful accelerators of charged particles. The numerous flare stars are important contributors to flare particles in the Galaxy [14].

The next stage, that boosts particles at $1X10^6$ eV up to a mean energy of $1X10^9$ eV, and a small fraction to higher energies, can be provided by hydromagnetic shock waves of extended SN remnants.

The composition of cosmic rays supports the above three-stage acceleration process. The cosmic-ray primary source composition (i.e. the components derived by subtracting the secondary spallation-produced cosmic rays) resembles the coronal composition. Hence, it is natural to assume that the nuclei that get accelerated to cosmic ray energies ($E \simeq 1X10^9$ eV) are derived from stellar flare or possibly stellar wind particles. However, flare particles have energies of $1X10^6$ to $1X10^7$ eV, hence an acceleration process is needed. SN explosions, with magnetic shock waves, have enough energy to supply the cosmic ray energy requirements. One SN generates about $1X10^{51}$ ergs of visible energy (a total of about $1X10^{53}$ ergs escape as weakly interacting neutrinos).

Cosmic rays at energies below 10^{14} eV are probably derived from stellar flare particles and to a minor degree from energetic ($\simeq 10^5$ eV) Wolf-Rayet star wind particles, both of which are accelerated by supernova shock waves. But above 10^{14} eV, the radius of curvature of particles in magnetic fields is so large that they cannot be confined to the shock wave acceleration region. High energy particles, 10^{14} - 10^{19} eV probably are produced in binary stellar systems, one of which is a compact neutron star that accretes mass from a companion (Fig. 3). The evidence for this process is obtained from the high energy ($\simeq 10^{15}$ eV) gamma rays detected from Cygnus X-3 and Hercules X-1 [15] which are generated in

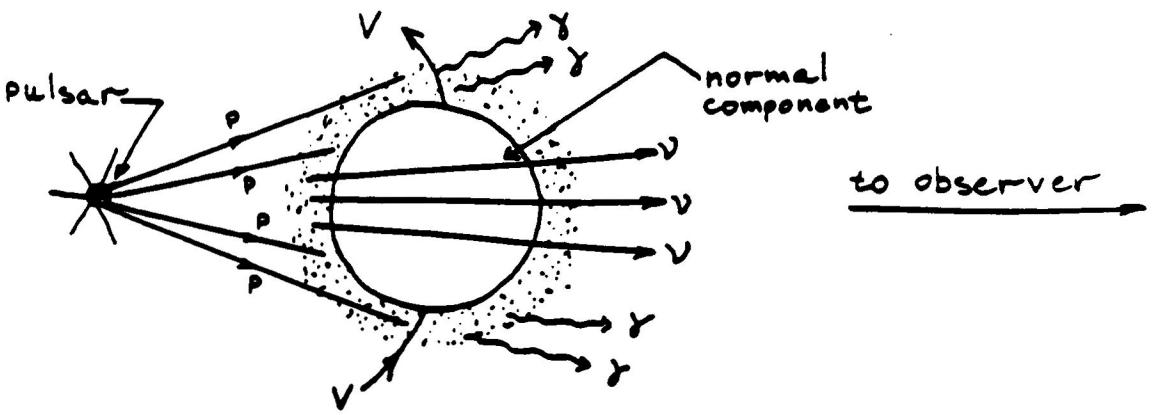

Fig. 3 Schematic Diagram of a Binary Stellar System

interactions of protons that have even higher energies, via π° production.

The Metagalactic theory links the origin of cosmic rays with the Metagalaxy, i.e., cosmic rays located or generated outside the Galaxy [16]. The energy input requirements for this theory exceed that for the galactic model by 10^4. This requirement is very unlikely because, (a) no such powerful sources have been identified, and (b) the gamma-ray intensity falls off slowly in the outermost parts of the Galaxy, implying a galactic origin, though with a large extensive cosmic-ray halo [17], maybe to 50 Kpc about the Galaxy. Of course, the Active Galaxies (Seyfert Galaxies and Radio Galaxies) are powerful cosmic-ray sources, but not enough to fill the vast inter-galactic space with the density observed in our Galaxy. However, the highest energy cosmic rays observed at Earth, those above 10^{19} eV, are likely to originate in these galaxies.

These particles are considered to be extragalactic because of the discontinuity ("flattening") in the energy spectrum at 10^{19} eV, because of their anisotropy, with preferential arrival direction near the galactic north pole in the direction of the center of the Virgo Supercluster of galaxies, and because of the inability of the galactic magnetic field to contain particles with gyroradii of galactic dimensions. Ultra-high energy cosmic rays produced in the Galaxy leak out on a rapid time scale, maybe in 10^4 years rather than 10^7 years deduced for particles with a mean energy at 10^9 eV.

In the "hierarchial" and similar theories, the Sun, galactic objects (stars and supernova shells) and certain galaxies

(radiogalaxies in particular) are included as sources. In this case the part played by one source or another depends upon the range of energies under discussion and the spatial region of cosmic rays under consideration.

Origin of the cosmic-ray material in young supernovae is not satisfactory because selection effects that depend upon the first ionization potential (discussed in the section on abundances) imply injection at 10,000°K, while matter in young supernova remnants is much hotter. There, many electrons are stripped as opposed to a single electron being stripped. Origin in interstellar gas is not accepted because it contains grains, i.e., cosmic rays would then be poor in silicon, magnesium, and iron. To melt grains, the gas (if it has low interstellar density) must be hotter than 10,000°K. This, too, conflicts with the ionization potential requirements. And an origin in sputtered grains also has difficulties because it is hard to see how the composition could then be as similar to solar and stellar abundances as observed.

The evidence on the origin of cosmic rays strongly favors the galactic theory rather than the other theories presented. This leaves stellar outer coronal matter, after acceleration to flare particle energies, as the likely origin of the nuclidic material and supernova shock waves that plough into this matter as the probable energy source.

There are probably more than 10^5 sources of cosmic rays strewn throughout the Galaxy. Hence, to pinpoint one source as "the source" is not possible. The large number of sources and diffusive scattering

of the charged cosmic rays renders the nature of this radiation isotropic. Gamma rays maintain their direction, and hence those gamma rays that originate in source regions can be used to make a "Galactic Map" of the source regions. A careful investigation of the propagation of the charged particles can aid in the determination of mean path length and the distribution of path lengths from sources to Earth (in units of g/cm^2 of interstellar material traversed).

c. propagation

Now that the problem of cosmic-ray origin has been narrowed to the galactic model, the mode of propagation of the primary and secondary particles, from the many sources to Earth, is the next step in the understanding of this radiation.

Our Galaxy has a radius of about $3X10^{22}$ to $5X10^{22}$ cm. The distance traversed by cosmic rays ($3X10^{26}$ cm) is considerably greater than the radius of the Galaxy. Thus one can conclude that cosmic rays are scattered back and forth in the Galaxy (Fig. 4). This diffusive behavior enables cosmic rays to escape eventually from the confinement region. The presence of numerous cosmic-ray source regions and diffusive propagation results in the broad exponential-like distribution of path lengths (i.e., many short paths lengths and some long ones).

The ratio of secondary-to-primary nuclei permit the determination of the amount of matter traversed by cosmic rays between acceleration and escape from the Galaxy. The corresponding path length

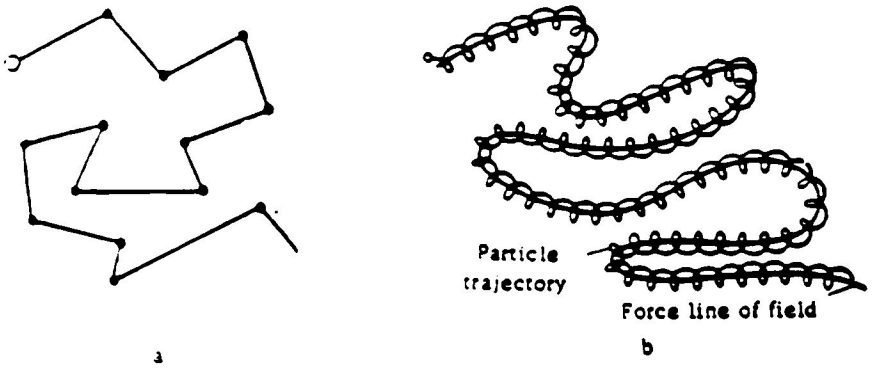

Fig. 4 Particle Motion in a (a) gas and (b) in a Magnetic Field

traversed is about 6 g/cm^2 of interstellar medium, made up mainly of hydrogen and helium. The path length of 6 g/cm^2 is representative of particles at energies of 4 GeV/nucleon. It is 9 g/cm^2 at 1 GeV/nucleon and 2 g/cm^2 at 30 GeV/nucleon. About half as much matter is traversed if there is some distributed acceleration [18].

Propagation of cosmic rays in the Galaxy has for many years been the subject of much attention [3,2]. There have been a number of "models" proposed to describe the confinement and propagation of the Galactic cosmic rays: (i) leaky box , (ii) nested leaky box, (iii) closed Galaxy, (iv) dynamic halo, (v) diffusion , (vi) and the combined model.

In the simplest model, the leaky box [19,20] , cosmic rays are considered to be confined to a region with partially reflecting boundaries from which they slowly "leak out". The volume from which cosmic rays eventually escape from is the volume taken up by the Galactic disk and its halo (Fig. 5). The confinement time in the halo, $\simeq 10^8$ years, is longer than the confinement time in the disk, $\simeq 10^6$ years.

There are certain isotopes in cosmic rays that are used as relativistic escape-time clocks: Be^{10}, Al^{26}, Cl^{36}, Mn^{53}, Mn^{54}, with the half lives of $\simeq 10^6$ years. Of the "escape clocks" mentioned, Be^{10} is the most interesting and most useful for measuring confinement time. Mn^{53} and Mn^{54} are more complicated because of the electron capture mode of decay. And Al^{26} and Cl^{36} are relatively short-lived and will become useful probes only after isotopic resolution is extended to energies of several GeV/ nucleon. Beryllium's half life is

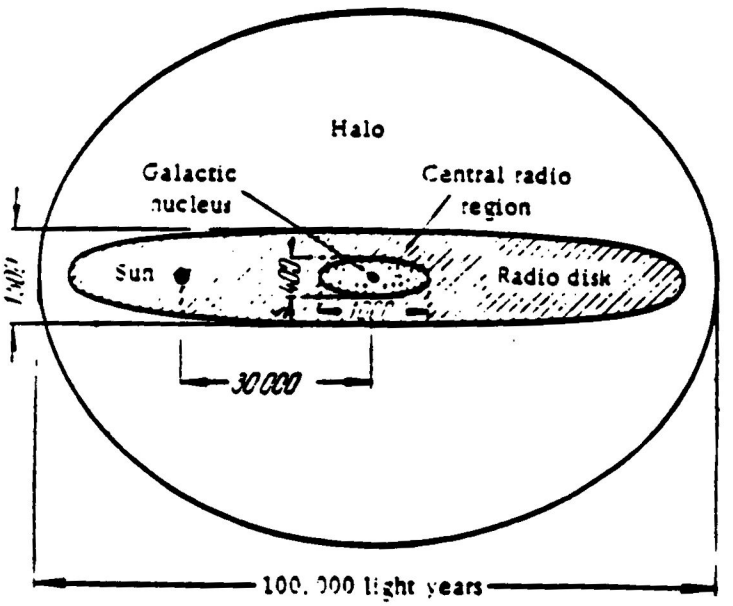

Fig. 5 Galactic Disk and Halo

$\simeq$ 1.5X10^6 years. Obviously, if T_{cr} >> $T_{1/2}$ of Be^{10}, no nuclei of Be^{10} should be observed in cosmic rays. On the other hand, if T_{cr} << $T_{1/2}$ of Be^{10}, all Be^{10} produced must be present. The complete decay of Be^{10} would confirm the existence of a galactic halo, if there were free circulation of cosmic rays back into the disk from the halo. The partial survival of Be^{10} implies that cosmic rays are relatively young (10-20 million years) and have traversed matter with a density of .2 - .3 atom/cm^3 within the confinement region. Before Be^{10} measurements, the leaky box model was proposed on basis of L/M = (Li,Be,B)/(C+N+O) $\simeq$ 0.25, which when combined with the density of 1 atom/cm^3, implies confinement of several X*10^6 years. Observed L/M decreases with increasing energy. Hence people suggested energy or rigidity dependent diffusion from the leaky box.

The nested leaky-box model [21,22] states that there are two confinement regions, one around the sources and the other corresponding to the Galaxy. The galactic cosmic rays (GCR) leak from both regions but at different rates. Rasmussen and Peters [23] proposed a closed Galaxy model where the boundaries of the confinement region are perfectly reflecting so particles cannot escape. They are destroyed by nuclear interactions and energy loss processes. This model cannot reproduce cosmic ray abundances unless one postulates some cosmic-ray sources from which particles reach the Earth with very little traversal of matter. This model was given up in favor of Peters and Westergaard's model [24] of rigidity-dependent confinement in Galactic arms, surrounded by closed Galaxy (this is somewhat like the nested leaky box).

Models that in addition to cosmic rays consider general galactic gas and magnetic field motions (dynamics) were developed. The diffusion model proposes that the cosmic ray particles are tied tightly to the magnetic field lines, which random walk, due to irregular/ turbulent motion, to the boundary of the confinement region where particles can escape. The dynamic halo model was developed by Jokipii in 1976 [25]. In this model our Galaxy has a galactic wind (much like the solar wind) which expels gas at a constant rate. This is a gas that moves outward, magnetic field lines are anchored in gas, and cosmic rays are bound to magnetic field lines. These diffuse around, but there is a component of outward pressure, resulting in the escape of gas, magnetic fields and cosmic rays. This could be the final phase of the diffusion model. While this model is more realistic, it has many poorly known parameters that are not pertinent to cosmic-ray propagation and interactions.

For cosmic-ray nuclear transformation calculations, it suffices to use the simple leaky box model with rigidity dependent escape from the Galaxy. The assumption of some reacceleration provides a better fit to energy dependence of secondary to primary (e.g. L/M) ratios. The nested leaky box model and Peters and Westergaard's (spiral arm and closed Galaxy) model yield rather similar results. Hence, after preliminary trials, people came back to the simple leaky box model. Also physical justification for these more complicated models is insufficient. In the nested leaky box model, there should be gamma ray concentrations from the sites of the source regions. While gamma-ray concentrations from clouds are seen, these

are due to gas concentration rather than cosmic-ray concentrations. And while gamma rays are somewhat enhanced along Galactic spiral arms, the inter-arm gamma-ray flux does not seem to be as low as in the Peters and Westergaard model. Even more complex models (e.g. Three Tier Model;Stephens(1981) [26]: Multi-Cloud-Model; Silberberg et al.,1983b [27] have been proposed.

Cosmic-ray propagation explains the changes induced on cosmic rays during confinement in the Galaxy (or other regions) (Fig. 6). There are two types of changes: composition and energy. The composition of the GCR is modified due to nuclear interactions in the interstellar medium where heavy nuclei fragment into lighter nuclei. The energies of the particles are modified through ionization energy losses in the ISM, for electrons also by synchrotron radiation in the galactic magnetic fields, and by inverse Compton collisions with the photon fields. Particles can gain energy due to stochastic acceleration and due to passage through the interstellar shocks.

The final step of propagation, moving from local interstellar space (LIS) to the orbit of Earth where the actual observations are made, involves the effects of solar and geomagnetic modulations. The cosmic rays that reach the Earth undergo solar modulation by the outflowing solar plasma that results in adiabatic deceleration and reduction of the intensity of low energy particles. There are several types of solar modulations: transient modulations, co-rotating solar wind flow, recurrent solar wind flows due to the period of rotation of the sun (27 days), series of Forbush decreases associated with the solar flare plasma outflow (cosmic ray intensity is reduced and then

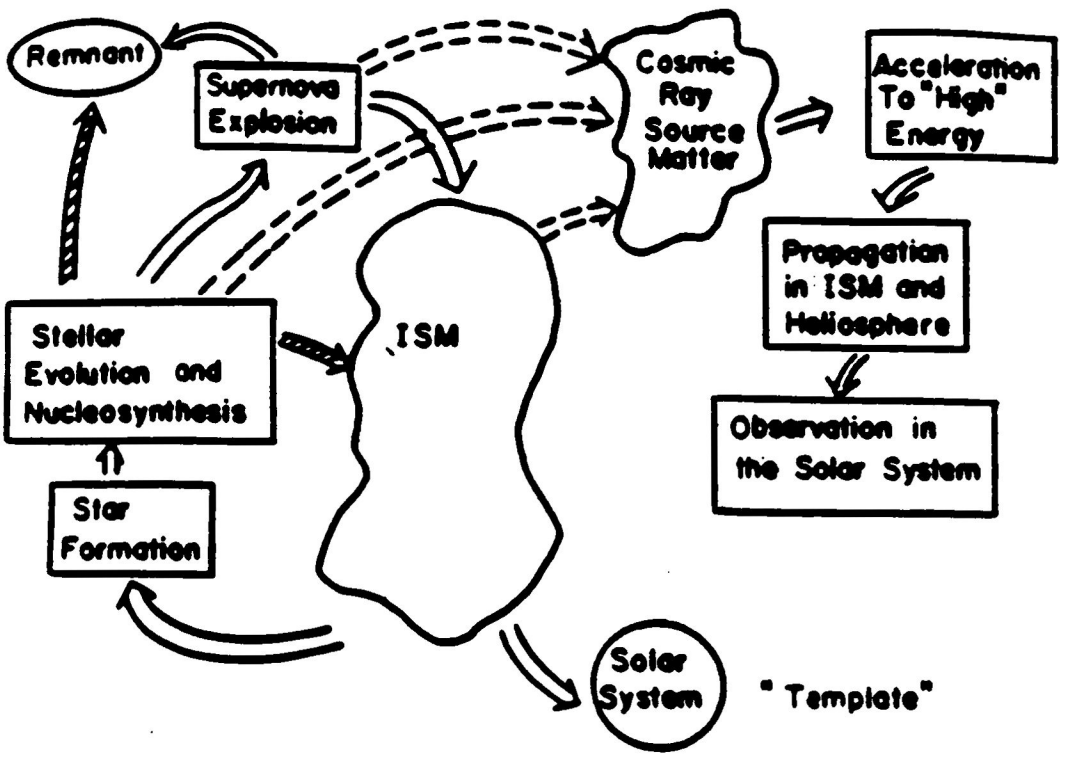

Fig. 6 Relationship between Cosmic-Ray Processes and Astrophysical Processes

recovers after some weeks or a month), and the 11-year solar cycle (produces maximum variation in total galactic particle flux density of about a factor of three, Fig. 7).

Containment within the Galaxy is mainly due to galactic magnetic fields, but the particles that reach the Earth also undergo geomagnetic modulation. The geomagnetic field acts as a natural spectrometer, suppressing the arrival of cosmic rays below a given rigidity threshold. The threshold or "cutoff" is a function of direction of incidence and geomagnetic latitude. It ranges from zero at the geomagnetic poles to 16 GeV at the geomagnetic equator in the vertical direction. Thus, the lower energy cosmic rays are deflected back by Earth's magnetic field. Close to the geomagnetic equator, even protons with energies of 10^{10} eV are prevented entry.

After injection from the stellar sources into interstellar space, the particles are accelerated to cosmic-ray energies. The changes these particles undergo are important and are elaborated upon in the next section. The abundances of cosmic rays change due to nuclear spallation reactions in the interstellar gas. Hence the composition at the sources differs from that observed near Earth.

Abundances

Measurements of the isotopic composition and the elemental composition imply that the sample of material that constitutes the primary cosmic rays has features in its composition that distinguishes it from solar system (general) abundances, but, perhaps more

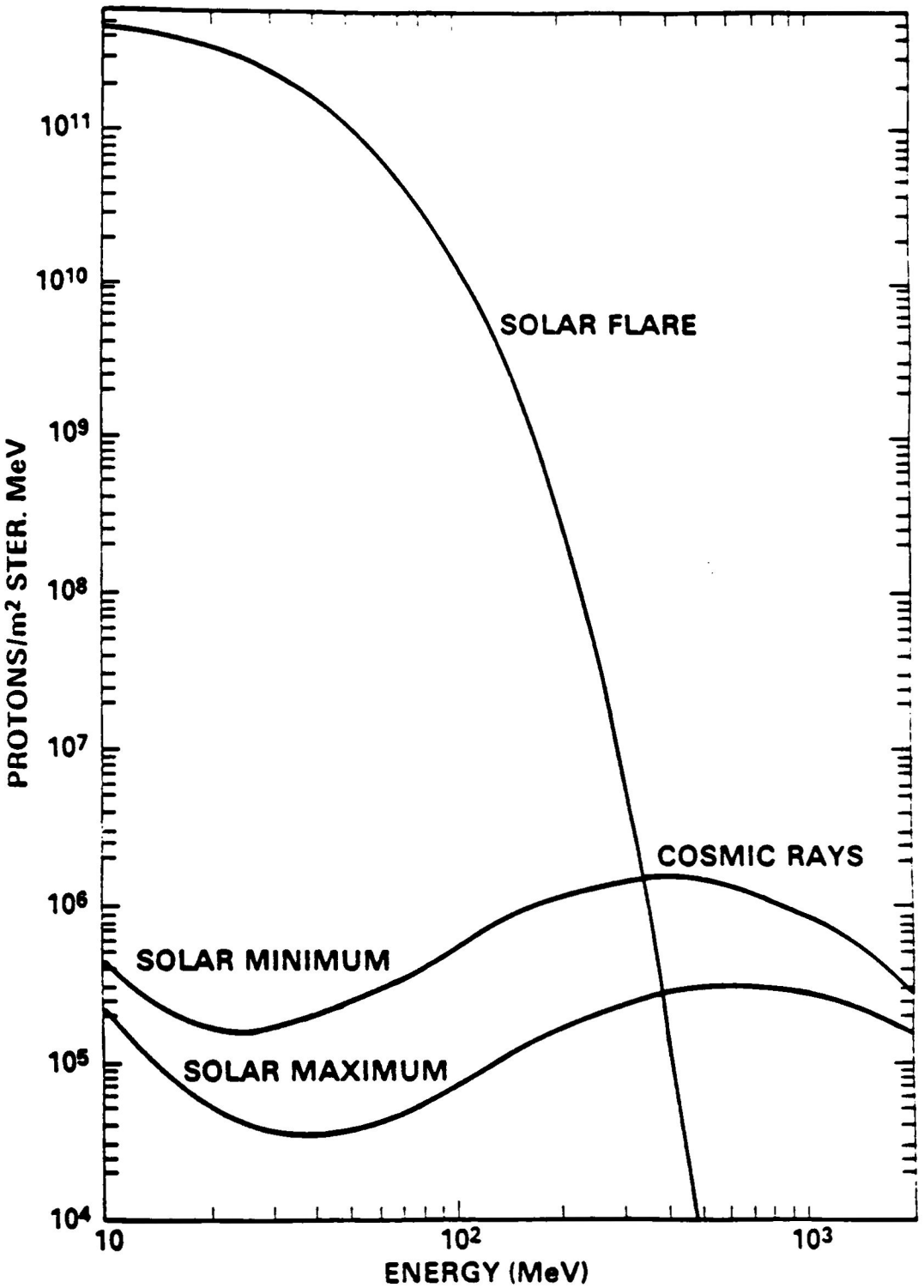

Fig. 7 Effects of Solar Modulation on Cosmic Rays and Solar Flare Spectrum

importantly, also from the abundances measured at Earth (Fig. 8a, Fig. 8b).

a. at the sources

One of the major goals of cosmic-ray research is to understand the composition of cosmic-ray nuclei at their source, i.e. just after acceleration to high energy. By definition, the cosmic ray source (CRS) abundances refer to the relative abundances of the various nuclear species prior to propagation through the interstellar space (i.e. at 0 g/cm^2). Table 1 gives the list of the primary source nuclei, along with other nuclei to be mentioned later.

There are three types of nuclides, stable, long-lived radioactive and those that decay by electron capture, that either originate in cosmic-ray sources or are formed by spallation during propagation through the interstellar space, each of which has a specific information content. A summary of the six different classes is given in table 2. While the set of nuclides that originate in cosmic-ray sources best fits into the section of source abundances, the nuclides that are formed by spallation will be discussed in the section covering abundances near Earth.

The stable nuclei that originate in cosmic-ray sources can give information about source composition and on injection and acceleration conditions. Table 3 shows the relative abundance of elements at the cosmic-ray sources. Havnes proposed a dependence of cosmic-ray composition on the first ionization potential (FIP) [28]. This theory

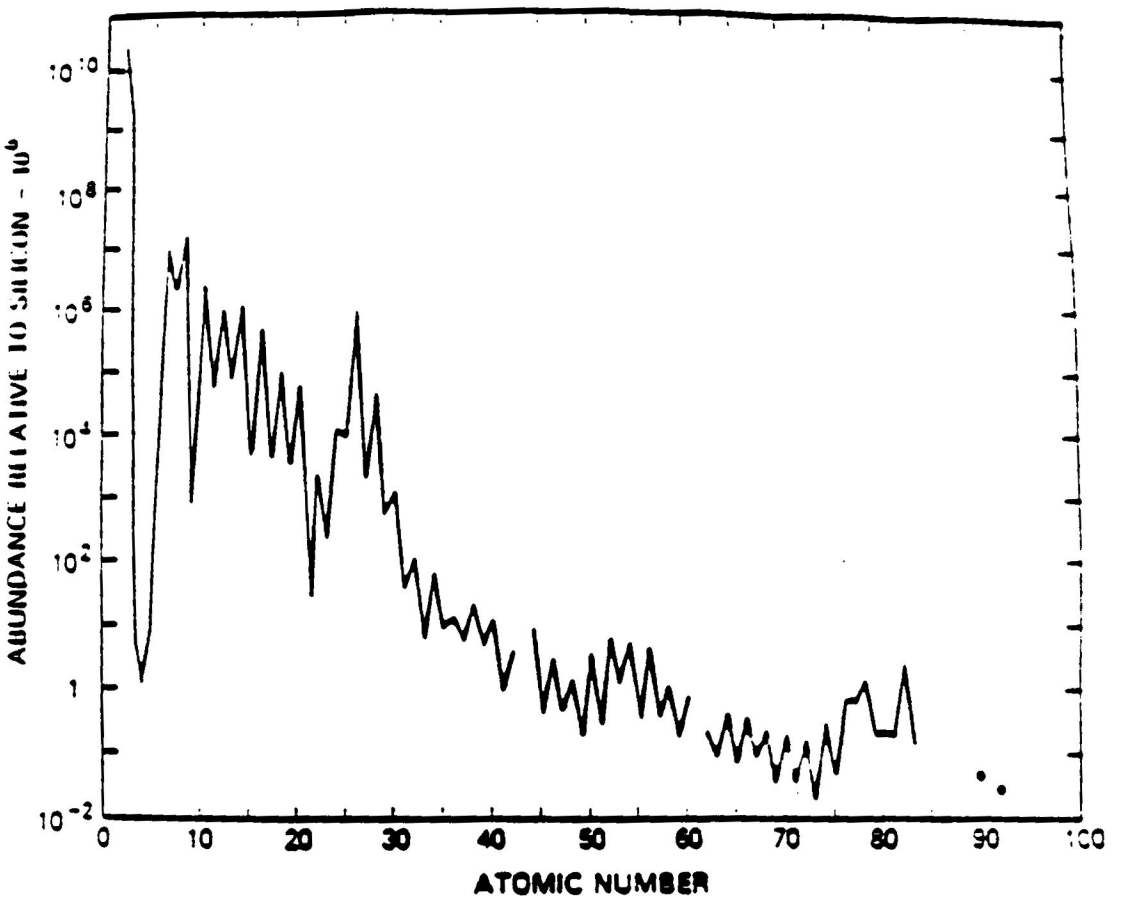

Fig. 8a General Abundances of Cameron

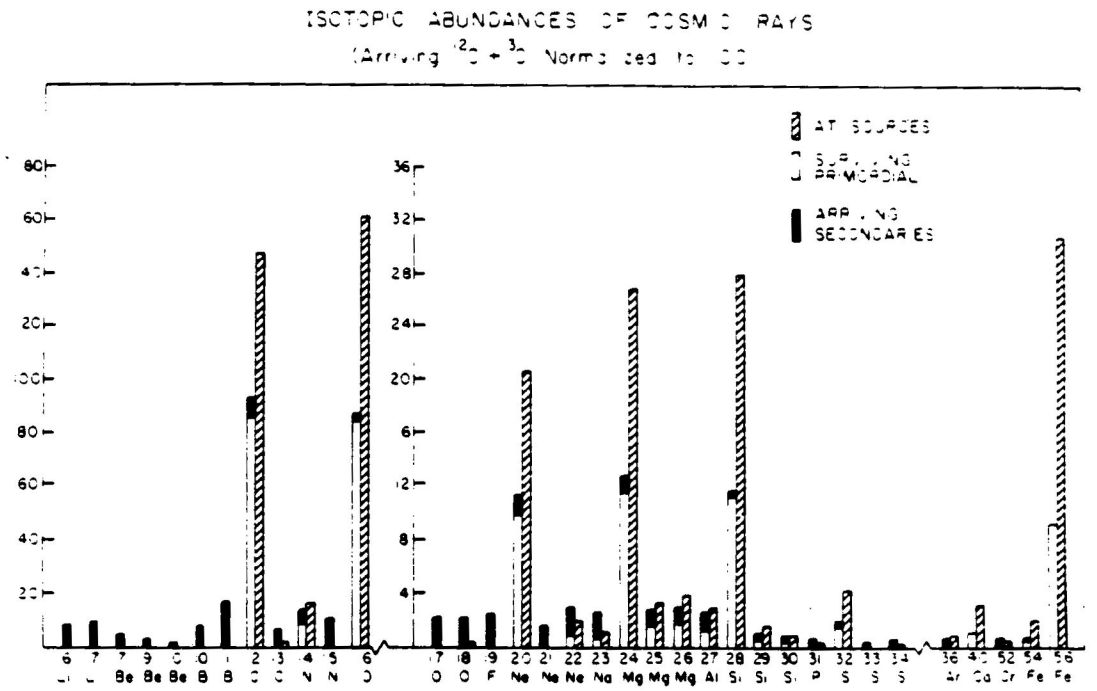

Fig. 8b Cosmic-Ray Source Abundances and Arriving Abundances

Table 1. Cosmic-Ray Primary Source Nuclei

MAINLY PRIMARY SOURCE NUCLEI	PARTLY PRIMARY/ PARTLY SECONDARY	MAINLY SECONDARIES
1H		2H
4He		3He
		6Li,7Li
		7Be,9Be,(10Be)
		10B,11B
12C	13C	
	14N	15N
16O		17O,18O
		19F
20Ne,22Ne		21Ne
	23Na	
24Mg,25Mg,26Mg		
	27Al	(26Al)
28Si	29Si,30Si	
	31P	
32S		33S,34S,36S
		35Cl,(36Cl),37Cl
36Ar		37Ar,38Ar,40Ar
		39K,40K,41K
40Ca,48Ca		41Ca,42Ca,43Ca,44Ca,
		46Ca
		45Sc
		44Ti,46Ti,47Ti,48Ti,
		49Ti,50Ti
		49V,50V,51V
	52Cr	50Cr,51Cr,53Cr,54Cr
	55Mn	53Mn,(54Mn)
54Fe,56Fe,57Fe,58Fe		55Fe
59Co		57Co
58Ni,60Ni,61Ni,62Ni, 64Ni		59Ni

* UNDERLINED:e-capture nuclei
* PARENTHESIS:long-lived partly decayed nuclei

Table 2. The Six Classes of Nuclides

1) COSMIC RAY COMPOSITION:

I. PRIMARY SOURCE COMPOSITION	II. SECONDARY SOURCE COMPOSITION
a) stable nuclides	a) stable nuclides
b) long-lived radioactive(244Pu)	b) long-lived radioactive(10Be)
c) e-capture(44Ti, 57Co, 59Ni)	c) e-capture

I-a) Tells about source composition, injection conditions, and sites

II-a) " " amount of material path length traversed, distribution of path lengths, energy dependence of Galactic confinement time

I-b) " " time since nucleosynthesis

II-b) " " time since acceleration

I-c (57Co,59Ni) II-b (10Be)
<----------><----------->

I-b (244Pu), U/Th U/Th changes w/236U,235U decay
<----------> |
| | | ---->time 232Th
nucl. syn. accel. observation

<---------->
1XE+7 years

I-c) Tells about time between nucleosynthesis and acceleration

II-c) e-capture and attachment starts to occur below ~ 200MeV/nucleon for 20<= Z <= 30; for highly charged nuclei 70<= Z <= 80, e-capture and attachment starts to occur below 1000 MeV/nucleon energy of affected nuclei can get shifted by subsequent reacceleration

Table 3. Cosmic Ray Source Abundance (Si = 100)

Element	Cosmic Ray Source	
H	0.089x10^6	(1.25)
He	0.012x10^6	(1.07)
C	431	(1.08)
N	31	(1.39)
O	511	(1.04)
F	<2.5	
Ne	64	(1.13)
Na	5.6	(1.80)
Mg	106	(1.06)
Al	10.2	(1.40)
Si	100	(1.06)
P	<2.5	
S	12.6	(1.17)
Cl	<1.6	
A	3.0	(1.25)
K	<1.9	
Ca	6.0	(1.30)
Sc	<0.8	
Ti	<2.4	
V	<1.1	
Cr	<2.9	
Mn	<3.7	
Fe	93	(1.06)
Co	0.32	(1.40)
Ni	5.1	(1.17)
Cu	0.064	(1.20)
Zn	0.067	(1.15)
Ga	0.0056	(1.50)
Ge	0.0064	(1.45)

* Numbers in brackets are uncertainty factors

has been further elaborated by Casse et al. [29]. (A previous theory that tried to relate source abundances to nucleosynthesis in supernovae was rejected because both Ar and Ca are produced in oxygen burning, but only Ar, with a high FIP, has a very low abundance, agreeing with the FIP model).

Cosmic-ray source abundances are similar to solar abundances modified by the FIP effect (Fig. 9). Elements that have a high FIP (>10 eV) have a lower abundance in cosmic rays. Elements with a high FIP are: H,He,C,O,N,Ne,Ar, and other noble gases (Fig. 10).Their atoms are neutral at 10,000°K. Neutral particles from the Sun (and we assume from stars) have difficulty in diffusing from the photosphere to the corona. These which are charged have an easier time escaping along the magnetic fields to the corona and other regions where particles are accelerated. H and He are less abundant by a factor of about 5 in the FIP model, but are still under abundant by another factor of 2 or 3. This can be explained by the preferential acceleration of heavier nuclei that the shock-wave theory suggests.

Some isotopes are over-abundant in cosmic-ray sources as compared to general abundances. The source abundance of Ne^{22}/Ne^{20} is 3.2 ± 0.5 times higher in cosmic rays and $Mg^{25,26}/Mg^{24}$ is 1.4 ± .3 times higher. The Ne^{22} anomaly in cosmic rays may have an origin in nitrogen burning in the helium zone (usual reaction: $N^{14} + He^4 \rightarrow F^{18} \rightarrow O^{18} + e^- + \nu \rightarrow O^{18} + He^4 \rightarrow Ne^{22}$ and $Ne^{22} + He^4 \rightarrow Mg^{26}$ or $Mg^{25} + n$). Woosley and Weaver [30] speculate that most of the cosmic rays observed at the Earth originate from remote metal-rich regions located a few Kpc away in the inner Galaxy. This could also enhance Ne^{22} and $Mg^{25,26}$ and

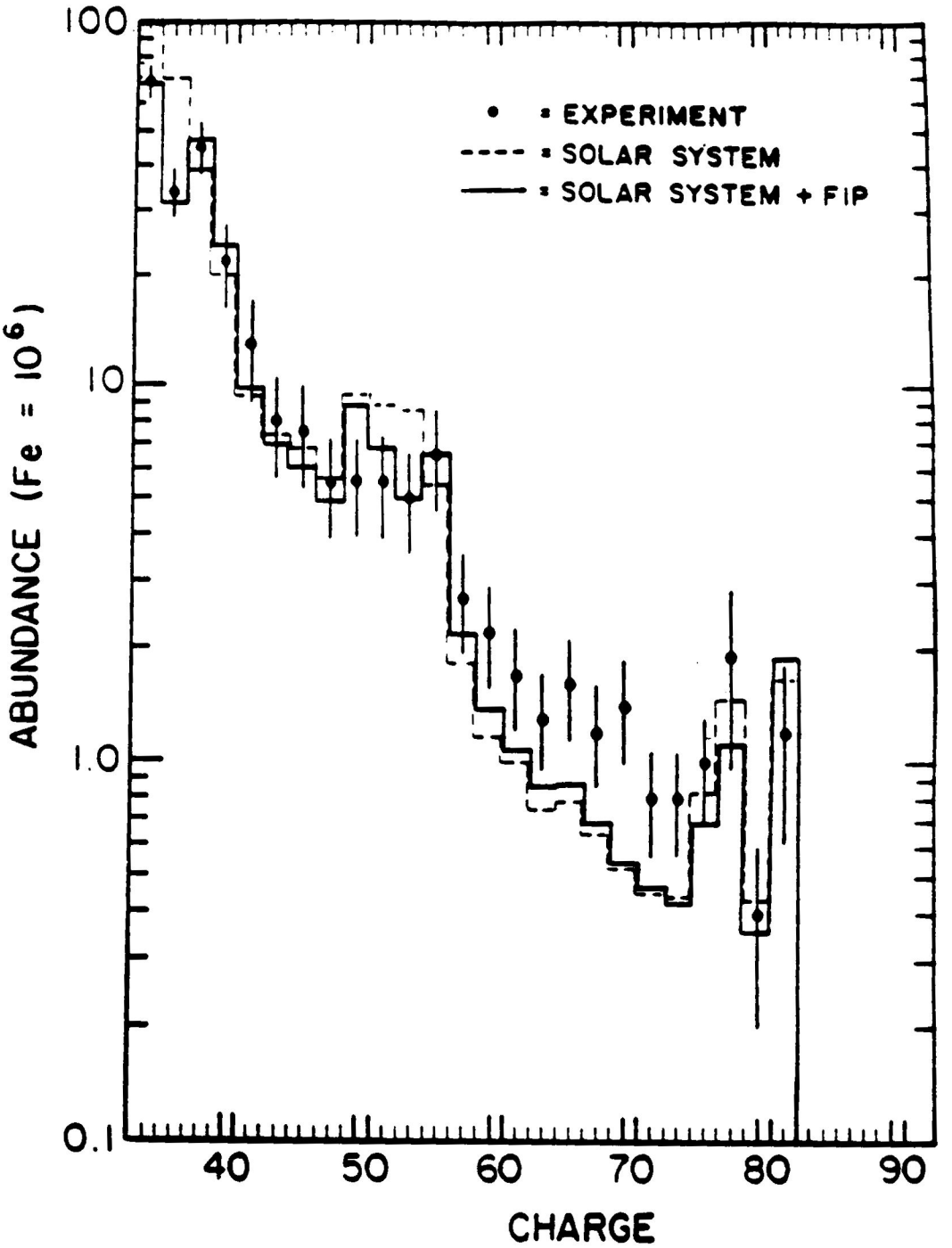

Fig. 9 Comparison of Cosmic-Ray Abundances and Propagated Solar System Abundances for Elements with Z Greater than 30 (with and without FIP)

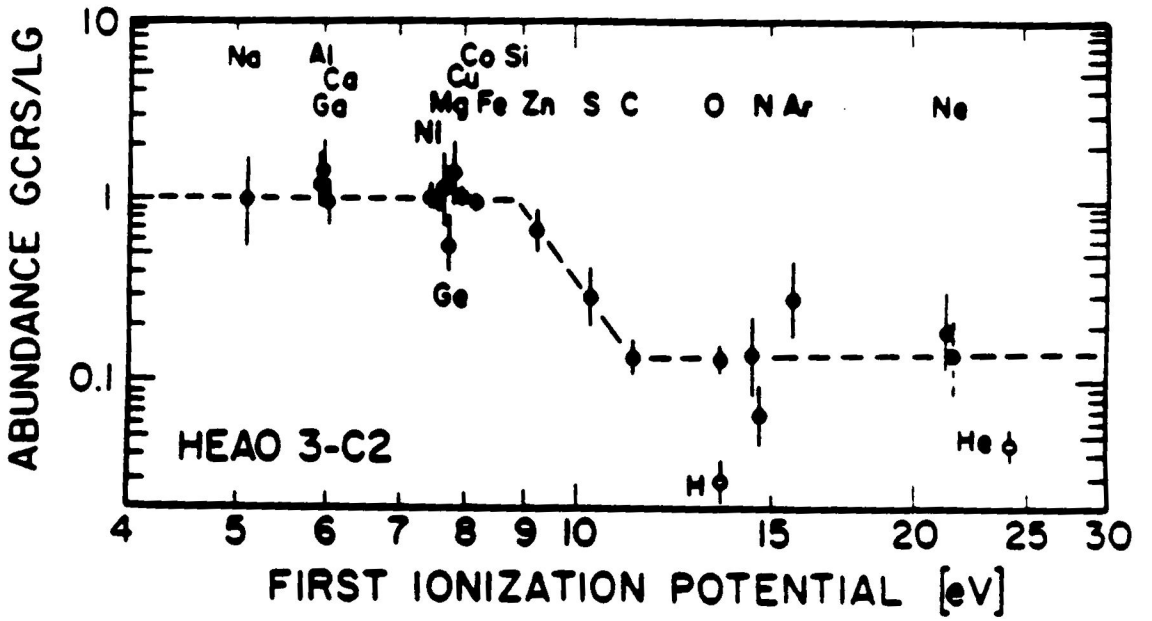

Fig. 10 Ratio of Galactic Cosmic Ray Source to Local Galactic Abundances as a Function of FIP

also Si^{29} and Si^{30}. Also, there is a very large Ne^{22} enhancement with respect to Ne^{20} (2 orders of magnitude) in Wolf-Rayet stars of the type WC (i.e. carbon rich) and also the enhancement of Mg^{25} and Mg^{26}, and of carbon relative to oxygen. Some admixture of material from WC stars can explain all four anomalies: Ne^{22}, Mg^{25}, Mg^{26}, C/O. A test between the Woosley and Weaver and the Wolf-Rayet star admixture models is given by the Si^{29}, Si^{30} vs. the C/O ratio. The former model predicts an enhancement of the above isotopes of Si, while the latter predicts enhancement of C/O.

The cosmological Big-Bang Nucleosynthesis only accounts for nuclides from hydrogen to lithium-7. It is harder to synthesize the heavier elements because of the low density involved and the gaps of stable or long-lived nuclides at mass numbers 5 and 8. A massive dense and hot star with an interior He^4 burning shell can also synthesize C^{12}. The reaction $3He^4 \rightarrow C^{12}$ can bridge this mass gap (if the temperature and density are high enough). This triple alpha reaction is followed by further nuclear reactions of type: $C^{12}(He^4,\gamma)O^{16}$ and $C^{12}(p,\gamma)N^{13}(He^4,p)O^{16}$, produced in a build-up toward heavier elements.

The long-lived radioactive nuclides that originate in cosmic-ray sources can be used to determine the time, T_n, that has passed since nucleosynthesis of cosmic-ray nuclides. A value of $T_n \leq 10^7$ years implies an origin in recent SN or in their shells, with cosmic ray confinement principally in the galactic disc. A value of $10^7 \leq T_n \leq 10^8$ would imply a similar origin, but confinement in the halo. If $T_n >> 10^8$ years, an origin in old SN material that has been incorporated into stars (e.g. the flare stars) is implied.

To tell the time from nucleosynthesis to present, one has to measure the abundance and the half-lives of U^{235}, Pu^{244} and isotopes of Cm (Fig. 11). The latter are measured in laboratories to within 10-20% accuracy . These isotopes are formed during rapid neutron capture (r-process) in SN. The time since nucleosynthesis, to be measured from the half lives of U and Pu and the abundance of these elements, is estimated $\simeq 10^7$ to 10^{10} years. The time has to exceed 10^7 years (based on Be^{10}), but will be less than $\simeq 10^{10}$ years, the age of the Galaxy. As shown in figure 11, also the ratio of U/Th permits one to measure the time since nucleosynthesis.

The nuclides that decay only by electron capture and originate in cosmic-ray sources permit a determination of the time between nucleosynthesis and acceleration (T_{na}) of cosmic ray nuclei [31]. In the synthesis of elements certain nuclides are produced that normally decay by electron capture. However, cosmic rays move with nearly the velocity of light and are completely stripped of their electrons. Thus, because they have no electrons to capture, they become stable. If primary Ni^{59} survives in cosmic rays, $T_{na} < 10^5$ years, if it has decayed to Co^{59}, then $T_{na} > 10^5$ years.

b. <u>general abundances and nucleosynthesis</u>

The cosmic rays which reach the solar system (the solar composition is representative of the general abundances, Fig. 12) are clearly identifiable, since they can be observed directly with detectors on balloons, rockets, satellites and interplanetary probes.

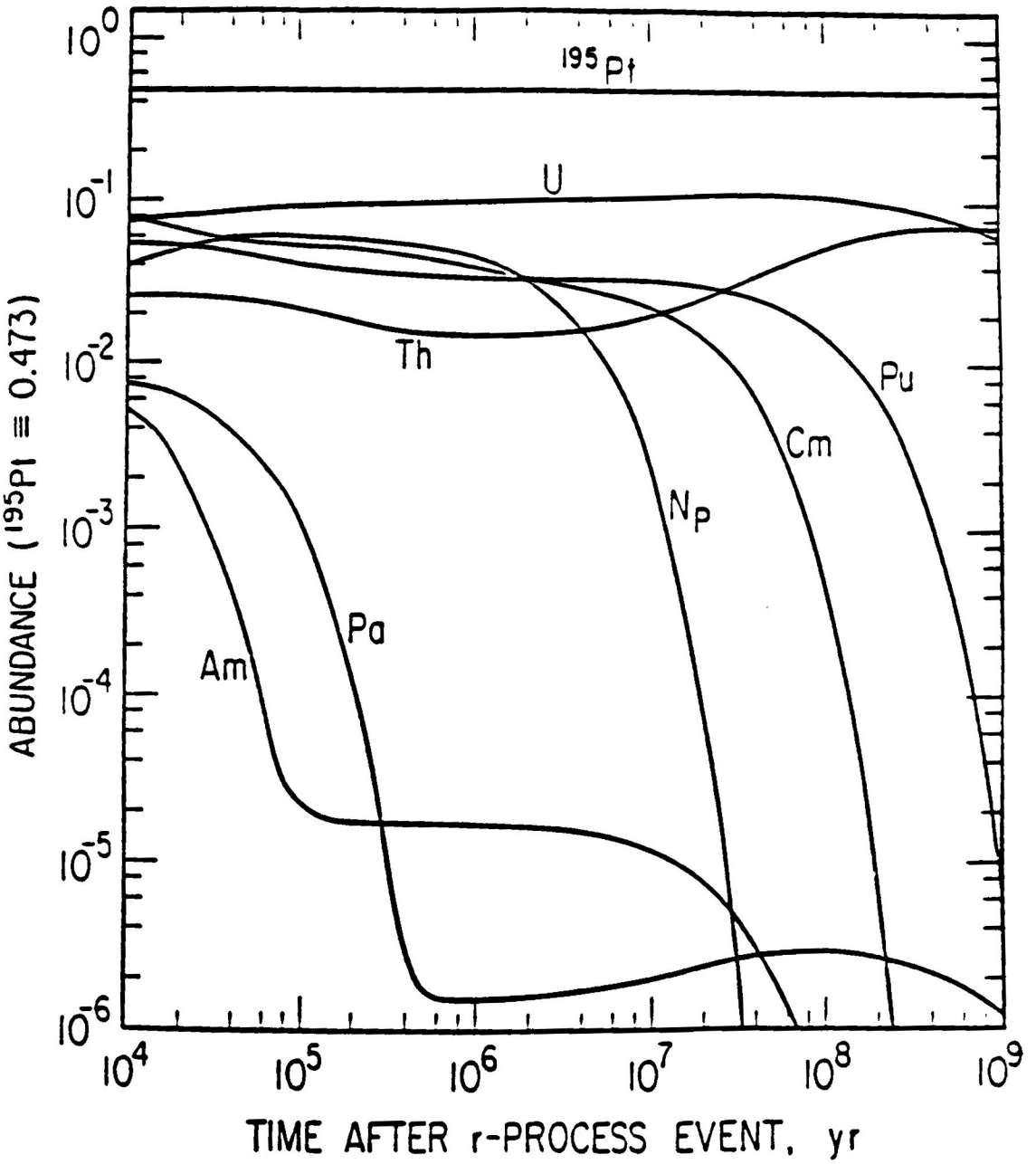

Fig. 11 Abundances of R-Process Actinides as a Function of Time

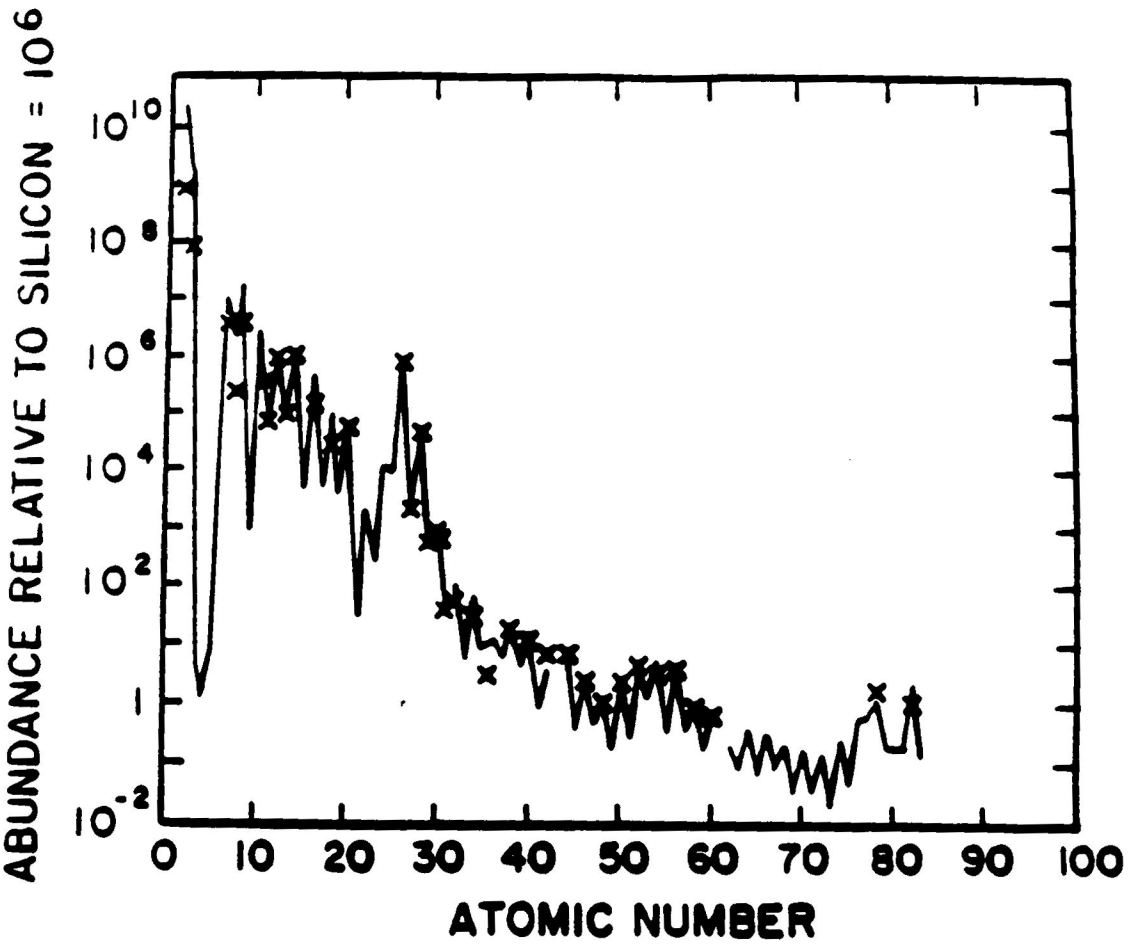

Fig. 12 Comparison of Cosmic-Ray Source Abundances (x)

and General Abundances (line)

The general abundances of elements reflect nucleosynthetic processes in various stars and SN. The relative solar abundances for H,He,C,N,O,Ne,S, and Ar are larger than the GCR abundances, which have been interpreted as suppression of elements with a high first ionization potential during the injection of particles that become cosmic rays.

The general abundances of elements are formed in three types of nucleosynthesis: 'Big Bang', stellar and explosive. In Big Bang nucleosynthesis, which is thought by some to have taken place some 15 ± 3 billion years ago, some 10^{80} protons and neutrons were produced. The nuclear interactions that took place were $p+p \rightarrow H^2+e^+ + \nu$, $H^2+p \rightarrow He^3$, $H^2+n \rightarrow H^3$ unstable and decays $\rightarrow He^3$, $H^2+H^2 \rightarrow He^4$, $He^4+He^4 \rightarrow Be^8$, but very short half life such that Be^8 decays $\rightarrow He^4+He^4$, $He^4+He^4 \rightarrow Be^7+n$, $He^4+He^3 \rightarrow Be^7+\gamma$, and $He^4+He^4 \rightarrow Li^7+p$. Because of the low density, the nuclei are not close enough to overcome the short half-life of Be^8 (which acts as a bottleneck of the interaction process) and thus the heavier elements are not formed. The gas is therefore composed of 90% H, 10% He^4, and traces of He^3, H^2, and Li^7.

Stellar nucleosynthesis starts with burning of hydrogen inside a star which leads to the production of the heavier elements. The starting interaction is between two hydrogen atoms: $H+H \rightarrow H^2 + e^+ + \nu_e$ (e^+ and ν_e for lepton conservation). With the cross section of two protons, $\sigma_{p+p} = 10^{-26}$ cm^2, and the weak interaction of ν_e, $\sigma_{\nu e} = 10^{-44}$ cm^2, i.e. only 1 interaction out of 10^{18} proton interactions will go into H^2. The very low cross section of the neutrino acts as the bottleneck of this reaction and prevents the sun from burning up in

seconds. The remaining reactions follow: $H^2+H^3 \rightarrow He^4+n$ (this is a strong reaction), $H^2+H^2 \rightarrow He^4+\gamma$ (this can occur, but infrequently because E_{thres} and T_{thres} are higher), $He^4+He^4 \rightarrow Be^8$, again this reaction is the 'bottleneck' of this process such that Be^8 must collide with another He^4 within 10^{-16} seconds (generally decays back into He^4). Since the density is much higher in stars, the heavier elements have a better chance of being formed and He^4 can collide with Be^8 to form C^{12}. And since He^4 is much more abundant than H^2, it fuses more frequently with existing elements to produce heavier elements, e.g. $C^{12}+He^4 \rightarrow O^{16}$ and $O^{16}+He^4 \rightarrow Ne^{20}$ and $Ne^{20}+He^4 \rightarrow Mg^{24}$.

In explosive nucleosynthesis, during the supernova phase, much heavier elements are formed through fusion reactions:

$C^{12}+C^{12} \rightarrow Ne^{20}+He^4$
$O^{16}+O^{16} \rightarrow Si^{28}+He^4$ (principal reaction)
-or- $\rightarrow P^{31}+p$ -or- $\rightarrow S^{31}+n$
(unstable and decays into P^{31}).

The step-by-step fusion of Si^{28} with He^4 continues in a quasi-equilibrium process that yields many nuclides (via S^{32}, Ar^{36}, Ca^{40}, etc.) until Ni^{56} is formed, which decays into stable iron. Once Fe is formed, the gravitational pressure is greater than the energy outflow and causes the star to collapse releasing gravitational energy (SN). The r-process (rapid neutron capture) and the s-process (slow neutron capture) produces the heavier elements beyond iron. Other isotopes are formed when combined with protons (p-process) (Fig. 13).

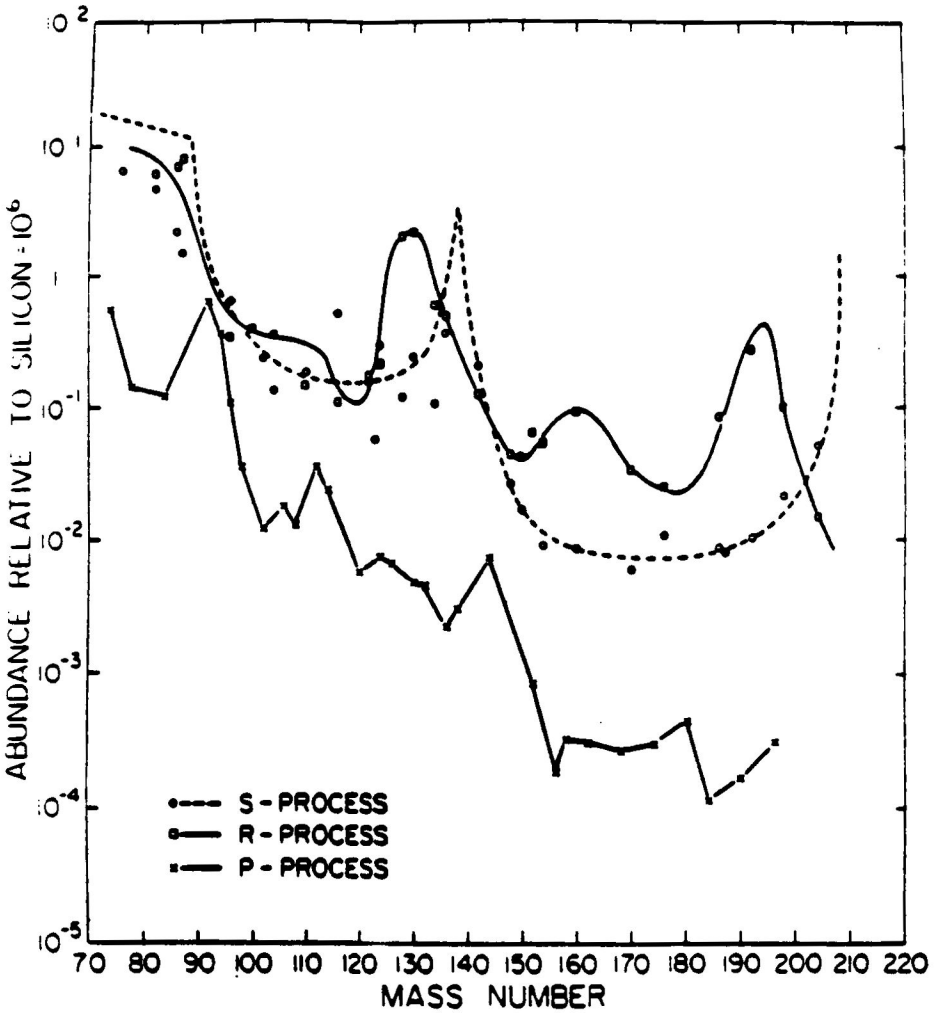

Fig. 13 Abundances of Heavy Nuclides Produced by the S-, R- P- Processes

c. during propagation and near earth

Figure 14 shows the measured abundances of arriving cosmic rays. The spallation of heavier cosmic-ray nuclei into lighter nuclei explains the discrepancy of the low source abundance of the lighter nuclei when compared to the nuclei measured at the top of the Earth's atmosphere. About half of the cosmic-ray carbon and oxygen nuclei (and more than half of the heavier nuclei) collide before reaching the Earth - then their collision products, the light elements Li, Be, and B, are built up.

The stable secondary nuclei that are formed by spallation are used to determine the amount of material path length traversed, the distribution of path lengths, and the energy dependence of Galactic confinement time. As mentioned in the propagation section, the mean path length is about 9 g/cm^2 for cosmic rays at energies $\simeq$ 1 GeV/nucleon, 6 g/cm^2 near 4 GeV/nucleon and 2 g/cm^2 near 30 GeV/nucleon. By comparing the secondary to primary abundances, these mean path lengths were calculated, and an exponential-like distribution was inferred after experimental and theoretical data were compared [radiation transport section]. Li, Be, B, are built up in cosmic rays by spallation of C and O, F from Ne, Mg and Si and Z = 17 to 25 are built up through spallation of Fe.

In the propagation section, some isotopes were discussed which are used as cosmic ray clocks. These isotopes, the long-lived radioactive nuclei, give information on the time since acceleration: Be^{10}, Al^{26}, and Cl^{36}. Stated earlier, Be^{10} is the most useful of the

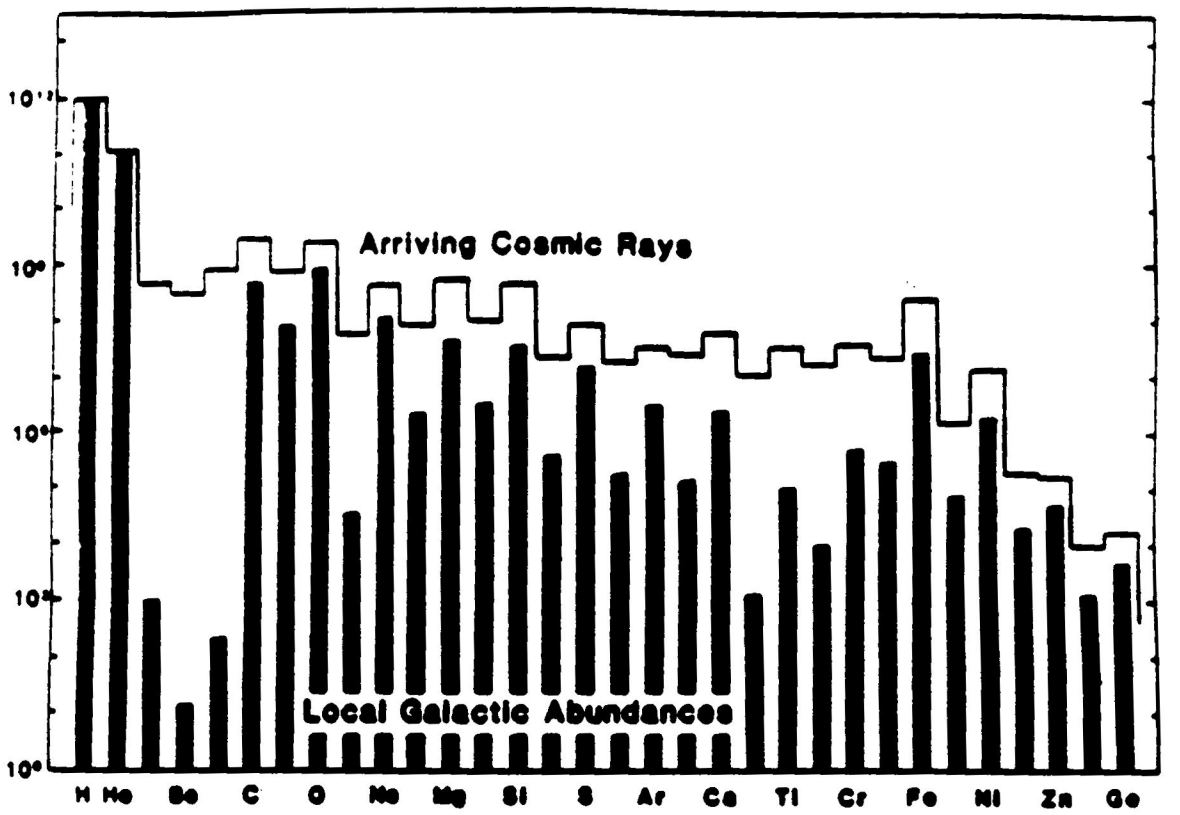

Fig. 14 Comparison of Elemental Arriving Cosmic-Ray and Local Galactic Abundances

so-called 'escape clocks '. Al^{26} and Cl^{36} need the aid of an upcoming experiment called the Astromag [32] as they decay below 1 GeV/nucleon. The Astromag can measure them at $\simeq$ 10 GeV/nucleon, at which energy their life-times are longer by the relativistic Lorentz factor.

The nuclides that decay by electron capture and are formed by spallation during propagation through space are the last type of the six classes. These nuclides can be employed to measure solar modulation with deceleration. Nuclides of this class are: Be^{7},Ar^{37},Ca^{41},Ti^{44},V^{49},Cr^{51},Mn^{53},Mn^{54},Fe^{55}, and about 50 more heavier than iron. At energies less than 200 MeV/nucleon, electron capture decay occurs. Below 200 MeV/nucleon, electrons can get attached to the above mentioned nuclides and cause them to decay. Cosmic-ray nuclei are close to fully ionized during their passage through the Galaxy. Electron capture decay is rare among these nuclides because most do not have bound electrons. If effects of decay are seen at 400 MeV (at which energy decay is negligible) it had to occur at or below 200 MeV, and then the nuclei were reaccelerated to 400 MeV. Thus, they can serve as probes for reacceleration. If such nuclei are formed below 200 MeV/nucleon, and decay ($V^{49} + e \rightarrow Ti^{49} + \nu_e$) and then are reaccelerated, say to 400 MeV/nucleon, the measurement at 400 MeV/nucleon would find an excess of Ti^{49} and deficiency of V^{49}. Thus, with distributed acceleration, effects of decay will be seen at higher energies. Under certain conditions, specifically low energies and/or high charges, electron capture becomes an essential factor in determining cosmic ray composition. (However, the analysis is complicated. While reacceleration shifts the effects of decay to higher

energies, deceleration during solar modulation shifts them to lower energies. The case of Ti^{44} is even more complicated; due to its long half-life, after electron attachment, the electron can be stripped off before decay, if formation of secondary nuclei occurs in dense interstellar clouds).

The observed cosmic-ray composition is likely to be derived from the superposition of different kinds of sources and/or different spectra at very low and very high energy, which are modified by nuclear spallation reaction in interstellar space.

Energy Spectra

There are three properties of cosmic rays that are measurable to some degree of accuracy: directional distribution, composition, and the energy spectrum for each species. The first two have been presented and the latest measurements included. The energy spectrum is added in this thesis because it helps to clarify where and how each species gets the energy to propagate through space and because the ratio of secondary-to-primary nuclei is energy-dependent. The energy spectrum describes the extraordinary energy of individual particles and the large total flux. Since the range of particles and cross sections depend on the energy, also the radiation doses and the single event upsets in computers depend on energy spectrum (discussed in the radiation exposure section). The large kinetic energy of cosmic rays sets them apart from the bulk of the material in our environment (Fig. 15). Cosmic ray energy extends over 14 orders of magnitude and

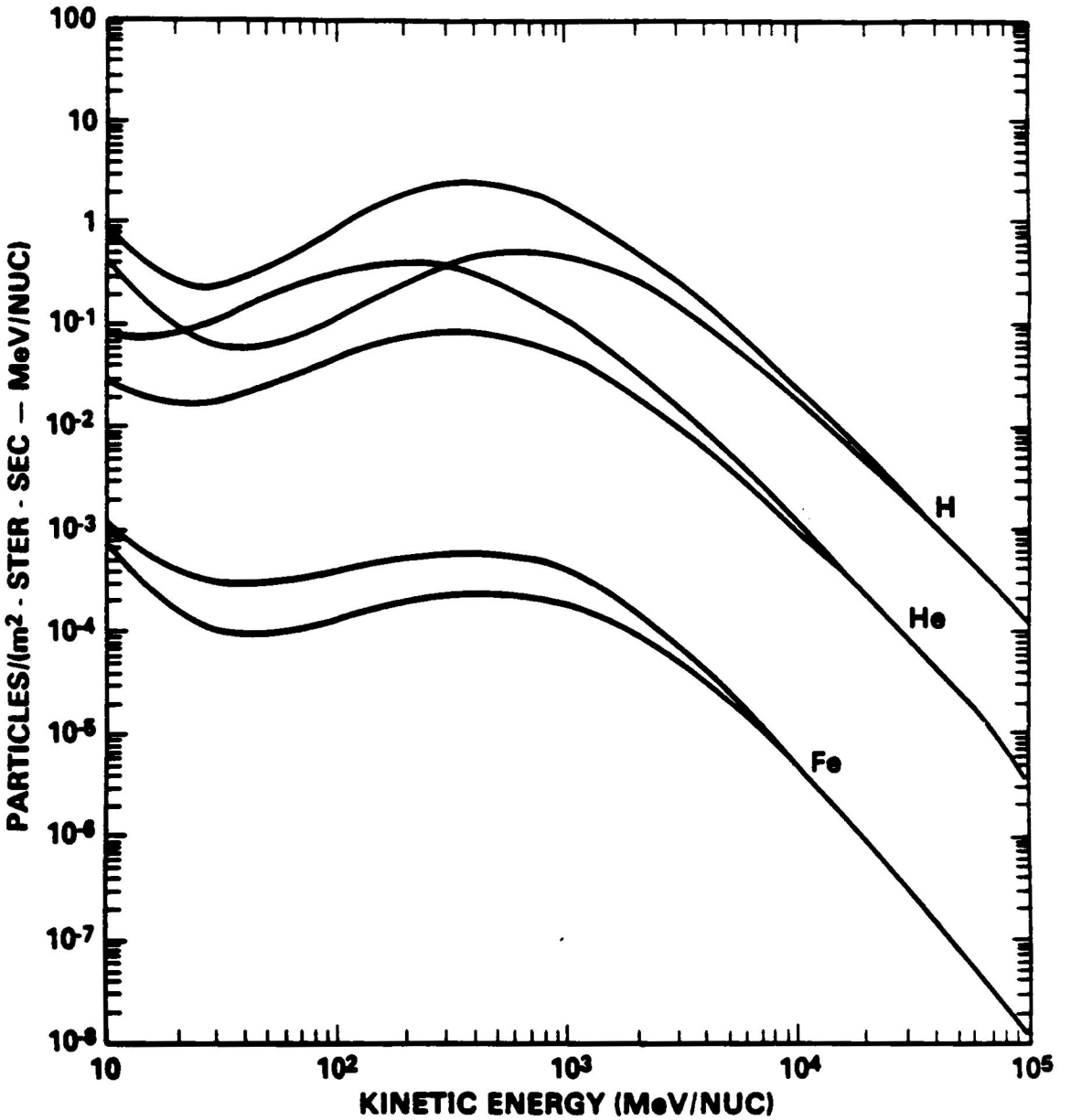

Fig. 15 Kinetic Energy of Cosmic Rays (per-nucleon spectrum)

can be divided into 4 characteristic regions: (a) below several GeV/nucleon, where solar modulation processes are important, (b) from several GeV/nucleon to $\simeq 10^6$ GeV/particle, where a single power law dominates, (c) between 10^6 and $\simeq 10^{10}$ GeV, where a steeper spectrum is evident, and (d) above 10^{10} GeV, a region most likely dominated by extragalactic cosmic rays.

Energy spectra of cosmic rays and of photons from pulsars, quasars, and active galactic nuclei are generally power laws. $dJ/dE = kE^{-\alpha}$ where generally $2 \leq \alpha \leq 4$. dJ/dE is the number of particles or photons in an energy interval dE.

For the energy interval: 10^{10} eV up to 10^{13} eV $\alpha \simeq 2.7$
10^{15} eV up to 10^{19} eV $\alpha \simeq 3.1$

dJ/dE is linear on a log-log scale:

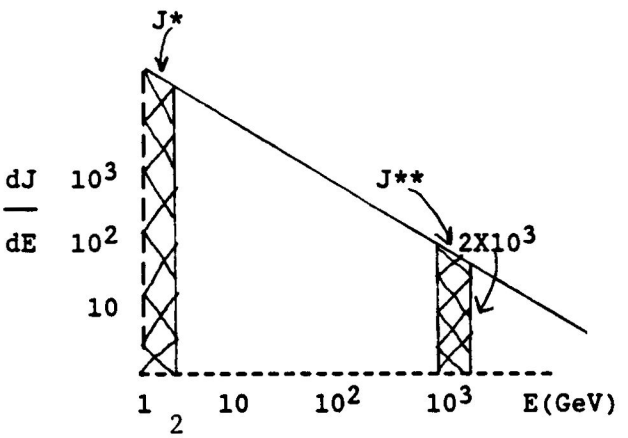

If alpha equals 2, then equally much energy is emitted in each interval.

PROOF:

$$dJ/dE = kE^{-2} \qquad\qquad dJ/dE = kE^{-2}$$

$$\int dJ = k\int_1^2 E^{-2}\,dE \qquad\qquad \int dJ = k\int_{1000}^{2000} E^{-2}\,dE$$

$$J^* = -k/E\Big|_1^2 \qquad\qquad J^{**} = -k/E\Big|_{1000}^{2000}$$

$$= k/2 \qquad\qquad = k/2000$$

The energy interval for J** is 1000 times larger: 1000 to 2000 vs. 1 to 2 for J*, and J** particles have 10^3 times higher energy, thus equally much energy carried by J** interval of particles as by J* interval of particles, though there are 10^6 times more particles per energy interval of the J* particles. For alpha equal to 4, the slope is much steeper, thus more energy is carried by particles at lower energies than at higher energies.

While the changes in slope of the cosmic ray spectrum have been confirmed by several independent experiments (0-10^6 GeV:satellites, 10^6-10^7 GeV:atmospheric Cerenkov light instruments and muons, >10^7 GeV:extensive air showers), there is still the troubling question of some possible systematic effects. Energy spectra of cosmic-ray particles, whose atomic numbers are measurable, have been measured with detectors on satellites and balloons at heliocentric distances of the order of 1 A.U. Present satellites have reached 30 A.U. with a constant outward movement of 1-2 A.U./year.

As seen in figure 16, the latest measured energy spectrum [33] exhibits a "knee" at 10^{15} eV and an "ankle" at $\simeq 10^{19}$ eV. Above the knee ($3X10^{15}$ eV), the flux drops more steeply, and the anisotropy increases and changes phase, as though the rate of leakage from the galactic 'box' increases. Since magnetic fields control the leakage rate (which increases as R, the rigidity, becomes larger), the change should occur at an energy-per-nucleus proportional to 'Z' for different nuclei; one thus expects the composition to change, with protons being lost first, and then the lighter elements in the neighborhood of the knee. The explanation of the ankle is due to the entry of ultra-high energy extra-galactic particles whose spectrum has not been steepened.

The origin, propagation, abundances, and the energy spectra of cosmic rays must be well defined because they are the foundation of cosmic ray research. The foundation of any subject must be set in order to build a better understanding. For this reason, these properties are constantly being researched and improved. And these improvements aid in the theoretical calculations of the mathematical properties of cosmic rays.

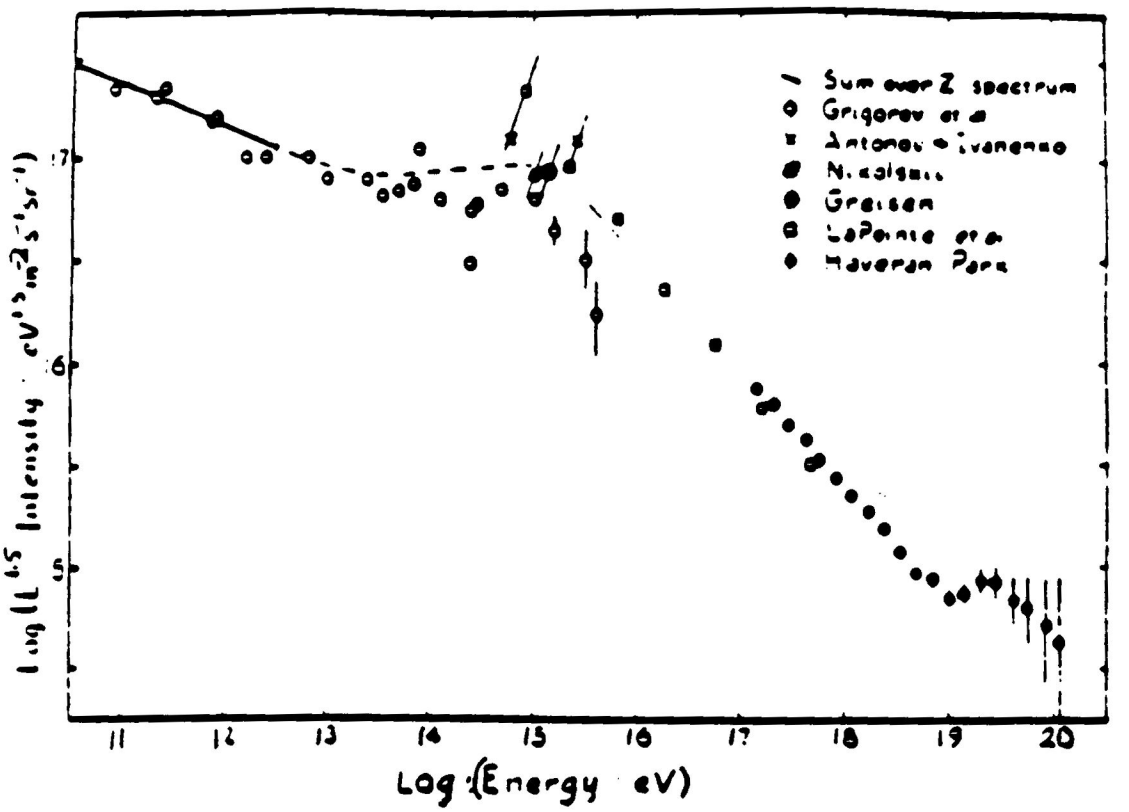

Fig. 16 Energy Spectrum of Cosmic Rays (per nucleus, very high energy)

III. CALCULATIONS

The previous chapter presented theories on the origin, acceleration, and propagation of cosmic rays. Also, the abundances and energy spectra of cosmic rays based on experimental data were discussed. In this chapter, those theories and experimental data along with propagation and cross section calculations will be combined so that reliable theoretical predictions may be made within an acceptable percent error.

Radiation Transport

Cosmic rays diffuse through interstellar medium (ISM) undergoing nuclear fragmentation and decay and suffering energy loss in atomic collisions. To explain this diffusion, the propagation of cosmic rays can be described by the equation [34]:

$$(1) \qquad dJ_i/dX = -J_i(N/\rho)\sigma_i + \Sigma_{j>i}[J_j(N/\rho)\sigma_{ij}] + \delta/\delta E[J_i(dE/dX)_i]$$

↑	↑	↑
depletion of primaries	increase in secondaries	ionization energy loss

where,

J_i = flux of particle 'i'

N = atomic density in medium (atoms/cm^3)

ρ = density in g/cm^3

σ_i = cross section in millibarns (1 mb = 10^{-27} cm^2)

λ_i = interaction mean free path = $(N\sigma_i/\rho)^{-1}$

and N/ρ = atoms/g = $6.02X10^{23}/1.007$ for hydrogen.

Rewriting in terms of mean free path yields,

(2) $$dJ_i/dX = -J_i/(\lambda_i) + \Sigma_{j>i}\, J_j/(\lambda_{ij}) + \delta/\delta E[J_i(dE/dX)_i]$$

(which is too complicated to solve analytically i.e. it is solved by computerized numerical integration). The decay calculations have been excluded because in general the decay lifetimes are shorter than the combined mean free paths for fragmentation and escape from the Galaxy; thus all nuclei with half lives < 10,000 years are considered to decay immediately. And the electron-capture decay mode is disregarded since most nuclei in the ISM have been stripped of their electrons. (Any discrepancies in cosmic-ray abundances caused by excluding nuclear decay will be corrected in calculations).

The most important physical process in propagation is nuclear fragmentation, which involves the total inelastic cross section (σ_i) and the partial cross section (σ_{ij}). The earliest attempts to systematize high energy cross section measurements into a useful analytical relationship describing the systematics of these reactions are generally credited to Rudstam [35]. These analytical relationships have been revised and improved by many workers as new cross section data have become available.

The most reliable calculations of still unmeasured partial cross sections are obtained with empirical formulae of Silberberg and Tsao [36]. The equation is applicable for calculating cross sections (in units of mb) of targets that have mass numbers in the range $9 \leq A_j \leq 209$ and products with $6 < A_i < 200$ at energies >100 MeV/nucleon:

(3) $$\sigma_{ij} = \sigma_o f(A_i) f(E) \exp(-P\Delta A) \exp(-R|Z - SA_i + TA_i^2|^{\nu}) \Omega \eta \xi$$

In equation (3), σ_o is the normalization factor. It is derived by integrating over all partial cross sections ($\sigma_i = \Sigma\sigma_{ij}$). It is slightly energy dependent and different for different target masses. The factors f(A) and f(E) are corrections factors and are applicable to products from heavy targets (with atomic number $Z_j > 30$, when ΔA is very large as in the case of fission, fragmentation, and evaporation.) The factor exp(-PΔA) describes the diminution of cross sections as the differences of target and product mass, ΔA, increases. The factor exp(-R|Z-SA+TA^2|$^\nu$) describes the distribution of cross sections for the production of various isotopes of an element of atomic number Z. The parameter Ω is related to the nuclear structure and number of ' particle-stable levels' (Book of Isotopes [37]) of a product nuclide. The factor η depends on the pairing of protons and neutrons in the product nucleus; it is larger for even-even nuclei (more stable, more abundant) than for odd-odd, odd-even, and even-odd. And the parameter ξ represents the enhancement of light evaporation products.

Equations are available to calculate the three different types of cross sections: total inelastic cross sections, elastic cross sections, and partial inelastic cross sections. The total inelastic cross sections, σ_i, permit the determination of the fraction of nuclides that survive passage in the interstellar gas. The elastic cross sections are used to calculate nuclear recoils at very low energies, when the nucleus does not break up, while partial inelastic cross sections are used when the nucleus break up. Both are used to determine the radiobiological effects and single event upsets; the amount of energy deposited by a nuclear recoil in such a small volume

is of great concern (see the radiation exposure section). The partial inelastic cross sections, σ_{ij}, give the probability of a given incident nuclide to yield a given product nuclide upon colliding with some target nucleus, e.g. with a proton (spallation).

Ionization loss through atomic collisions is the other factor in the propagation equation that must be computed to explain cosmic ray diffusion through interstellar gas. The ionization equation, $\delta/\delta E[J_i(dE/dX)_i]$, contains the stopping power of the interstellar medium, dE/dX. The stopping power depends on the composition of the ISM, the projectile charge, mass, and energy. The ionization loss is a velocity and charge dependent effect.

The propagation calculations performed in this thesis utilized the total and partial cross sections of Silberberg and Tsao with corrections, when needed, based on experimental data of Webber et al. [38].

The program used for these calculations was named PROP5EHE (Appendix B) and was revised 5 times. The original program contained a double exponential calculation for the distribution of path lengths traversed by cosmic ray primaries. The first file opened in the program, LMH59.lis (table 4,5,6; source column), is the calculated primary source composition of cosmic rays. Originally, there were five different calculated source compositions used (old S&T, old Cameron, new Cameron, new Cameron [7] with FIP effect and Wolf-Rayet contributions, and new S&T). The experimental data used in these calculations came from Simpson (table 7) [39] in the 1000-2000 MeV/nucleon range (high energy). The PROP5EHE program approximated the

Table 4. Calculated Source and Arriving Composition of Silberberg and Tsao (normalized to carbon)

Element	Source	Arriving
Li	0.0	20.35
Be	0.0	12.08
B	0.0	27.57
C	100.0	100.00
N	3.4	23.90
O	110.0	89.65
F	0.0	1.95
Ne	16.0	15.11
Na	.9	2.62
Mg	24.0	18.61
Al	2.3	2.73
Si	21.0	13.95
P	.3	.74
S	3.0	3.10
Cl	.1	.55
Ar	.9	1.74
K	.1	1.10
Ca	4.4	3.60
Sc	0.0	.43
Ti	.1	1.55
V	0.0	.78
Cr	.5	1.49
Mn	.1	.47
Fe	22.0	9.54

Table 5. Calculated Source and Arriving Composition Using Cameron's General Abundances (normalized to carbon)

Element	Source	Arriving
Li	0.0	20.97
Be	0.0	12.63
B	0.0	29.91
C	100.0	100.00
N	20.7	38.66
O	164.4	122.78
F	.01	1.47
Ne	23.2	16.95
Na	.5	1.14
Mg	9.5	7.24
Al	.8	1.06
Si	8.9	5.83
P	.1	.42
S	4.4	2.91
Cl	.04	.22
Ar	1.0	.97
K	.03	.40
Ca	2.4	1.63
Sc	0.0	.15
Ti	.02	.52
V	.002	.27
Cr	.11	.49
Mn	.10	.19
Fe	7.4	3.25

Table 6. Calculated Source and Arriving Composition Using Camerons's General Abundances with FIP and WR Contributions (normalized to carbon)

Element	Source	Arriving
Li	0.0	20.39
Be	0.0	12.12
B	0.0	27.71
C	100.0	100.00
N	8.7	25.21
O	110.2	89.64
F	.02	1.90
Ne	12.2	12.67
Na	1.8	3.25
Mg	26.8	20.55
Al	2.0	2.60
Si	22.4	14.75
P	.3	.72
S	4.1	3.65
Cl	.1	.53
Ar	2.5	2.41
K	.1	.96
Ca	3.2	2.86
Sc	.001	.39
Ti	.1	1.39
V	.01	.71
Cr	.3	1.28
Mn	.25	.49
Fe	19.9	8.61

Table 7. Experimental Arriving Composition of Simpson (normalized to carbon)

Isotope	Abundance
3Li 6	10.7143
3Li 7	9.8902
4Be 7	5.684
4Be 9	3.9585
4Be 10	.5075
5B 10	9.297
5B 11	21.693
6C 12	94.0
6C 13	6.0
7N 14	12.6454
7N 15	14.8446
8O 16	85.1904
8O 17	1.7748
8O 18	1.7748
9F 19	1.99
10Ne 20	8.3334
10Ne 21	1.7544
10Ne 22	4.5322
11Na 23	3.11
12Mg 24	11.8755
12Mg 25	3.1059
12Mg 26	3.2886
13Al 26	.0975
13Al 27	3.1525
14Si 28	12.7194
14Si 29	1.0234
14Si 30	.8772
15P 31	.77
16S 32	2.009
16S 33	.4305
16S 34	.4305
17Cl 35	.414
17Cl 36	.069
17Cl 37	.207
18Ar 36	.72
18Ar 37	.12
18Ar 38	.42
18Ar 40	.06
19K 39	.276
19K 40	.184
19K 41	.46
20Ca 40	.1328
20Ca 41	.096
20Ca 42	.48
20Ca 43	.288
20Ca 44	.288

21Sc 45	.48
22Ti 46	.798
22Ti 47	.266
22Ti 48	.266
23V 49	.201
23V 50	.134
23V 51	.335
24Cr 50	.133
24Cr 51	.133
24Cr 52	.665
24Cr 53	.1995
24Cr 54	.1995
25Mn 53	.276
25Mn 54	.184
25Mn 55	.460
26Fe 54	.6195
26Fe 55	< .6195
26Fe 56	7.965
26Fe 57	< .708
26Fe 58	< .2655

path length distribution by a series of weighed slabs, (paths in g/cm^2). The program assumes that the ISM is comprised of 100% hydrogen and propagates the primary cosmic ray source nuclei through this medium, opens up the second file, QLMH59.lis (Appendix C), to put in partial cross sections, calculates the total inelastic cross sections, and yields the calculated arriving composition at Earth.

The five revisions of the propagation program were based on of the comparison of experimental data (Simpson at 1 A.U.) and the calculated data of the arriving composition. The comparison was made using the ratio of the L (light nuclei: Li,Be,B) and M (medium nuclei: C,N,O,F) (.28) and the ratio of sub-iron (Sc,Ti,V,Cr,Mn) to iron (.49). The double exponential path length distribution originally written into the program was reduced to a pure exponential in order to agree with the new experimental data and thus proving the exponential distribution of path lengths (Fig. 17), with $\langle x \rangle = 5.4502\ g/cm^2$. Of the five source compositions used, the new S&T calculated source composition came closest to yielding the measured arriving composition, after putting it into the propagation program.

After the exponential model was introduced, a plot was constructed for comparing the experimental and calculated arriving abundances at Earth. Discrepancies were noticed at Z=4, 15, 17, and 25. The Z=4 and Z=25 discrepancies were due to the nuclear decay that was ignored in the propagation calculations. Approximately 80% of Be^{10} decays into B^{10} and most nuclei tabulated as Cr^{54} should be Mn^{54}, instead, i.e. most Mn^{54} (when stripped of electrons) has not decayed into Cr^{54}. These corrections were added by hand because the propagation

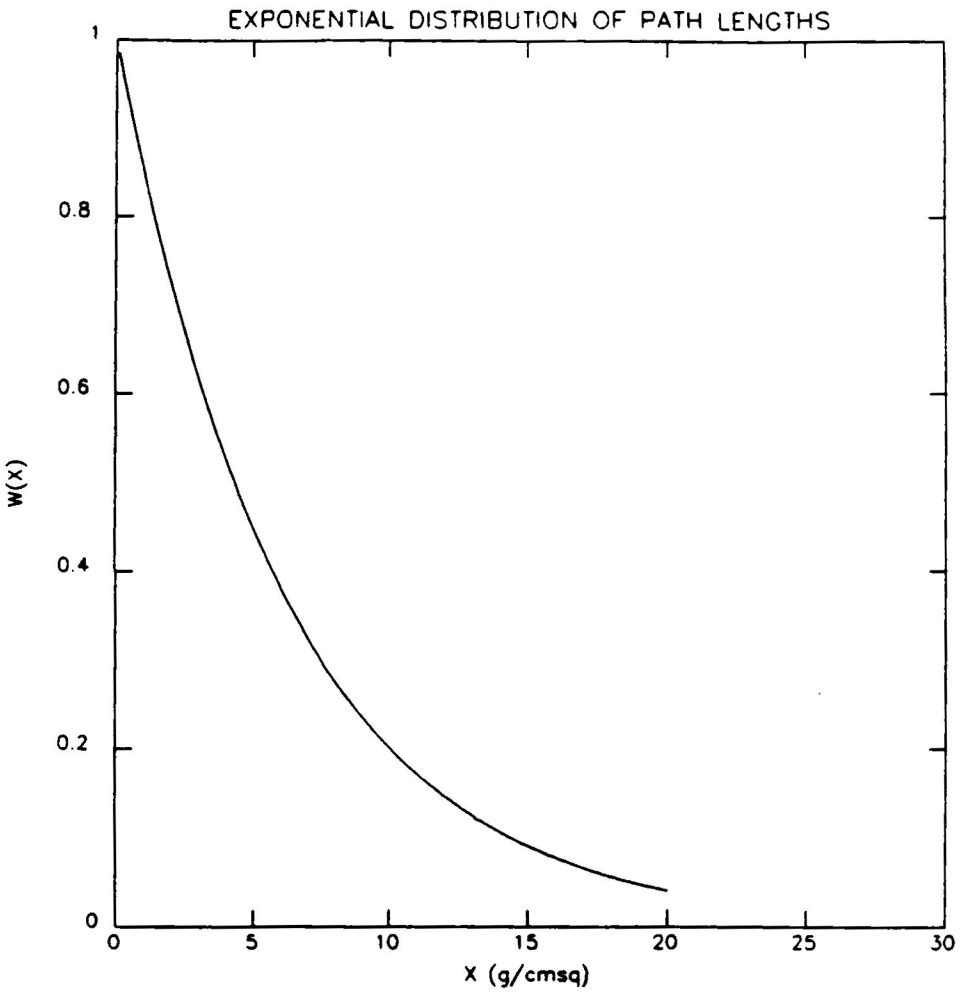

Fig. 17 Exponential Distribution of Path Lengths for Cosmic Rays

program does not account for them. The discrepancies at Z = 15 and Z = 17 were due to uncertainties in the cross section calculations used.

The Z = 15 and Z = 17 anomalies are corrected by the recently measured cross sections of Webber et al.[38]. The correction is made by assuming the proportionality of the nucleon stripping reactions (p,pn), (p,2p), (p,p3n), and (p,2p2n) for Ar^{40}, Ar^{38}, and Ar^{36} because Webber et al. did not measure the cross sections for the isotopes Ar^{36} and Ar^{38} used, but measured only Ar^{40}: $Ar^{40} \rightarrow Cl^{39}$ (Webber et al.) to $Ar^{36} \rightarrow Cl^{35}$ (Silberberg and Tsao) resulted in a 25% increase in S&T's cross section calculation, $Ar^{40} \rightarrow Cl^{37}$ to $Ar^{38} \rightarrow Cl^{35}$ resulted in a 100% increase, $Ar^{40} \rightarrow Cl^{39}$ to $Ar^{38} \rightarrow Cl^{37}$ resulted in a 50% increase, and $S^{32} \rightarrow P^{31}$ was measured directly by Webber et al. and resulted in a 25% increase in the calculated cross sections of Silberberg and Tsao.

Figure 18a illustrates the experimental vs. the measured arriving abundances at Earth after the anomalies at Z = 4, 15, 17, and 25 were corrected. Figure 18b presents the same comparison but on a linear, linear scale to show the higher abundance of C and O. Figures 19a and 19b show the FIP effect and the Wolf-Rayet contribution [40]. Table 8 lists the factors which contribute to these effects.

The remaining small discrepancies illustrated in figure 18a may be attributed to measurement errors in the experiments, to further errors in the cross section calculations, and to the assumption that the ISM is made up of 100% hydrogen ($\simeq$ 93% hydrogen and $\simeq$ 7% helium).

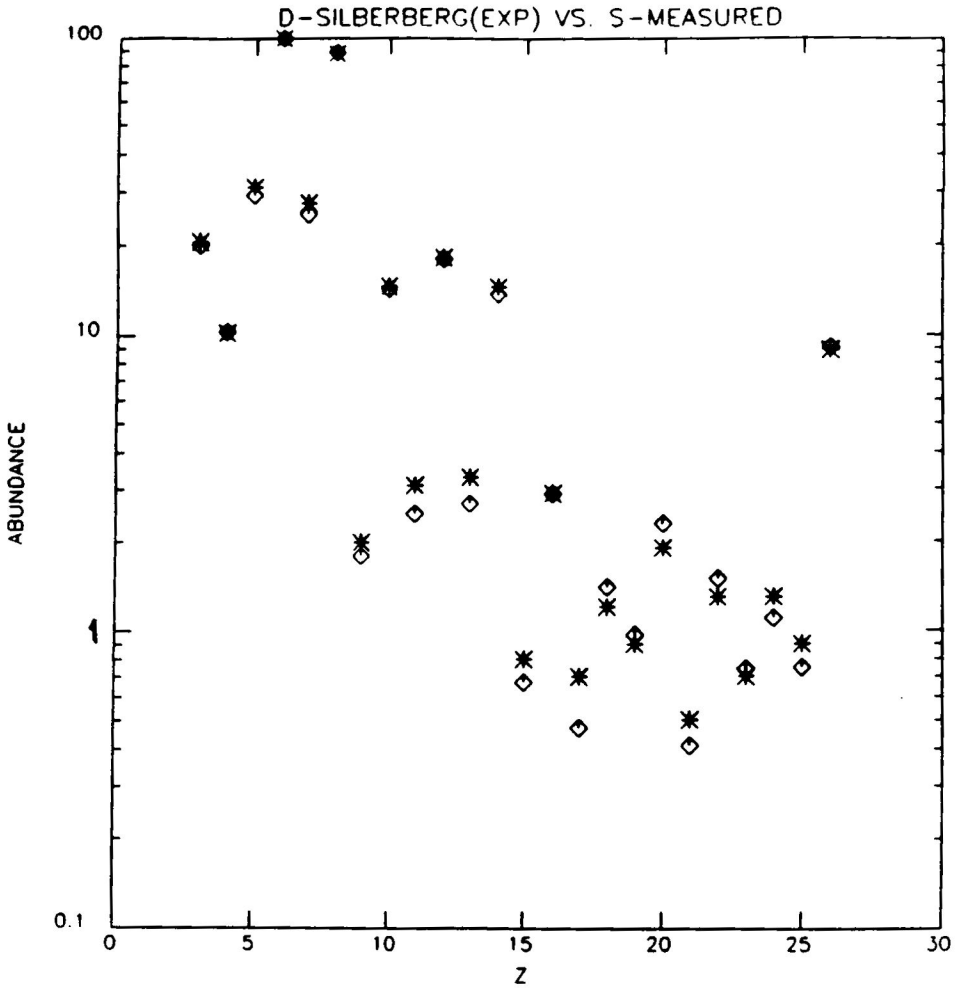

Fig. 18a Experimental (star) vs. Calculated (diamond)

Arriving Abundances on a Log-Linear Scale

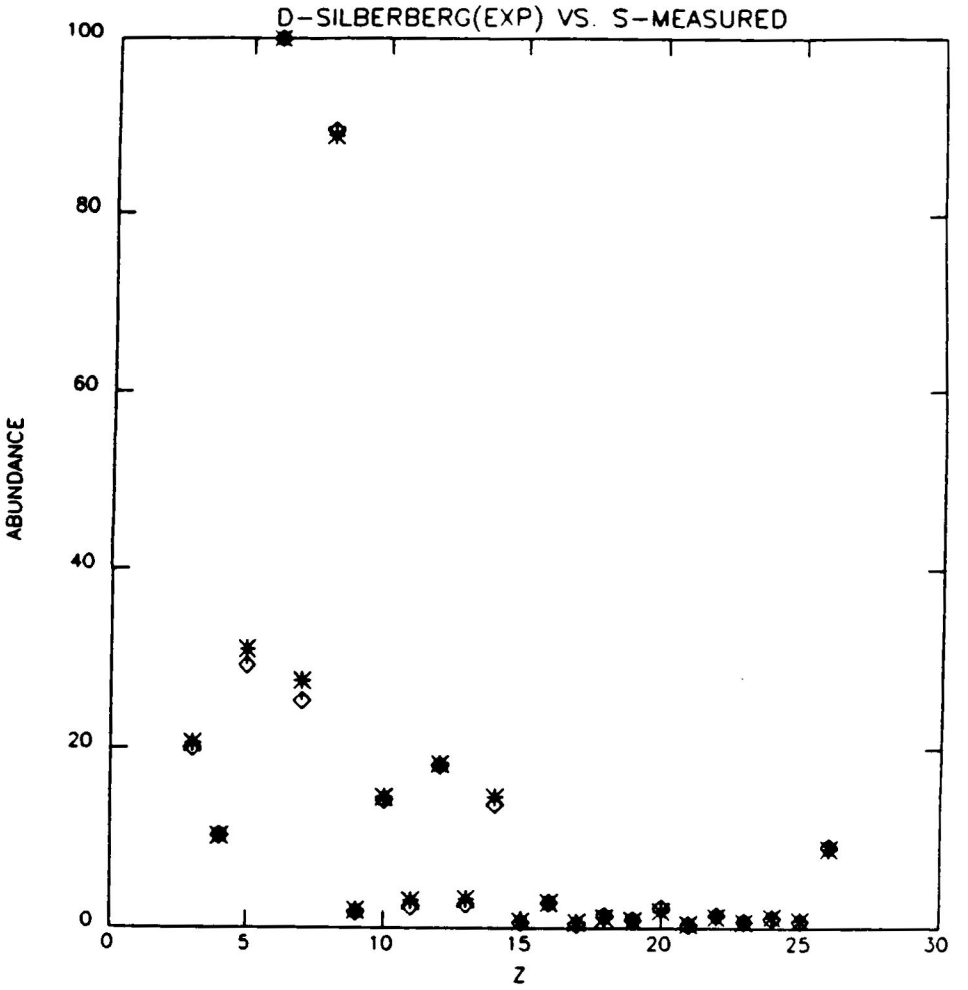

Fig. 18b Experimental (star) vs. Calculated (diamond)
Arriving Abundances on a Linear-Linear Scale

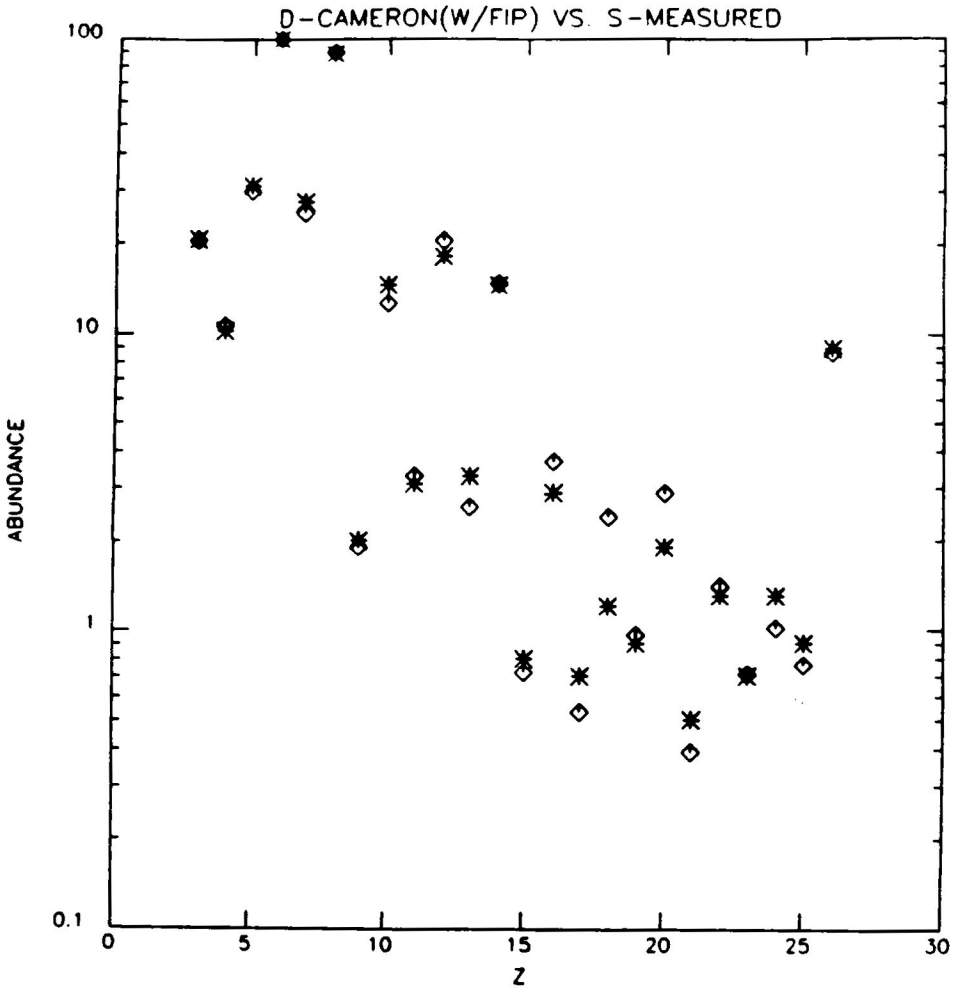

Fig. 19a Arriving Abundances Calculated with Cameron's Source Abundances with FIP and WR Contributions

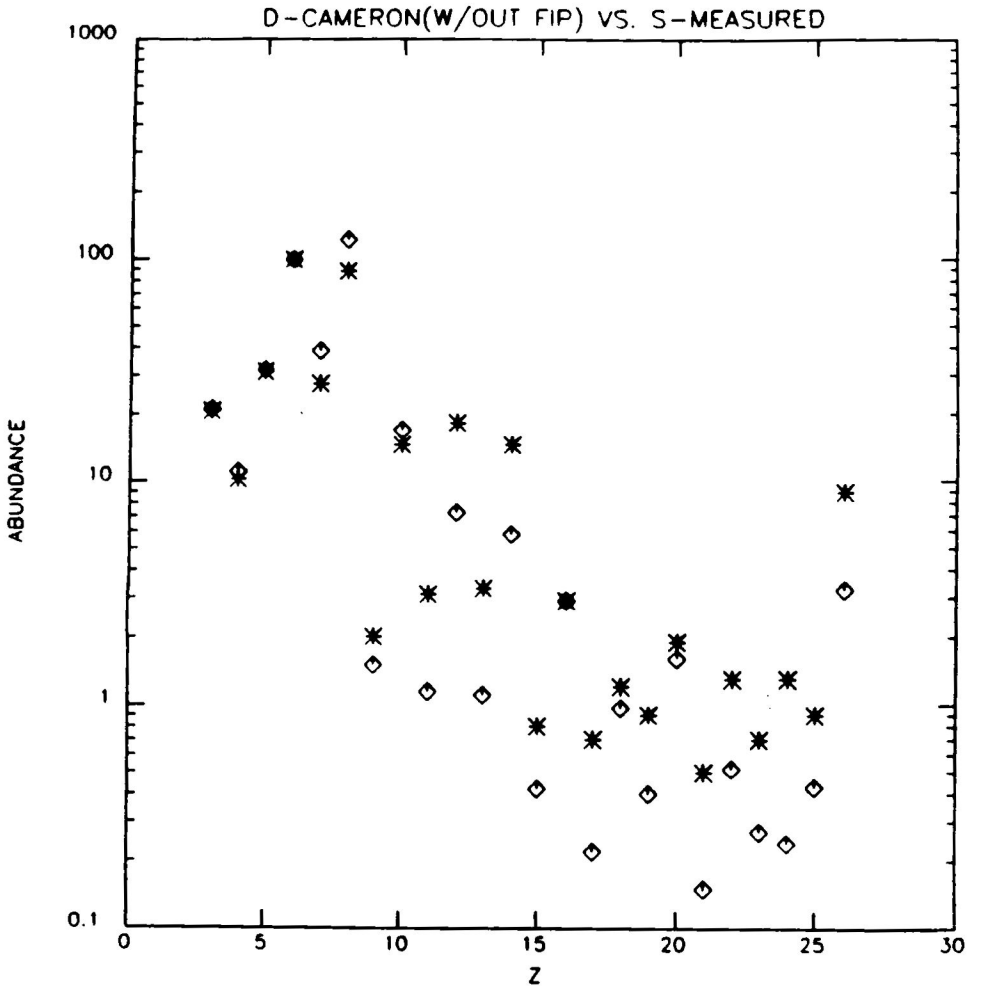

Fig. 19b Arriving Abundances Calculated with Cameron's Source Abundances without FIP and WR Contributions

Table 8. FIP and Wolf-Rayet Contributions to Abundances

12C	* 1/6(FIP) * 2.4(WR)
13C	* 1/6(FIP)
14N	* 1/6(FIP)
15N	* 1/6(FIP)
16O	* 1/6(FIP) * 1.6(WR)
17O	* 1/6(FIP)
18O	* 1/6(FIP)
20Ne	* 1/6(FIP)
21Ne	* 1/6(FIP) * 2.0(WR)
22Ne	* 1/6(FIP) * 3.3(WR)
23Na	* 1.4(WR)
25Mg	* 1.6(WR)
26Mg	* 1.5(WR)
32S	* 1/3(partial FIP)

Nuclear Recoils

Elastic and partial inelastic cross sections aid in the interpretation of nuclear recoils. An atomic nucleus recoils because of (1) a collision with a nucleon or a nucleus, or because of (2) the emission of particles from it. The direction and magnitude of the recoil are determined by the conservation of energy and momentum. Nuclear recoils are of such great importance because they deposit large amounts of energy in small volumes (biological damage to tissue and SEUs).

The calculations that were performed for such reactions permitted a comparison of the experimental data of Kwiatkowski et al. [41] and the theoretical predictions of HETC (High-Energy Transport Code [42]). The experimental data were energy spectra of fragments with A = 7, 16, and 22 produced in the 180 MeV p+Al^{27} reactions. The experimental data were collected at three different angles: 20°, 40°, and 70° degrees. The theoretical data were obtained by integrating over all angles. The experimental data were weighted according to the solid angles; a single straight-line approximation was found to fit the nuclear recoil energy spectrum summed over three solid angle intervals. This straight-line approximation was computed for A = 7, 16, and 22 (Fig. 20). The calculated equation for the energy spectrum of nuclear recoils was the straight line, on a semi-log scale, of the form $\exp(-E/E_o)$, where $E_o=1.6+.305(A_t-A)$ MeV.

Comparisons could only be made for A=16 and A=22 because data on A=7 had not been computed by HETC. A statistical average over the

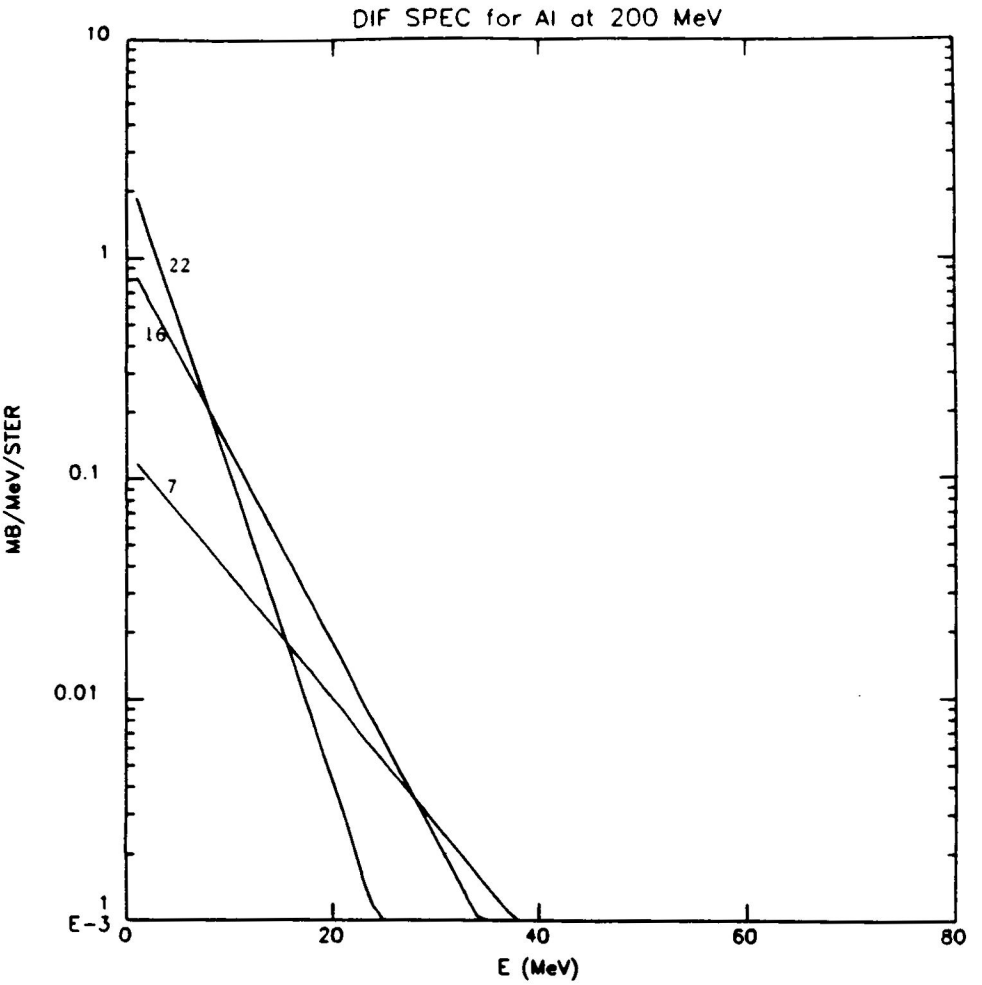

Fig. 20 Straight Line Approximation of Nuclear Recoil Energy Spectrum for A = 7, 16, and 22

isotopes of Ne had to be made because the experimental data was a function of atomic mass A = 22 while the HETC calculations were a function of atomic number. The program for this comparison (Appendix B) opens two files, A1200.0 and A1200.Ne, which contain the atomic mass, charge, and energy distribution (all calculated by HETC). And QA(I) in the program is the cross section normalization computed by Silberberg and Tsao (for Ne, with <A> = 20.4, σ_o=30.8 and for A=16, σ_o=8.1).

The comparison showed that the HETC calculations near recoil energies of 15 MeV deviated from the experimental data by a factor of 5 (Figs. 21a and 21b). A correction factor of exp(.03E) was calculated for HETC and inserted into the program. Figures 22a and 22b show the comparison of the experimental data and the HETC calculations that includes the new correction factor. Any remaining deviations within this comparison may result from the straight line approximation calculation for the experimental data.

The radiation transport calculation, comparisons with the cross section measurements of Webber et al., and the nuclear recoil calculations made in this thesis uncovered some systematic errors in cross section calculations, and in HETC-generated nuclear recoil energy spectra. The radiation transport calculations comprised a list of elements and isotopes for the cosmic ray source composition, derived a near-Earth cosmic-ray composition that agrees well with observations, and gave the energy spectra of the particularly damaging nuclear recoils. These calculations will serve as a model for future calculations.

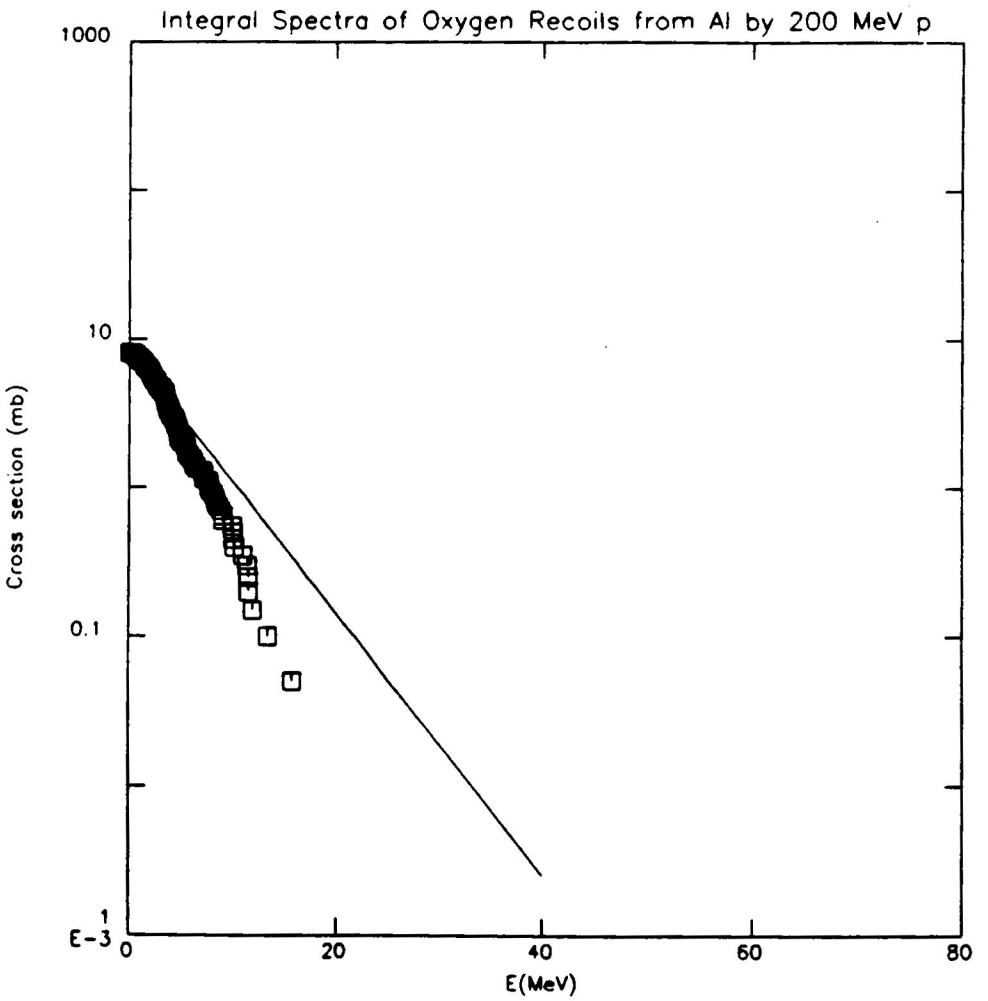

Fig. 21a HETC-Calculated vs. Measured Nuclear Recoil Energy Spectrum for A = 16

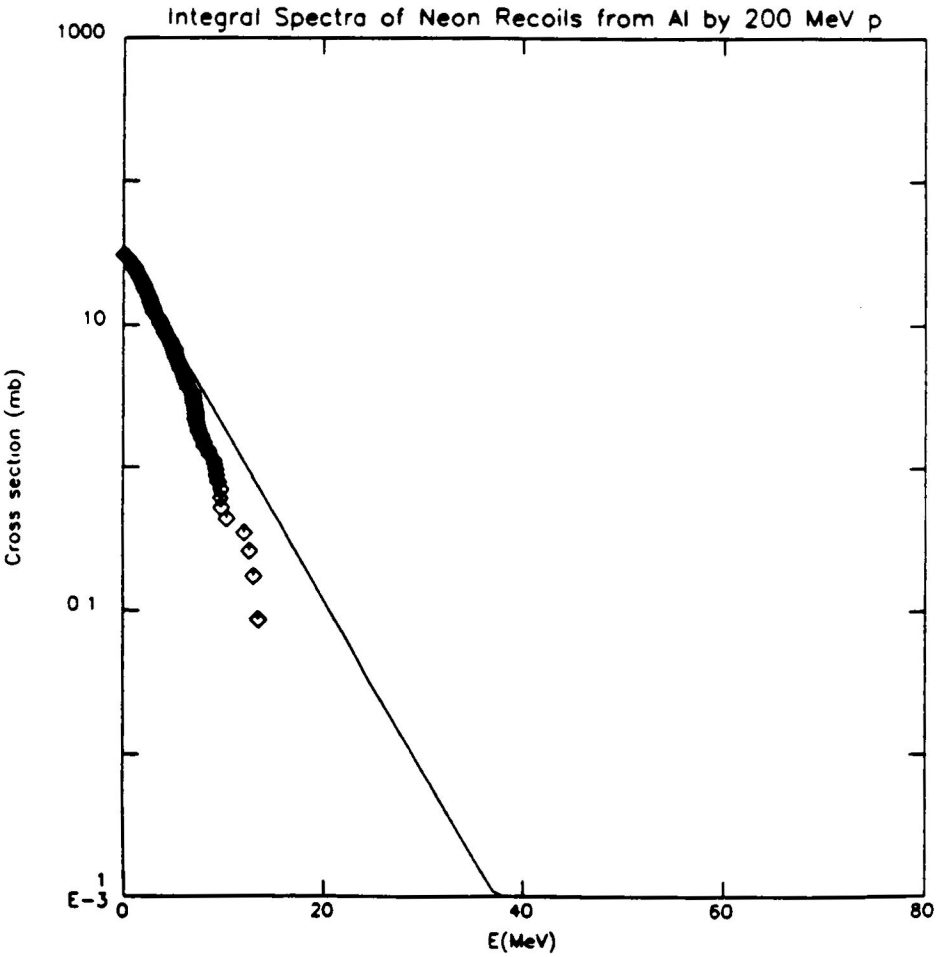

Fig. 21b HETC-Calculated vs. Measured Nuclear Recoil Energy Spectrum for A = 22

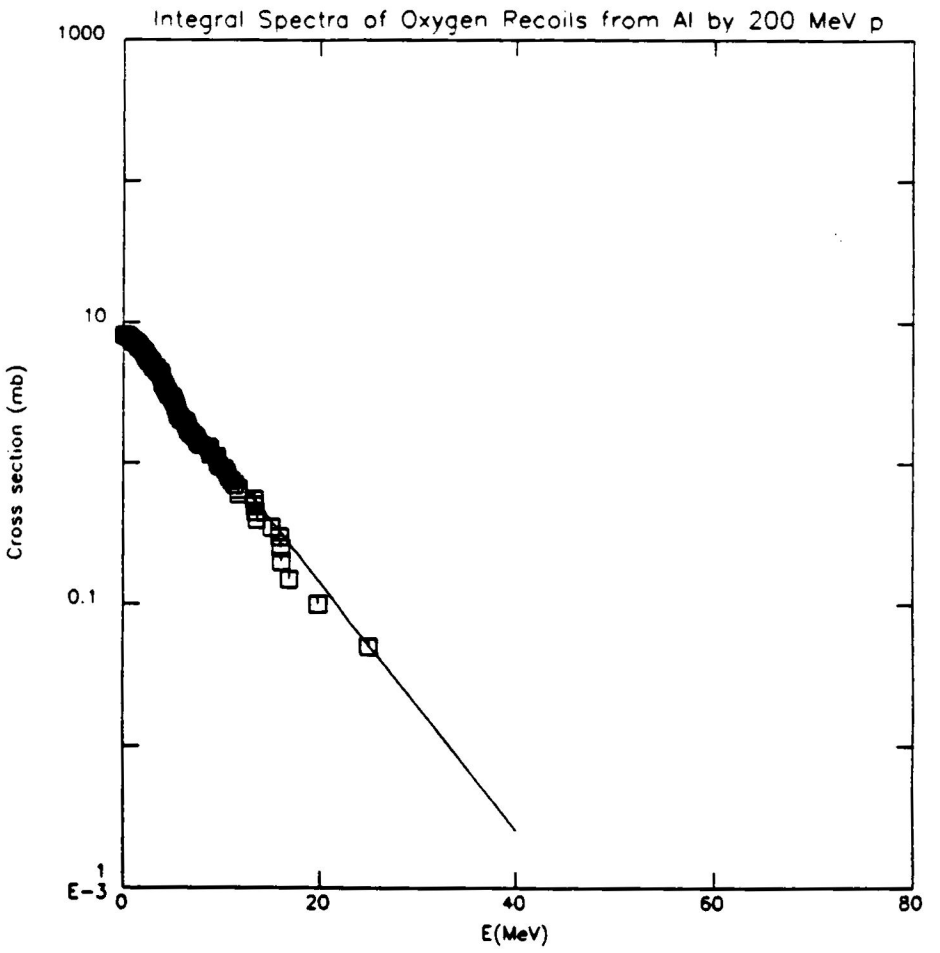

Fig. 22a HETC vs. Measured Nuclear Recoil Energy Spectrum for A = 16 with Correction Factor

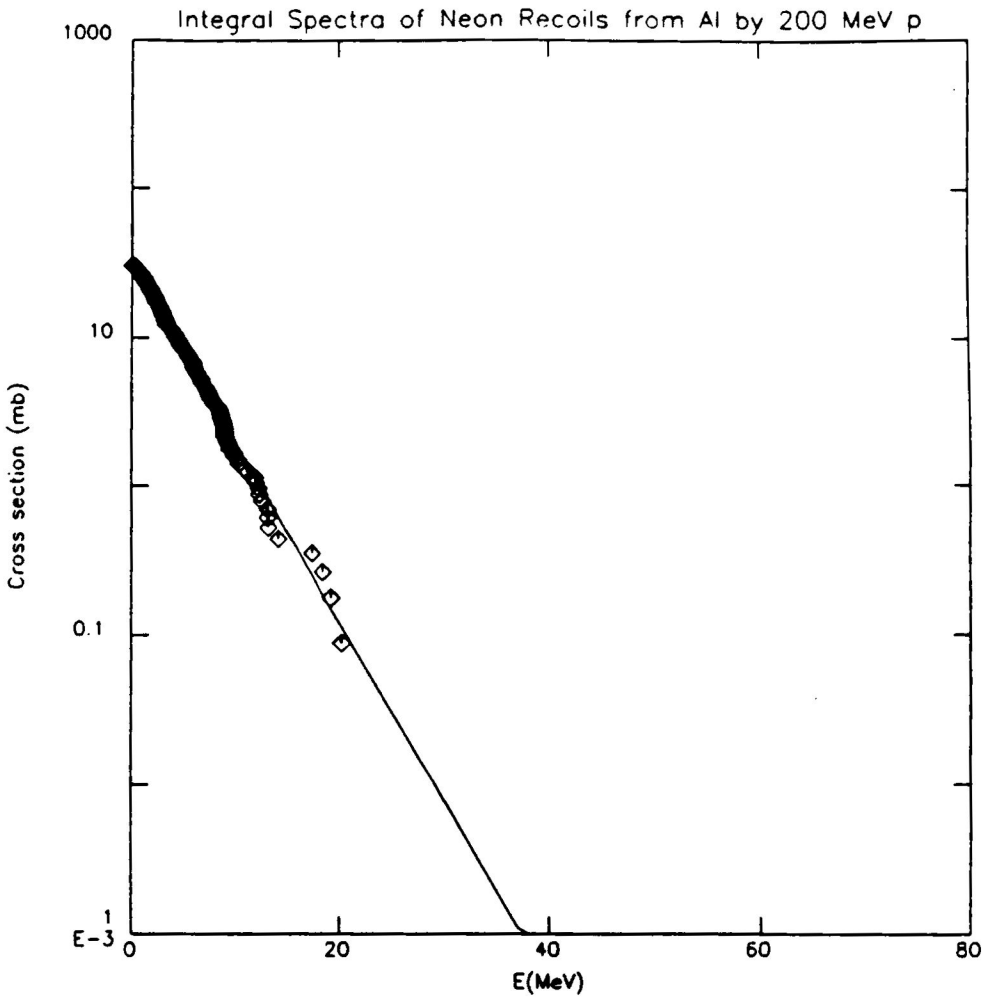

Fig. 22b HETC vs. Measured Nuclear Recoil Energy Spectrum for A = 22 with Correction Factor

IV. RADIATION EXPOSURE

In the preceding sections, this thesis outlined the environment in which cosmic rays exist, and their nuclear interactions. Because of space exploration, spacecrafts and satellites have to operate in this environment. And because cosmic-ray primaries possess such high energies, cosmic-ray secondaries and elementary particles like muons reach down to sea-level, and even into deep mines. In either case, possible radiation hazards (upsets in spacecraft electronics or high radiation dose to human tissue) make prognoses of cosmic-ray fluxes and interactions a problem of practical importance.

Biological Damage To Humans

Radiation of various forms (natural and man-made) is a normal part of man's natural environment, but only in the last seventy-five years has he been aware of the presence of penetrating ionizing radiation. Appropriate protection criteria will differ for individuals engaged in various classes of radiation work, for individuals in the general population, and for special population groups.

Cosmic radiation is a form of natural radiation that makes up ~ 8% of all natural radiation at sea-level and much more at the top of the atmosphere as discussed below. This means that there is no way to avoid some exposure, but there are ways to limit the amount of exposure. Every second approximately 10,000 relativistic charged particles enter the atmosphere from outer space and hit an area of 1 m^2

near the top of the Earth's atmosphere. Due to geomagnetic shielding this flux is about 20 times less near the Earth's equator. Without the 1000 g/cm^2 of air mass between the Earth's surface at sea-level and the cosmic radiation field in interplanetary space, the absorbed dose would be about 100 times greater. For dose equivalent, it is 1000 times more.

Biological effects vary from one kind of particle to another (Fig. 23). The rate at which charged particles deposit energy for each unit path length is proportional to their ionic charge squared; thus an iron nucleus deposits energy at a rate that is 26*26 or 676 times that of a proton having the same velocity. The rate of energy deposition is also energy dependent, e.g. the rate dE/dX is about 200 times greater for protons at energies of 0.1 MeV than at 1000 MeV. Furthermore, the biological damage increases faster by a factor Q than the rate of ionization dE/dX. 'Q' is defined as the "quality factor" for equivalent radiation damage. Thus the "dose equivalent" is Q * "absorbed dose". Figure 24 shows the relative contributions of various charge groups to the dose equivalent, which is expressed in units of "rem" (Q*dose in "rad" = dose in rem). Note that heavy ions are the most important component of the dose in the upper atmosphere, i.e. at depths down to about a few tens of g/cm^2, i.e. down to a couple of percent of the atmospheric thickness of about 1000 g/cm^2.

Guidelines for radiation protection have been developed by the National Council on Radiation Protection and Measurements (NCRP) and International Commission on Radiological Protection (ICRP). The annual dose, set by these two protection agencies, for the general public is .5 rem for stochastic effects and 5 rem for non-stochastic effects.

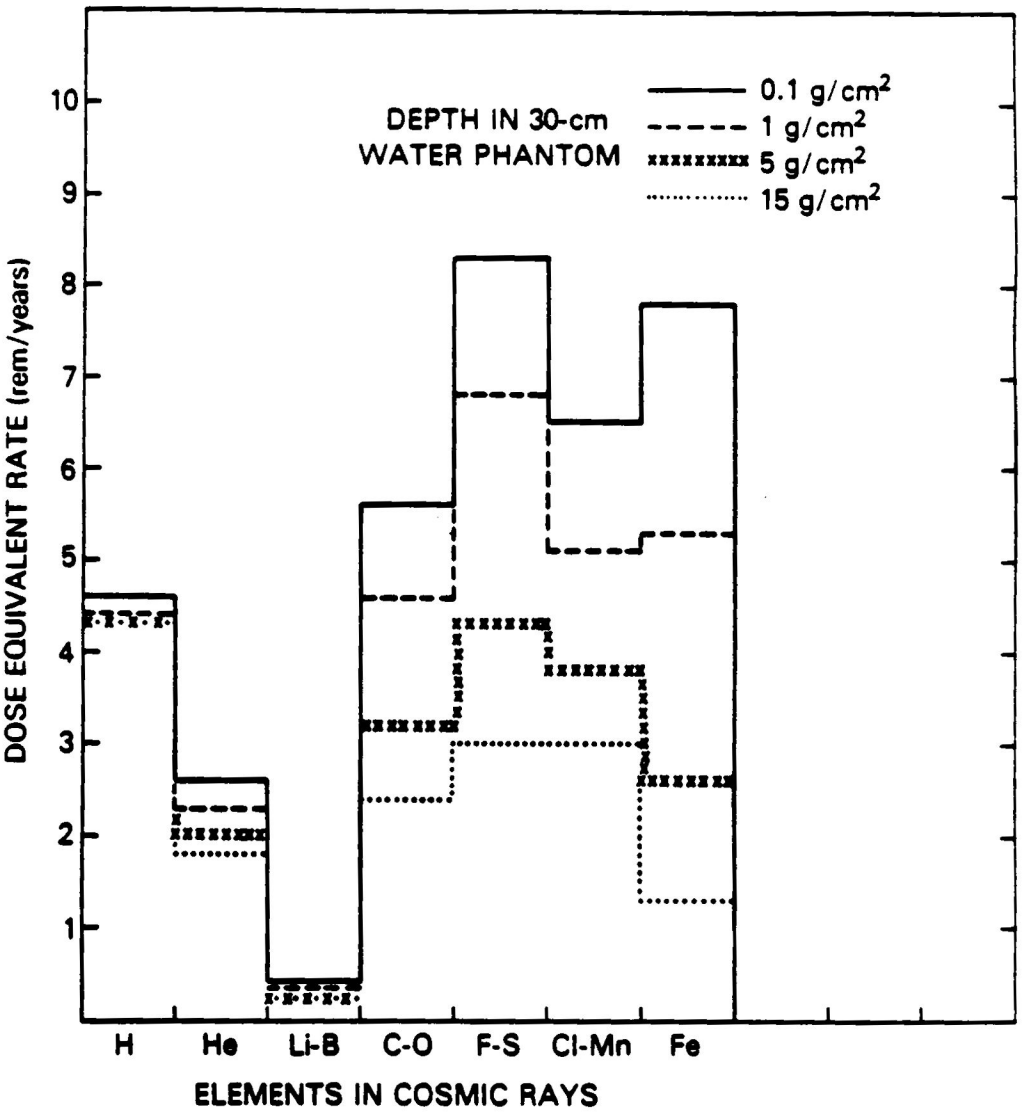

Fig. 23 Biological Effects of Individual Particles

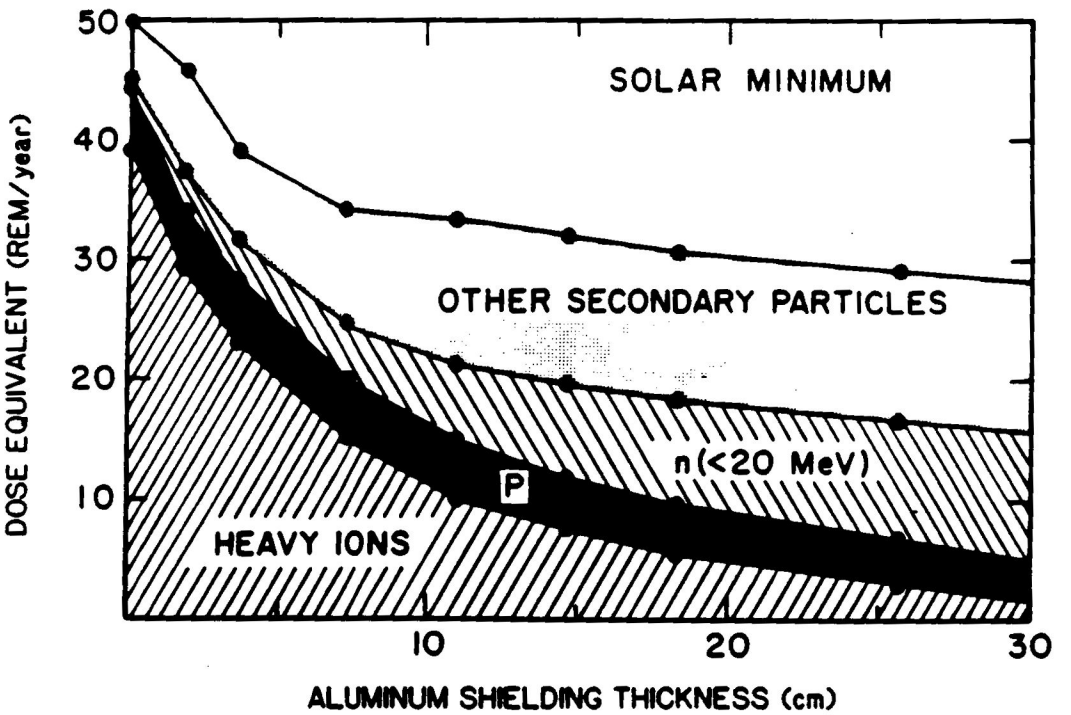

Fig. 24 Contributions of Various Charge Groups to Dose Equivalent

Since radiation hazards are also a function of altitude as well as latitude, the cosmic-ray dose rates to which aircraft passengers are exposed are considerably higher than the typical environmental radiation dose rates at ground altitudes. To keep the dose less than .5 rem/year, the crew and passengers on supersonic flights may spend a maximum of 14 hrs/wk at flight altitude with the quality factor of 1971 for neutrons (7.8) corresponding to 6 rem/year. With the new quality factor of 1986 for neutrons (13.7) corresponding to 11 rem/year, a crew member or passenger can spend a maximum of 7.6 hrs/wk. The annual dose for the flight crew could be higher, but is not to exceed that of radiation workers, 5 rem/year. The above quality factors for neutrons were derived in this thesis by integrating the energy dependence of the quality factor over the energy spectrum of the secondary neutrons.

As altitudes exceed the magnetosphere, the cosmic-ray environment becomes more hazardous because the Earth's magnetic field no longer provides protection. However, the trapped protons in the Van Allen radiation belts are most intense in the magnetosphere, and dominate the radiation dose there. Radiation exposures in space and the upper atmosphere are due to various sources: galactic cosmic rays, solar flare particles, trapped radiation, and secondary particles. The personnel working in such an environment, mainly astronauts, require special considerations for protection to see that the NCRP and ICRP's radiation dose limits, 13 rem/month; 38 rem/year and 200 rem/career, are met.

Since heavy cosmic-ray nuclei contribute a large portion of the dose equivalent during space flights, and since their nuclear

interaction mean free paths in materials are short, it is essential to carry out radiation propagation calculations with accurate spallation cross sections. Partial inelastic nuclear cross sections of Silberberg and Tsao are utilized in the radiation transport calculations. The latter includes separately all the isotopes of cosmic rays (matrix method of Letaw et al. [43]). The understanding of the transport of high-energy nuclei in materials helps to define the shielding requirements; thus leads to defining structures and procedures for protecting astronauts from space radiation.

There is a significant difference between cosmic rays and solar flare particles in the relative contribution of heavy nuclei ($Z \geq 6$) to the total dose equivalent as a function of shielding. The heavy nuclei in cosmic rays dominate to about 8 g/cm^2 and contribute significantly to about 15 g/cm^2 in material like Al [44]. The relative contribution of heavy nuclei in solar flare particles is attenuated much more rapidly because their energy spectrum is steeper, hence their ranges are shorter. As seen in figure 7 , the outflowing solar wind modulates the cosmic-ray intensity so that it is anti-correlated with the general level of solar activity. Hence the times when the cosmic-ray flux is most reduced, the risk of having a solar flare is largest. Some solar energetic particle events can deliver more energetic particles in a few hours than cosmic rays could deliver in 10 years- enough for a lethal dose under light shielding. Trapped radiation is most intense at altitudes from 1000 - 30,000 km with peaks at 3000 km and 22,000 km [45].

If a future spacecraft moves with a velocity close to that of light, a new hazard develops. The stationary interstellar gas looks in the frame of the rocket like a beam of relativistic cosmic-ray nuclei. Using the interstellar gas density of 1 atom/cm^3, and distance nearly $3X10^{10}$ cm traversed per second, and assuming that $3X10^7$ relativistic protons/cm^2 deposit a dose of 1 rad and slightly over 1 rem, a dose equivalent of 1000 rem/sec can be calculated. And in .35 seconds the dose would be lethal. Such a space craft would need a stripping foil that ionizes the atoms and a superconducting magnet that bends away ions [Appendix A].

The free space environment has the full intensity of cosmic radiation in the vicinity of the Earth. The lunar surface is shielded from cosmic radiation over one hemisphere by the moon itself. Mars has a thin atmosphere of CO_2 which provides some shielding to astronauts on the martian surface.

With such missions as the Manned Mars Mission [46], the exploration of Venus and the moon, shielding requirements are needed in addition to the self-shielding environment of these planets. Silberberg et al. have performed calculations that yield these shielding requirements. Figures 25a and 25b shows the LET (linear energy transfer) integral distributions of the dose-equivalent rate (rem/year) of cosmic rays at depths of 0.1, 1.0, 5.0, and 15.0 cm within a 30-cm diameter water sphere, which is commonly used to represent the human body. The cosmic-ray flux at solar minimum outside the Earth's magnetosphere is unshielded in (a) and shielded by 4 g/cm^2 Al in (b). Nuclear interactions result in a buildup of a significant

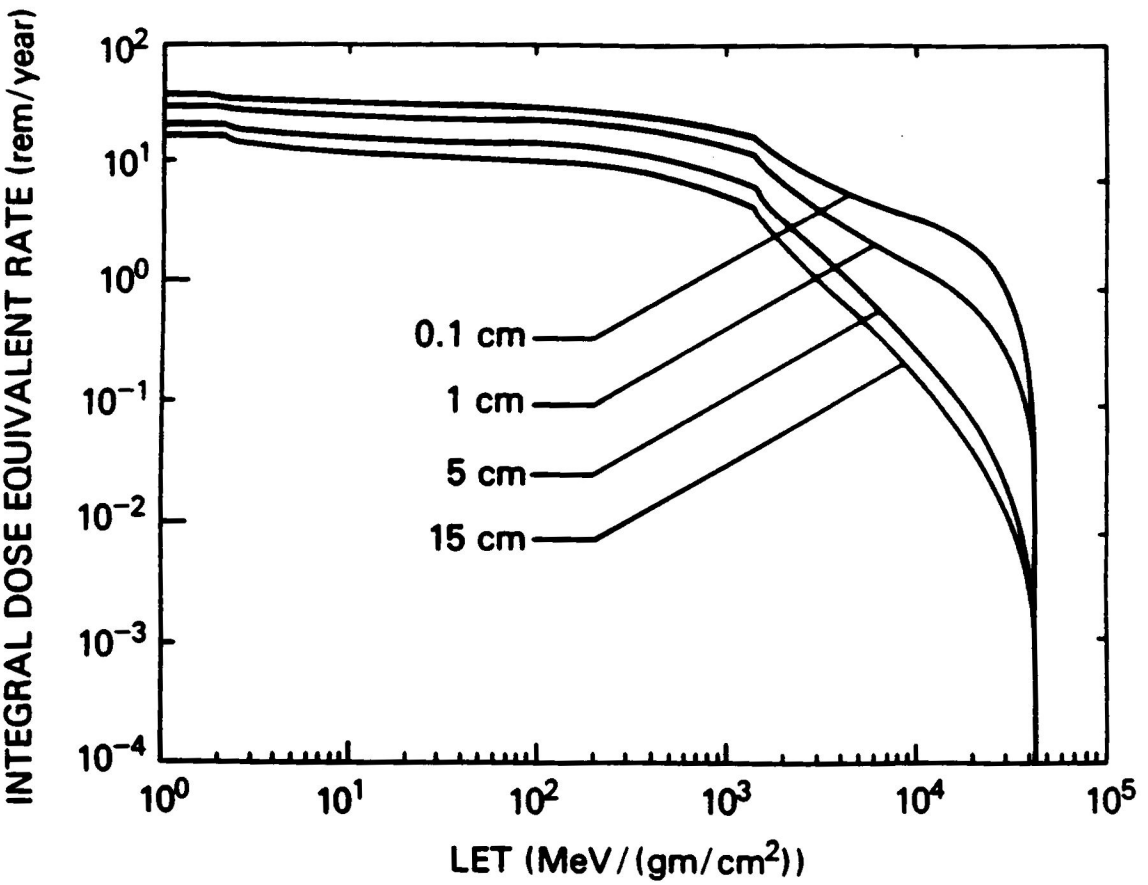

Fig. 25a Unshielded LET Integral Distribution of Cosmic Rays at Various Depths in a Water Sphere

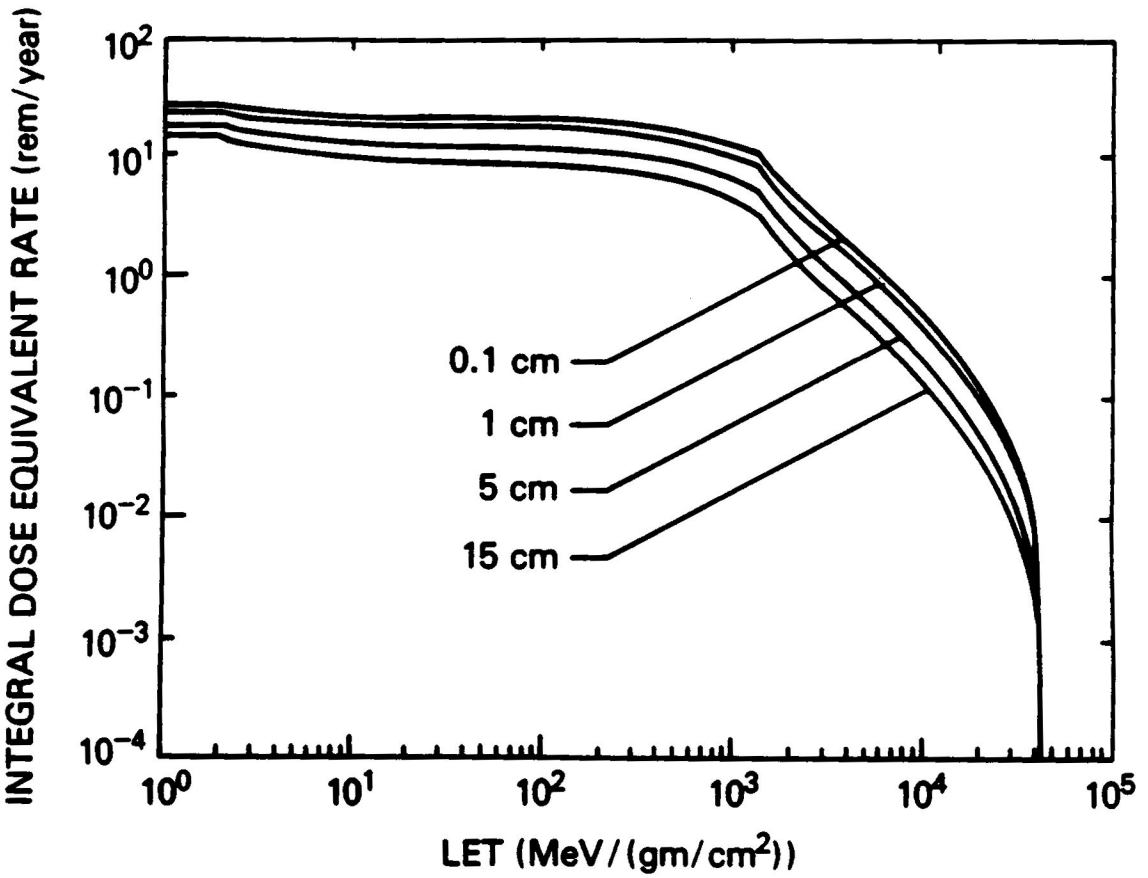

Fig. 25b Shielded LET Integral Distribution of Cosmic Rays at Various Depths in a Water Sphere

quantity of neutrons, which have a high biological effectiveness. Figure 26 shows a comparison of the annual dose equivalent due to cosmic-ray nuclei and secondary neutrons, as a function of depth in lunar material. Note that to reduce the dose to 5 rem/year (the tolerance limit for radiation workers) requires a shielding of over 400 g/cm^2 of lunar soil, i.e. a lunar habitat has to be covered by about 2 meters of lunar soil, and the work periods on the lunar surface have to be restricted to 30 hours (20% of a week) or less per week. The radiation dose equivalent as a function of aluminum shielding depth, as calculated by Letaw et al.[47], is shown in figure 27. Various shielding strategies can be conceived which would limit the production of secondary particles and absorb neutrons (Fig. 28). In particular, hydrogen-rich materials like water (or methane) is a much better shield than aluminum because it yields fewer neutrons, is more effective at fragmenting and slowing down heavy ions, and is an efficient neutron moderator. Thus the required drinking and washing supply of water on long-duration space flights also will provide radiation shielding in an appropriate geometric configuration.

Single Event Upsets In Electronic Components

The radiation environment outside the Earth's magnetic field affects not only people, but electronic systems as well. The high-intensity trapped protons in the magnetosphere and neutrons produced by them can generate highly ionizing nuclear recoils that also affect electronic systems. Higher energy cosmic rays penetrate the

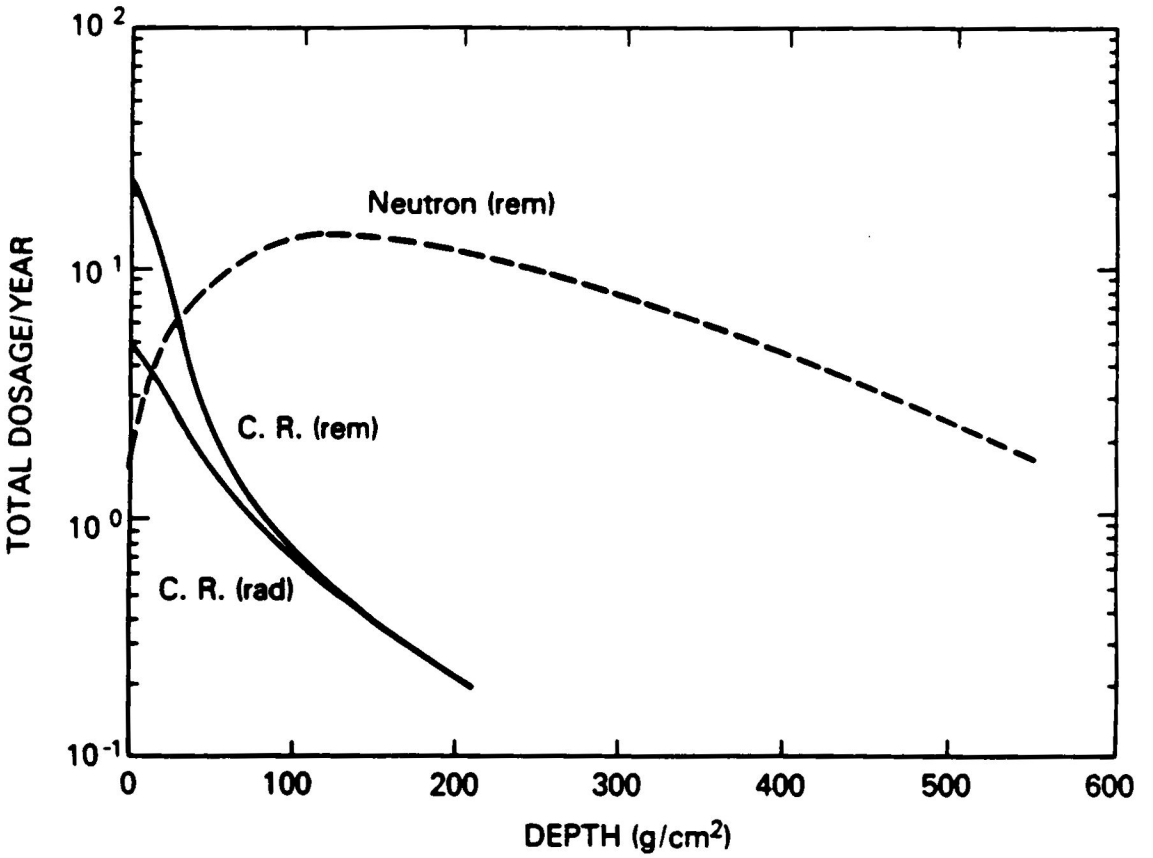

Fig. 26 Annual Dose Equivalent due to Cosmic Ray Nuclei and Secondary Neutrons

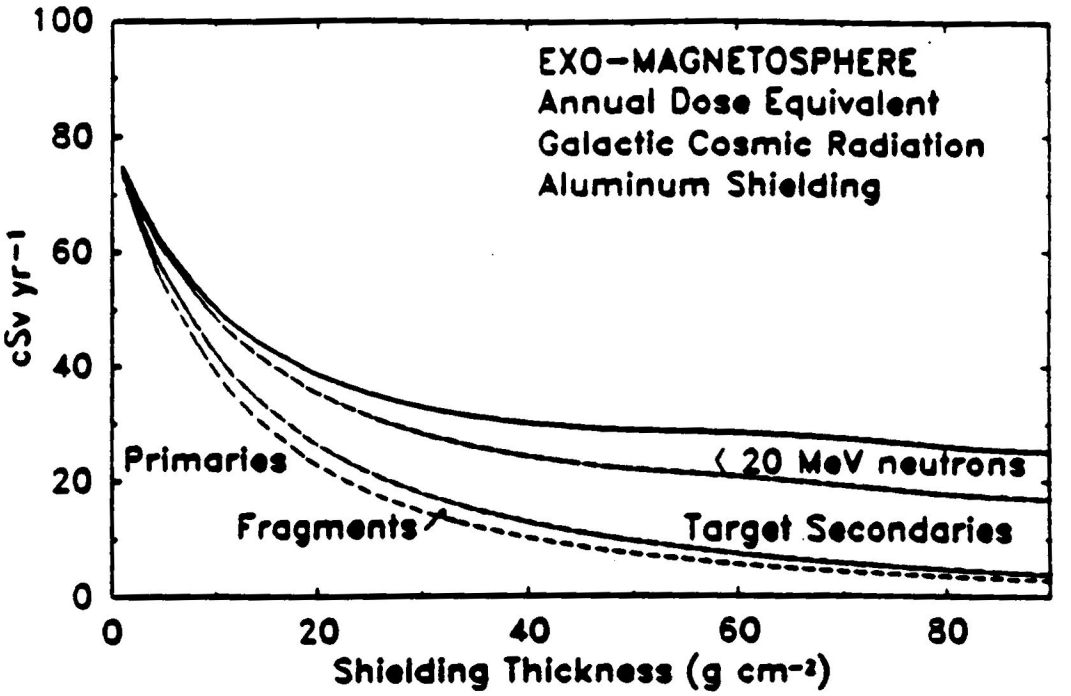

Fig. 27 Dose Equivalent vs. Aluminum Shielding

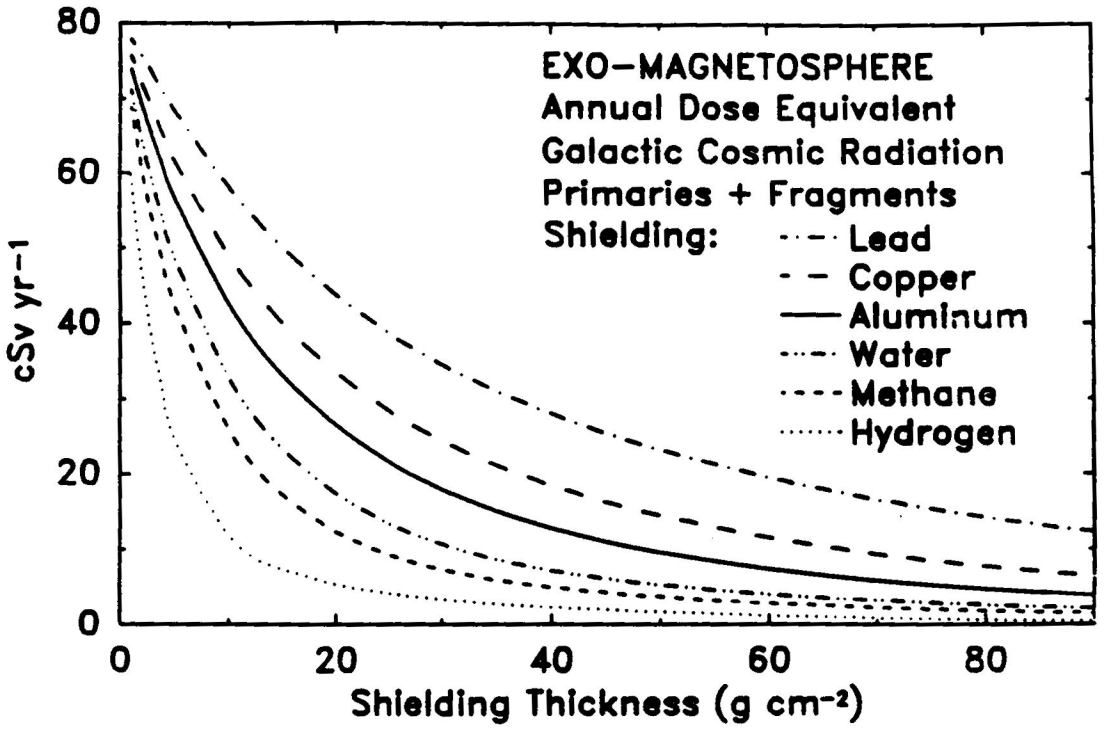

Fig. 28 Various Shielding Strategies

magnetosphere and produce electronic malfunctions in the upper atmosphere. Electronic components are affected by the total radiation dose they have accumulated. This radiation produces damage due to charge deposition, changes in conductivity or shifts in device threshold that cause a malfunction of the electronic circuit. There are two types of malfunctions or failures: soft fails, in which there is a spontaneous, temporary change in codes or a sudden stop and hard fails, in which the electronic circuit must be replaced. Soft fails occur more frequently than hard fails because of the energy required to produce each. For this reason, soft fails will be addressed in this thesis. And silicon will be the electronic component referred to because most electronic circuits are fabricated of it.

To produce computer code errors, cosmic rays, along with other sources of radiation, must interact within the silicon crystal either by ionization energy loss of a heavy cosmic-ray nucleus like iron, or by producing a moving charged particle that generates a burst of electron-hole pairs of sufficient quantity and density to affect electronic circuit components. Only certain types of particle interactions with silicon semiconductors produce electronic bursts that can affect electronic circuits: ionization wakes along the path of the particles, recoiling silicon from close collisions, and nuclear fragmentation of silicon. There is a threshold, a critical charge (the number of free electron-hole pairs necessary in the neighborhood of a junction to cause an upset), that must be liberated by the ionizing particle in a very short pathlength. Below this Q_C, soft errors do not occur. The properties of nuclear recoils and ionization losses were

defined in the section on calculations. Figure 29 illustrates the burst generation rate as a function of the neutron energy for various recoil energies E_b. The burst generation rate 'b' or charge deposition by nuclear recoil in a chip was adopted from Ziegler and Lanford [48] and was modified by Silberberg et al. [49] by including the energy spectrum of the residual nuclei induced by spallation.

Shielding against cosmic-ray-induced upsets is difficult because cosmic rays are highly penetrating and have measurable fluxes at extremely high energies. Shielding depends on specific mission requirements (cosmic-ray flux has an altitude and latitude dependence). The latitude dependence of the flux can be determined from figure 30. Cosmic rays with rigidities below the cutoff rigidity (given in units of GV/c in Figure 30) are deflected by the Earth's magnetic field. The upset rate also depends on the depth (neutrons are extraordinarily penetrating due to the absence of ionization losses; atmospheric shielding acts as a generator of neutrons which in turn generate nuclear recoils), and device sensitivity and orientation (the more compact, i.e. with small components, and lower power a device is made, the more sensitive it becomes to cosmic rays). The CREME programs of Adams et al. [6] are a group of Fortran routines that permit scientists to calculate differential and integral energy spectra of cosmic rays incident on the electronics inside a spacecraft in any Earth orbit and the SEU rates that result. LET spectra are then converted into upsets vs. critical charge (Figs. 31a and 31b).

To calculate the upsets/day in microelectronic computer components due to neutron generated recoils at aircraft altitudes of

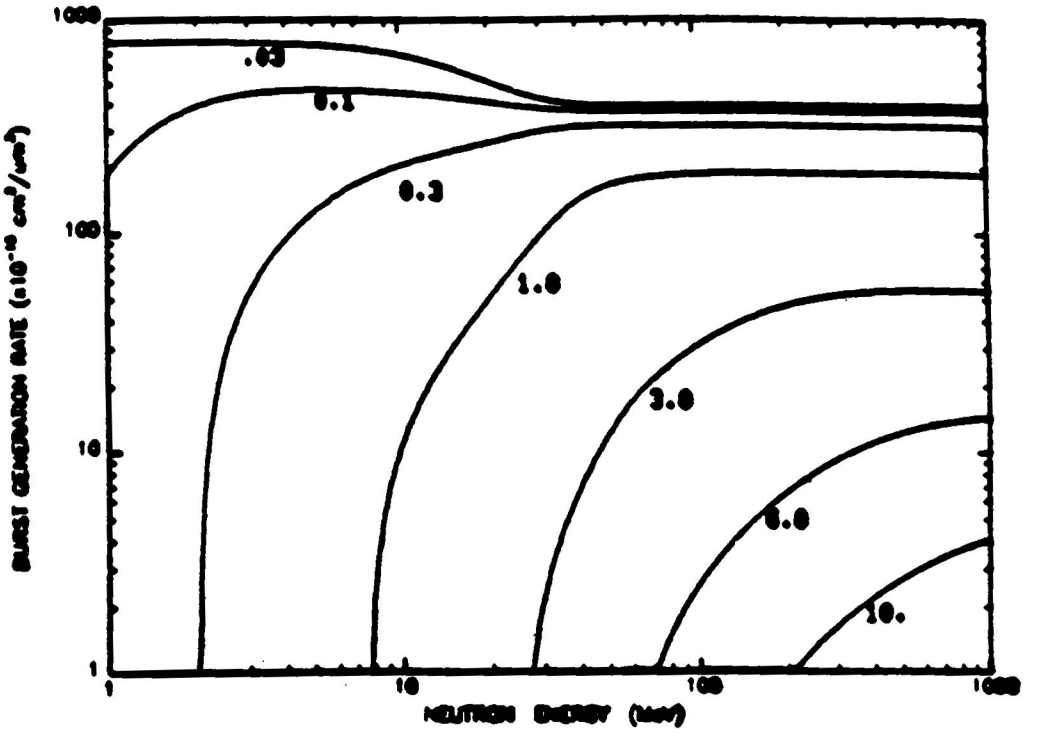

Fig. 29 Burst Generation Rate vs. Neutron Energy

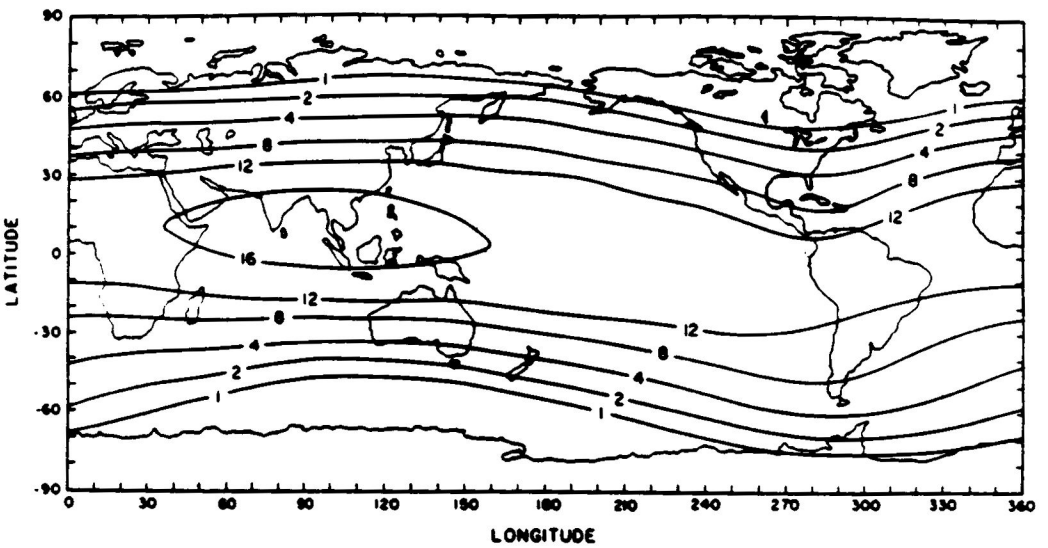

Fig. 30 Cutoff Rigidity (units of GV/c)

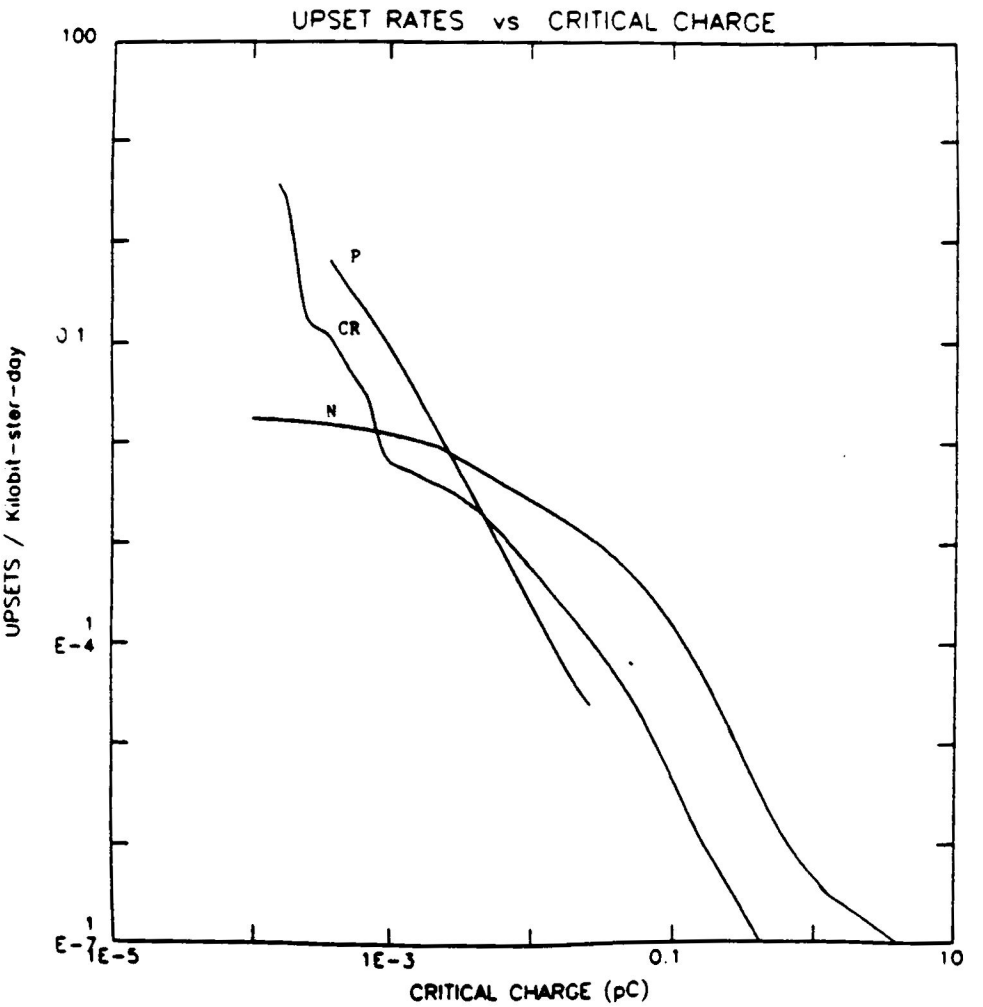

Fig. 31a Upsets vs. Critical Charge for p, n, and Cosmic Rays

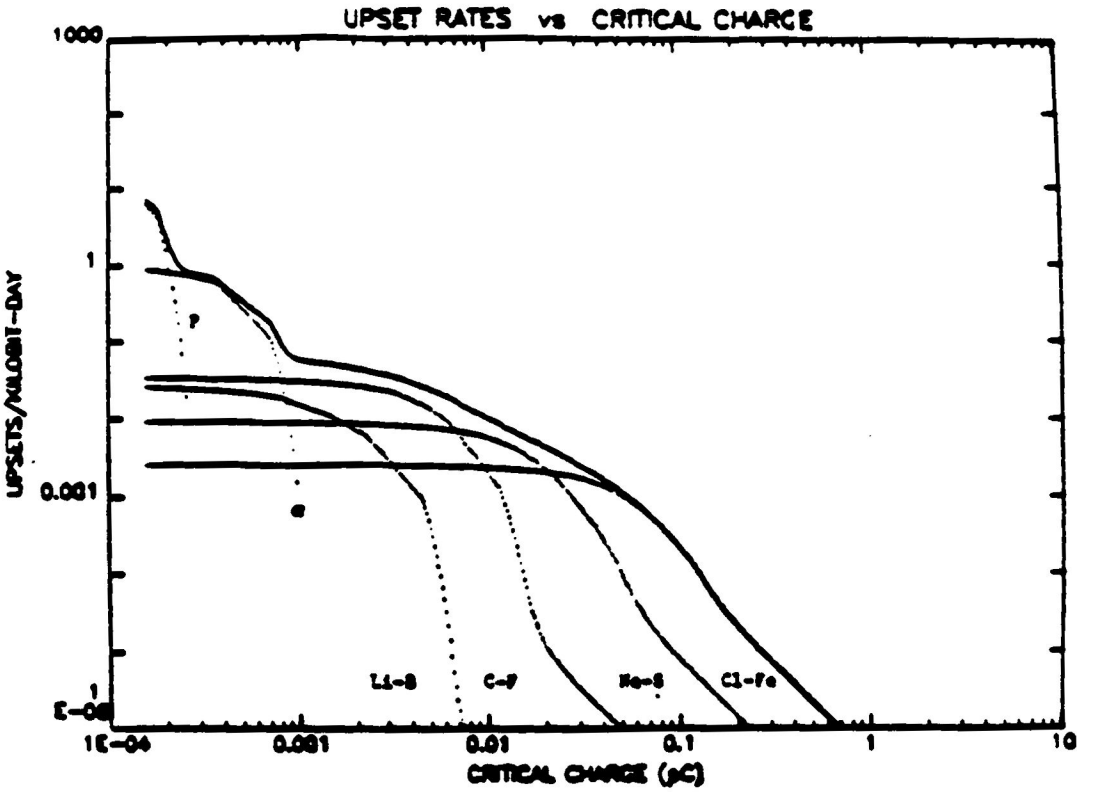

Fig. 31b Upsets vs. Critical Charge for Hydrogen to Iron

55,000 ft., the neutron flux must be computed. The calculations yield $3X10^5$ n/cm^2 day, out of which $1.0X10^4$ will interact in 1 cm of silicon. If less sensitive components are used and .133 pC charge is needed for an upset, the calculated E-burst in units of MeV, (using 3.6 eV as the mean energy of an electron-hole pair production in silicon), is 3.0 MeV. And the computed reduced neutron flux that can generate upsets is 120 n/cm^2 day. Since more characteristic computers are flown in space that have $1X10^3$ or $1X10^6$ microcomputer components of volume 10^3 μ^3, a proportionality is taken to the previous flux calculations that yield .01 upsets/day in $1X10^3$ microcomponents (that are very sensitive) and $1.0X10^{-4}$ upsets/day (that are less sensitive). For $1X10^6$ microcomponents, using the same proportionality, the corresponding upsets/day are 11.0 (in very sensitive) and .12 (in less sensitive components). At 55,000 ft., neutrons will generate upsets in microelectronic components at rates of 10^{-3}, 10^{-4}, and 10^{-6} upsets per kilobit per day for critical charges of .01, .1, and 1.0 pC respectively [50]. Figures 32,33,34, and 35 show soft upset rates at various altitudes, geomagnetic cutoff, elemental group, and for various sensitive volumes.

While the instantaneous SEU rate can vary dramatically around an orbit, these variations occur on time scales that are usually small compared to the mean time between SEU's . Therefore the orbit-average SEU rate is a useful guide for designing spacecraft digital electronics.

The many areas of physics (astrophysics, nuclear-, plasma-, particle physics) that are associated with cosmic-ray studies

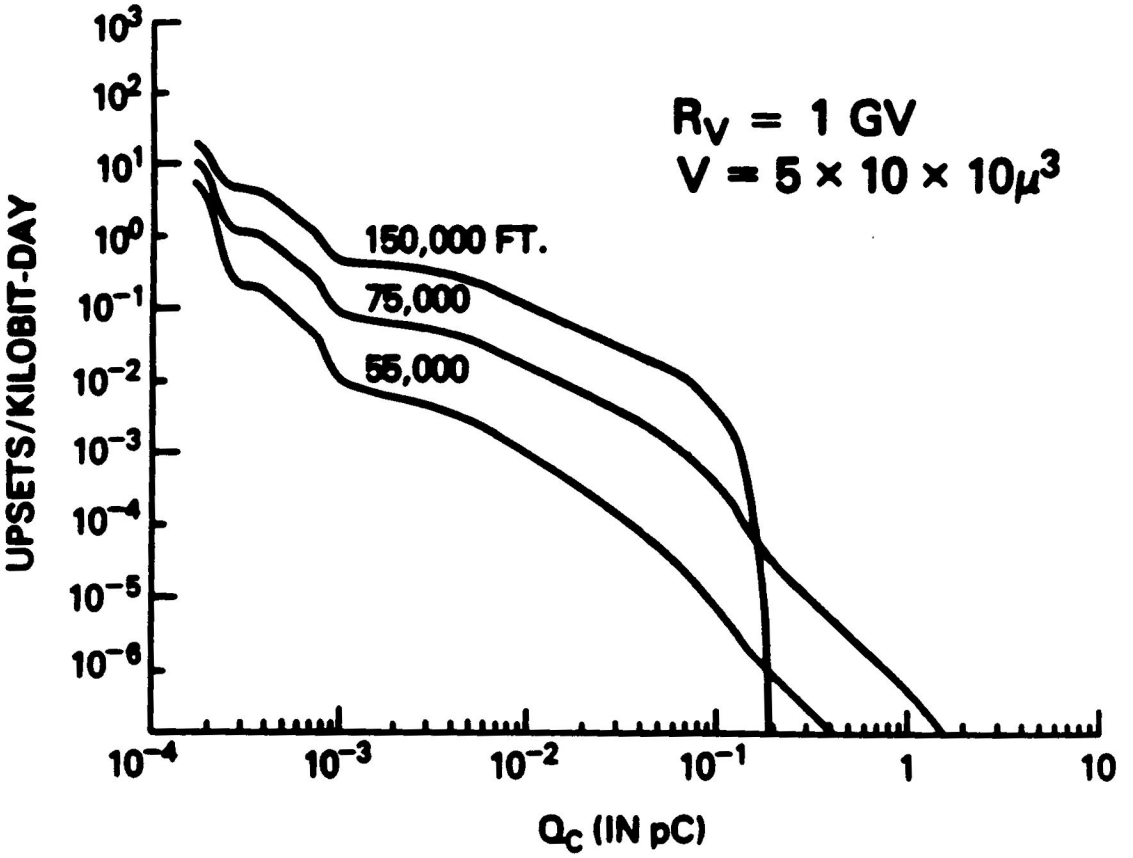

Fig. 32 Upsets vs. Critical Charge as a Function of Altitude

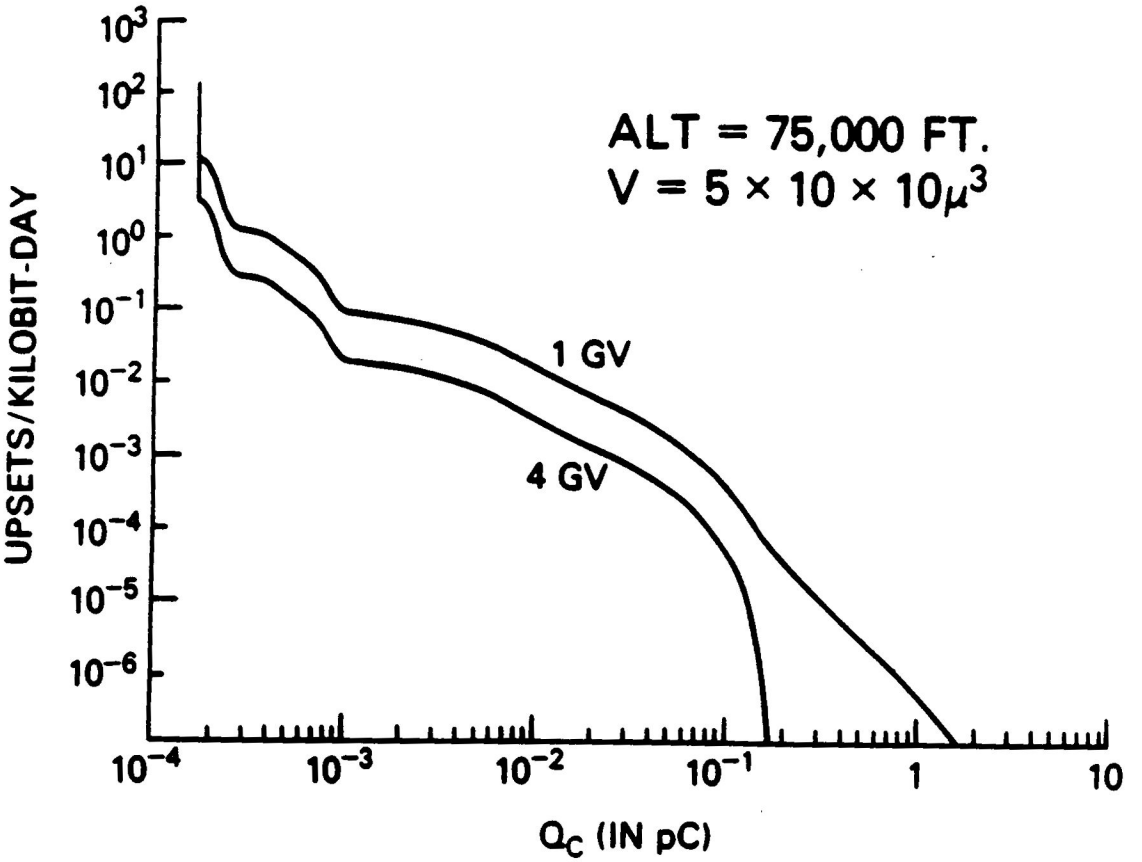

Fig. 33 Upsets vs. Critical Charge as a Function of Rigidity

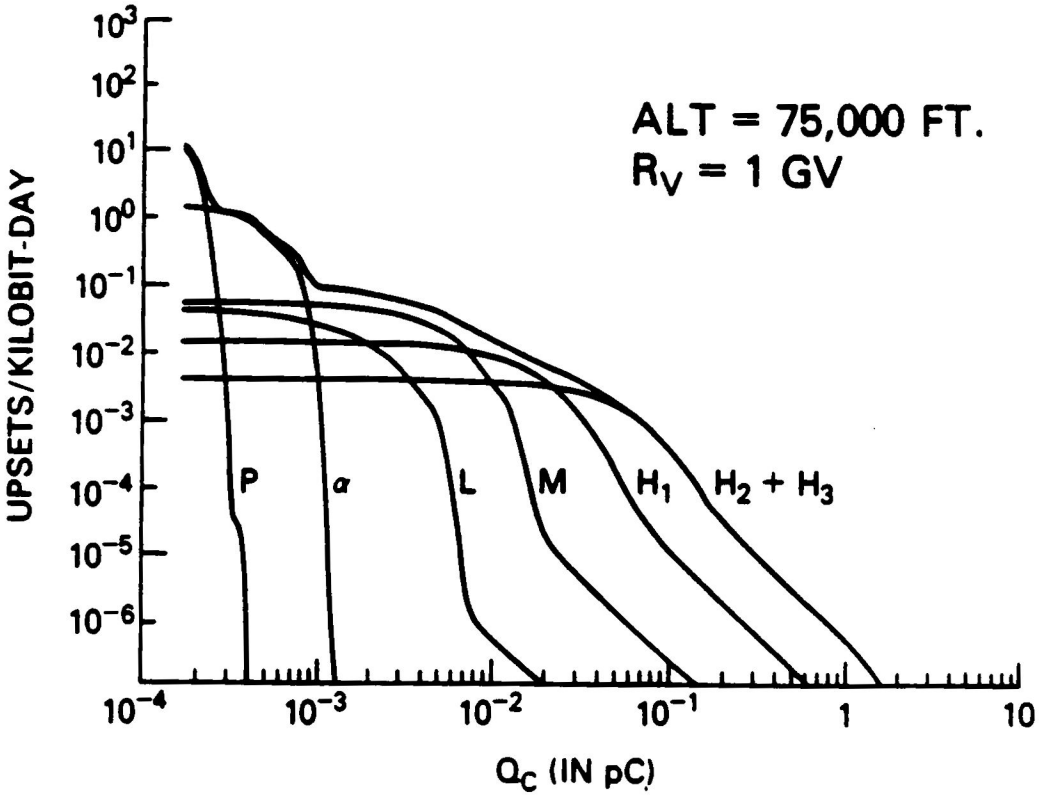

Fig. 34 Upsets vs. Critical Charge as a Function of Element Group

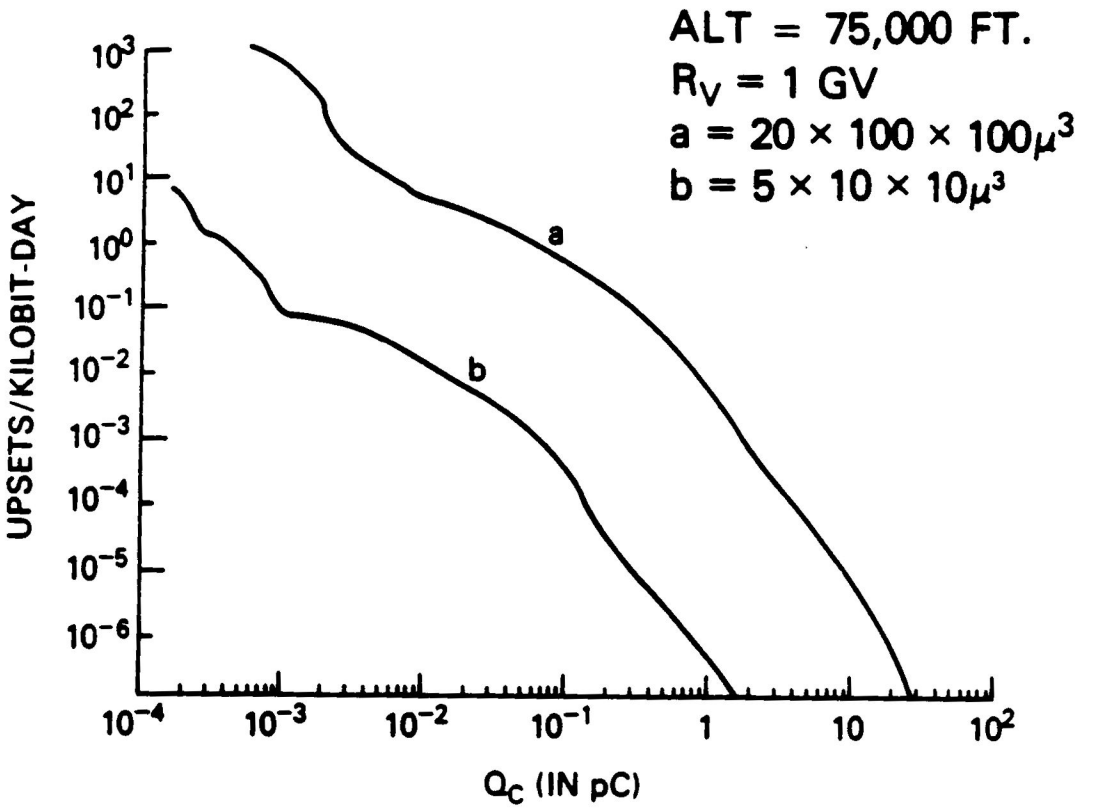

Fig. 35 Upsets vs. Critical Charge as a Function of Sensitive Volume

emphasizes the importance of this research. Cosmic-ray investigations have supplied astrophysical information on particle and nuclear abundances and energy spectra. This basic information can be employed to formulate radiation transport equations, which in turn, can be applied to physical situations for protection against radiation hazards, which these highly penetrating particles present.

APPENDIX A: CALCULATIONS

SUPPLEMENT 1: CALCULATION OF ENERGY CONTENT OF COSMIC RAYS IN THE GALAXY.

ENERGY DENSITY= $1 eV/cm^3$

VOLUME OF GALACTIC DISK = $(\pi)(r^2)(l)$

where $r = 15X10^3$ parsec
$l = 300$ parsec
1 parsec = $3.1X10^{18}$ cm
1 eV = $1.6X10^{-12}$ ergs

ENERGY CONTENT OF COSMIC RAYS IN THE GALAXY = (ED)(VOL)

ENERGY = $(1eV/cm^3)(3.14)(4.65X10^{22}cm^2)(9.3X10^{20}$ cm)

= $1.01X10^{55}$ ergs

SUPPLEMENT 2: CALCULATION OF TIME TO TRAVERSE $5g/cm^2$ BY COSMIC INTERSTELLAR RAYS IN H-GAS.

EQUATION: $x = (\rho)(v/c)(c)(t)$

where $x = 5.0g/cm^2$
$\rho = 1.7X10^{-24}$ g/cm^3
$v/c \simeq 1$
$c = 3.0X10^{10}$ cm/sec

CALCULATION: $t = (5.0\ g/cm^2)/(1.7X10^{-24}\ g/cm^3)(1)(3.0X10^{10}$ cm/sec)
$= 9.8X10^{13}$ sec
$= 3.1X10^6$ years

Q1: WHAT FRACTION OF A YEAR CAN BE SPENT AT 50 OR 100 g/cm^2 DEPTH IN ATMOSPHERE TO KEEP DOSE LESS THAN 0.5 rem?

OLD QUALITY FACTOR(1971)	NEW QUALITY FACTOR(1986)
ANNUAL DOSE: 6.0 rem/yr	ANNUAL DOSE: 11.0 rem/yr
.5 is 8.3% of 6.0	.5 is 4.5% of 11.0
.083 X 365 = 30.4dys	.045 X 365 = 16.4dys
in hrs/wk: 14.0 hrs/wk	in hrs/wk: 7.6 hrs/wk

Q2: FOR LUNAR BASE, HOW MUCH SHIELDING IS NEEDED TO KEEP DOSE RATE BELOW 5.0 rem/yr.

OLD QUALITY FACTOR(1971)	NEW QUALITY FACTOR(1986)
Q.F. IS 7.8	Q.F. IS 13.7
W/PROPORTIONALITY TO Q.F.OF 10.0,THE NEEDED SHIELDING IS: 320 g/cm^2. THE DENSITY= 2.5 g/cm^3; 320 g/cm^2 = 1.28 m	W/PROPORTIONALITY TO Q.F. OF 10.0,THE NEEDED SHIELDING IS:440 g/cm^2. THE DENSITY= 2.5 g/cm^3; 440 g/cm^2 = 1.76 m

DOSAGE CALCULATIONS USING QUALITY FACTOR FROM 1971:

DEFINING EQUATION:(QF)(FLUX)(ABSORB DOSE(RAD))(ENERGY INTERVAL)

QUALITY FACTOR	ENERGY INTERVAL(MeV)	DOSAGE(REM/SEC)
2.0	.003 - .0003	1.0E-9
2.5	.03 - .003	1.0E-9
7.5	.3 - .03	16.0E-9
11.0	.7 - .3	40.0E-9
11.0	1.3 - .7	42.0E-9
9.0	3.7 - 1.3	29.0E-9
8.0	6.3 - 3.7	14.0E-9
7.0	7.7 - 6.3	4.0E-9
6.5	12.3 - 7.7	5.0E-9
7.5	15.7 - 12.3	3.0E-9
8.0	24.3 - 15.7	6.0E-9
7.0	55.7 - 24.3	14.0E-9
5.5	64.3 - 55.7	3.0E-9
4.0	135.7 - 64.3	7.0E-9
3.5	264.3 - 135.7	5.0E-9
3.5	335.7 - 264.3	2.0E-9
3.5	464.3 - 335.7	3.0E-9

SUMMATION(1-17)= 195.0E-9
ANNUAL DOSE= 6.0 REM

DOSAGE CALCULATIONS USING QUALITY FACTOR FORM 1986:

DEFING EQUATION: (QF)(ABSORB DOSE(RAD))(ENERGY INTERVAL)

QUALITY FACTOR	ENERGY INTERVAL(MeV)	DOSAGE(REM/SEC)
13.0	.003 - .0003	7.0E-9
13.5	.03 - .003	7.0E-9
18.5	.3 - .03	39.0E-9
22.0	.7 - .3	81.0E-9
20.5	1.3 - .7	79.0E-9
15.0	3.7 - 1.3	49.0E-9
11.0	6.3 - 3.7	19.0E-9
9.0	7.7 - 6.3	5.0E-9
8.5	12.3 - 7.7	6.0E-9
8.0	15.7 - 12.3	3.0E-9
8.0	24.3 - 15.7	6.0E-9
8.0	55.7 - 24.3	16.0E-9
7.5	64.3 - 55.7	4.0E-9
6.0	135.7 - 64.3	11.0E-9
5.5	264.3 - 135.7	8.0E-9
5.5	335.7 - 264.3	4.0E-9
5.5	464.3 - 335.7	5.0E-9

SUMMATION(1-17) = 349.0E-9
ANNUAL DOSE = 11.0 REM

<Q> FOR QUALITY FACTORS FROM 1971 AND 1986

DEFINING EQUATION: SUMMATION(1-17)(QF)(NF)(AD)(E2-E1)/(NF)(AD)(E2-E1)

1971	1986
5.0E-10 RAD/SEC	5.4E-10 RAD/SEC
4.0E-10 RAD/SEC	5.2E-10 RAD/SEC
21.3E-10 RAD/SEC	21.2E-10 RAD/SEC
36.4E-10 RAD/SEC	36.8E-10 RAD/SEC
38.2E-10 RAD/SEC	38.5E-10 RAD/SEC
32.2E-10 RAD/SEC	32.7E-10 RAD/SEC
17.5E-10 RAD/SEC	17.3E-10 RAD/SEC
5.7E-10 RAD/SEC	5.6E-10 RAD/SEC
7.7E-10 RAD/SEC	7.1E-10 RAD/SEC
4.0E-10 RAD/SEC	3.8E-10 RAD/SEC
7.5E-10 RAD/SEC	7.5E-10 RAD/SEC
20.0E-10 RAD/SEC	20.0E-10 RAD/SEC
5.5E-10 RAD/SEC	5.3E-10 RAD/SEC
17.5E-10 RAD/SEC	18.3E-10 RAD/SEC
14.3E-10 RAD/SEC	14.5E-10 RAD/SEC
5.7E-10 RAD/SEC	7.3E-10 RAD/SEC
8.6E-10 RAD/SEC	9.1E-10 RAD/SEC
SUM = 251.1E-10 RAD/SEC	SUM= 255.6E-10 RAD/SEC
ANNUAL DOSE: .79 RAD	ANNUAL DOSE: .81 RAD
<Q> = 195.0E-9/251.1E-10	<Q>= 349.0E-9/255.6E-10
= 7.8	= 13.7

UPSETS IN MICROELECTRONIC COMPUTER COMPONENTS DUE TO NEUTRON-GENERATED NUCLEAR RECOILS AT AIRCRAFT ALTITUDES OF 55,000 FT. IN ONE DAY.

STEP (1): OBTAIN NEUTRON FLUX IN ENERGY INTERVALS BY INTEGRATING (SUMMING) NEUTRON DIFFERENTIAL ENERGY SPECTRUM OVER ENERGY INTERVALS Ea to Eb.

LET Ea = .7MeV, LOWER ENERGY NEUTRONS ARE UNLIKELY TO MAKE RECOILS.

Jo1 = (2 neu/cm^2/sec/MeV)(1.3MeV-.7MeV) = 1.2 neu/cm^2/sec
Jo2 = (.34)(3.7 - 1.3) =.816 neu/cm^2/sec
Jo3 = (.13)(6.3 - 3.7) =.338 neu/cm^2/sec
Jo4 = (.06)(7.7 - 6.3) =.084 neu/cm^2/sec
Jo5 = (.025)(12.3 - 7.7) =.115 neu/cm^2/sec
Jo6 = (.016)(15.7 - 12.3) =.054 neu/cm^2/sec
Jo7 = (.011)(24.3 - 15.7) =.095 neu/cm^2/sec
Jo8 = (.0065)(55.7 - 24.3) =.204 neu/cm^2/sec
Jo9 = (.005)(64.3 - 55.7) =.043 neu/cm^2/sec
Jo10= (.0018)(135.7 - 64.3) =.129 neu/cm^2/sec
Jo11= (.0007)(264.3 - 135.7) =.090 neu/cm^2/sec
Jo12= (.0005)(335.7 - 264.3) =.036 neu/cm^2/sec
Jo13= (.00034)(464.3 - 335.7) =.044 neu/cm^2/sec

SUMMATION (1-13) = 3.248 neu/cm^2/sec

STEP (2): SOLVE THE DIFFERENTIAL EQUATION FOR NEUTRON INTERACTIONS IN PATH LENGTH OF MATERIAL X(g/cm^2), FOR A TOTAL VOLUME OF $1cm^3$ OF SILICON.

DIFFERENTIAL EQUATION: $dJn/dX = -(Jn)(N/\rho)(\sigma)$

LET Jo,n = incident neutron flux

Jo,n - Jn = # interactions in X(g/cm^2)

N = atoms/cm^3 = $5.01X10^{22}$

ρ = density of silicon in g/cm^3 = 2.33 g/cm^3

σ = 300 mb for En > 130 MeV

900 mb for En = .7 to 20 MeV

300 mb $\exp((130^{-En/100})$ for 20 MeV< En <130 MeV

SOLVED DIFFERENTIAL EQUATION: $J_n = J_o \exp-((N/\rho)(X)(\sigma))$

$J1=(1.2n/cm^2/sec)(exp-((5.01X10^{22}atoms/cm^3)/(2.33g/cm^3)(2.33g/cm^2)(900mb)$

$= 1.147$ neu/cm^2/sec

$J2=(.816)(exp-((5.01X10^{22}/2.33)(2.33)(9.0X10^{-25}cm^2)) = .780$ neu/cm^2/sec

$J3=(.338)(.956) = .323$ neu/cm^2/sec

$J4=(.084)(.956) = .080$ neu/cm^2/sec

$J5=(.115)(.956) = .110$ neu/cm^2/sec

$J6=(.054)(.956) = .052$ neu/cm^2/sec

$J7=(.095)(exp-((5.01X10^{22}/2.33)(2.33)(300mb\ exp((130-20)/(100))$

$= .091$ neu/cm^2/sec

$J8=(.204)(exp-((5.01X10^{22}/2.33)(2.33)(300mb\ exp((130-40)/(100))$

$= .197$ neu/cm^2/sec

$J9=(.043)(exp-((5.01X10^{22}/2.33)(2.33)(300mb\ exp((130-60)/(100))$

$= .042$ neu/cm^2/sec

$J10=(.129)(exp-((5.01X10^{22}/2.33)(2.33)(300mb)) = .127$ neu/cm^2/sec

$J11=(.090)(exp-((5.01X10^{22}/2.33)(2.33)(300mb)) = .089$ neu/cm^2/sec

$J12=(.036)(exp-((5.01X10^{22}/2.33)(2.33)(300mb)) = .035$ neu/cm^2/sec

$J13=(.044)(exp-((5.01X10^{22}/2.33)(2.33)(300mb)) = .043$ neu/cm^2/sec

that have interacted in 2.33g/cm^2 or 1cm of silicon:

Jo1 - J1 = .053 neu/cm^2/sec
Jo2 - J2 = .036 neu/cm^2/sec
Jo3 - J3 = .015 neu/cm^2/sec
Jo4 - J4 = .004 neu/cm^2/sec
Jo5 - J5 = .005 neu/cm^2/sec
Jo6 - J6 = .002 neu/cm^2/sec
Jo7 - J7 = .004 neu/cm^2/sec
Jo8 - J8 = .007 neu/cm^2/sec
Jo9 - J9 = .001 neu/cm^2/sec
Jo10- J10= .002 neu/cm^2/sec

Jo11- J11= .001 neu/cm^2/sec
Jo12- J12= .001 neu/cm^2/sec
Jo13- J13= .001 neu/cm^2/sec

SUMMATION(1-13): .132 neu/cm^2/sec
11,404.8 neu/cm^2/day

STEP(3): SUPPOSE USING LESS SENSITIVE COMPONENTS, AND .133pC CHARGE IS NEEDED FOR UPSET. CALCULATE REQUIRED ENERGY OF NUCLEAR RECOILS,E-burst in units of MeV, FOR GENERATING .133pC, USING 3.6 eV AS THE MEAN ENERGY OF ELECTRON-HOLE PAIR PRODUCTION IN Si, AND 1.6XE-19 C AS ELECTRON CHARGE.

CALCULATIONS: .133XE-12C/1.6XE-19C = 831,250.000

(3.6 eV)(831,250.0)= 2,992,500.0 eV = 3.0 MeV

STEP(4): TO CALCULATE HOW MUCH THE UPSET RATE IS REDUCED IN THE LESS SENSITIVE COMPONENTS, PUT IN WEIGHTING FACTORS TO THE NUMBER OF NEUTRON INTERACTIONS OBTAINED IN STEP (2). THE WEIGHTING FACTORS, AS A FUNCTION OF NEUTRON ENERGY, ARE OBTAINED FROM THE RATIO OF BURST GENERATION RATE FOR E-burst = 30 MeV TO THAT FOR E-burst = 1 MeV IN GIVEN En INTERVAL Eb=3.0MeV/Eb=.1MeV, USING FIG. 2a OF 1988 IEEE PAPER.

that have interacted in 2.33g/cm^2 or 1cm of silicon w/weighting factors:

w.f.

Jo1 - J1 = (.053)(0) = 0.000

Jo2 - J2 = (.036)(0) = 0.000

Jo3 - J3 = (.015)(0) = 0.000

Jo4 - J4 = (.004)(0) = 0.000

Jo5 - J5 = (.005)(0) = 0.000

Jo6 - J6 = (.002)(0) = 0.000

Jo7 - J7 = (.004)(7/400) = 7.0XE-5 neu/cm^2/sec

Jo8 - J8 = (.007)(12/350)= 24.0XE-5 neu/cm^2/sec

Jo9 - J9 = (.001)(18/260)= 6.923XE-5 neu/cm^2/sec

Jo10- J10= (.002)(26/200)= 26.0XE-5 neu/cm^2/sec

Jo11- J11= (.001)(40/180)= 22.0XE-5 neu/cm^2/sec

Jo12- J12= (.001)(44/185)= 23.78XE-5 neu/cm^2/sec

Jo13- J13= (.001)(52/200)= 26.0XE-5 neu/cm^2/sec

SUMMATION(1-13): 135.703XE-5 = .001 neu/cm^2/sec

117.247 neu/cm^2/day

MORE CHARACTERISTIC COMPUTERS FLOWN IN SPACE HAVE 1.0XE+3 OR 1.0XE+6 MICROCOMPONENTS OF VOLUME 10X10X10 MICRONS. CALCULATE UPSET/DAY.

CALCULATIONS: for 1.0XE+3 microcomponents using proportionality to previous calculations.

very sensitive: (11,404.8)(1.0XE-6) = .0114 upsets/day

less sensitive: (117.247)(1.0XE-6) = 1.172XE-4 upsets/day

CALCULATIONS: for 1.0XE+6 microcomponents using proportionality to previous calculations.

very sensitive: (11,404.8)(1.0XE-3) = 11.405 upsets/day

less sensitive: (117.247) (1.0XE-3) = .117 upets/day

Here we explore the dose in a relativistic velocity spacecraft, that moves e.g. with a Lorentz factor $\gamma = 5$. In the frame of the spacecraft, the interstellar gas strikes the spacecraft with energies $m_o\gamma c^2$, i.e. with energies like cosmic rays, but with a huge flux of $3x10^{10}$ protons/cm^{2}sec. This would deposit a dose of 1000 rem/sec, a lethal dose is obtained in 0.35 sec. A procedure to protect against this dose is outlined here.

Explore the following radiation protection device: a stripping foil some distance in front of the space ship, that strips electrons from atoms, and ionizes the incident interstellar gas. Have a superconducting magnet(s) behind the stripping foil, that sweeps away the particles before they strike the space ship. Here is a limiting factor: The stripping foil provides material for nuclear reactions, and hence for neutron production. The neutrons are not swept out by the magnet, and will reach the astronauts. Find:

(a) the stripping cross section of interstellar hydrogen gas incidented on an aluminum stripping foil, using equation (B5) of the propagation paper in Astrophysical Journal Supplement 56,369 (1984).

$$\sigma_s = 4\pi a_o^2 \, (\alpha/Z_p\beta)^2 \, (Z_t^2 + Z_t) \, C_1(\ln 4\beta^2\gamma^2/C_2\alpha^2Z_p^2 - \beta^2)$$

where,

$C_1 = .285$
$C_2 = .048$
$a_o = 5.292X10^{-8}$ cm
$\alpha = 1/137$
$Z_p = 1$
$Z_t = 13$
$\beta \simeq 1$
$\gamma = 5$

and $\sigma_s = 1.603X10^{12}$ mb

(b) What fraction of atoms are stripped in 10,15, or 20 stripping mean free paths? (x in terms of λ_s)

Np ≡ incident flux

Np $\exp(-x/\lambda_s)$ ≡ remaining unstripped hydrogen flux that reaches the spacecraft

Np$(1 - e^{-x/\lambda_s})$ ≡ stripped hydrogen (i.e. proton flux)

for,

$x = 10\lambda_s$ → 1000 rem/sec or $3X10^{10}$ p/cm^{2}sec * $1 - e^{-10} = 999.95$ rem/sec

or $2.999863X10^{10}$ p/cm^{2}sec

≡ dose of particles that get stripped and deflected away from spacecraft. Dose that reaches spacecraft = 1000 rem/sec * e^{-10}.

For $x = 15\ \lambda_s$ and $20\ \lambda_s$ the answer is the nearly the same within 4 decimal places, for the flux deflected away. But the flux that reaches the spacecraft for $x = 20\ \lambda_s$ is $4.5X10^{-2} * 4.5X10^{-5} = 2.0X10^{-6}$ rem/sec.

(c) Using 400mb as the proton-aluminum nuclear cross section, and assuming two neutrons are emitted in each nuclear reaction, what is the optimum thickness of the foil? Hint: the ratio of p-Al nuclear cross section to atomic stripping cross section, times 2 for the 2 neutrons, times the number of stripping mean free paths has to equal $\exp(-x/\lambda_s)$. This yields optimum value of x/λ_s, when dose due to the unstripped hydrogen in the aluminum stripper and the generated neutron dose are equal. (i The proton flux into rem-dose and n-flux into rem dose conversion factors were assumed to be similar).

$2\ \lambda_n/\lambda_s = 2$ (400mb)$/1.603X10^{12}$ mb $= 4.99X10^{-10} \equiv e^{-y/y}$

let $y = x/\lambda_s \rightarrow y = 18.5$ and $x = 18.5\lambda_s$. As shown in (b) above, this yields a dose that is too high. The dose can be further reduced by having the stripping foil at a large distance from the spacecraft, and taking into account the geometry factor: most neutrons are isotropically emitted from the foil hence do not go toward the spacecraft. Take a boom at 1 km fromthe spacecraft, to which the foil is attached, and assume a spacecraft diameter = 10 m. What fraction of neutrons reach the spacecraft? Use ratio of areas: $\pi*5^2m^2/4*\pi*1\ km^2 = 6.25X10^{-6} \equiv F$. This ratio must be multiplied by existing factors.

(d) By what factor is the proton dose reduced, and what is the remaining p and n dose in rem/year taking into account the geometry factor?

The dose is reduced by $e^{-18.5}$

$(N_p)(F)(e^{-18.5}) = (1000\ rem/sec)(6.25X10^{-6})(e^{-18.5})$

$= 5.77X10^{-11}$ rem/year.

(e) Is the dose still too high, so that an inert shield has to be applied between the astronauts and the stripping foil? By what factor should the dose be reduced to bring it down to 50 rem/year?

The dose is no longer too high. However, the stripping foil is so thin that it is not rigid enough. Assume ~ .03 mm or 10^{-2} g/cm^2 Al is practical, i.e. that about 10^{-4} of proton mean free path is the practical limit; then $3X10^{10}$ p/cm^{2}sec $* 10^{-4} \rightarrow 3X10^6$ p_{inter}/cm^{2}sec; in a screen 2 n interact such that $(2n)(F)(3X10^6$ p/cm^{2}sec$) \rightarrow 37.5$ n/cm^2; and in one year $\rightarrow 1.2X10^9$ n/cm^{2}yr ~ 40 rem/year. If you want to reduce

dosage to 10 rem/year, either move the stripping foil to 2 Km or make the foil thinner by 4X. With the foil at 2 Km,

$F = 1.563X10^{-6}$

$(2n)(1.563X10^{-6})(3X10^{6}\ atom/cm^2sec)$

$\rightarrow 9.378\ n/cm^2sec \rightarrow 2.957X10^{8}\ n/cm^2yr$

$\rightarrow 9.9\ rem/year$

APPENDIX B: Propagation Program

```
      PROGRAM    PROP5EHE                    !abridged from props "/1.5-->*1.5"
C     output surviving primary and secondary isotope distrubution per slab path
      PARAMETER  NN=59, NL=30
      DIMENSION  FI(NN),FX(NN),SF(NN),SZ(NN),S1(NN),S2(NN),GM(NN,2)
      DIMENSION  F1(NN,NL),F2(NN,NL),D(NL),G(NL),W(NL),WX(NL)
      DIMENSION  CL(NN),C1(NN),C2(NN),EK(NN),EL(NN),ID(2)
      COMMON /I/ IX(NN),IY(NN),IZ(NN) /Q/ Q(NN,NN),P(NN),F(NN)
      DATA       G /0.2, 0.4, 0.6, 0.8, 1.0, 1.2, 1.4, 1.6, 1.8, 2.0    paths
     1,             2.2, 2.4, 3.0, 4.0, 5.0, 6.0, 7.0, 8.0, 9.0, 10.    in
     1,             11., 12., 15., 20., 25., 30., 35., 40., 45., 50./   grammage
C     path interval weighting factor and subslab thickness
      DATA       W /12*.2, 10*1., 8*5./                                  Bin size
      DATA       D /12*.2, 10*.5, 8*1./                                  Sub-slab
      DATA       ID/'VEL.', 'RIG.'/
      DATA       IE/2300/, RP/465./, RI/0.852/, JD/'    '/
      OPEN (1,FILE='LMH59.LIS',STATUS='OLD')          ! isotope abundances
      OPEN (2,FILE='QLMH59.DAT',STATUS='OLD')         ! Part. Cro. Sec. tables

      READ (1,1) (IZ(I),IX(I),IY(I),F(I),I=1,NN)      ! read in isotope & Flux
 1    FORMAT (I3,A2,I3,40X,F8.1)

      DO 10  I=1,NN                                   ! total inelastic xsec.
       P(I) = 10.*3.1416*1.31**2*IY(I)**(2./3.)*(1.-.47*IY(I)**(-.4))
 10    CONTINUE

      READ (2,2) (IZ(J),IX(J),IY(J),(Q(I,J),I=1,NN),J=1,NN)  ! read part. xsec
 2    FORMAT ((I3,A2,I3,4(/12F6.2)/11F6.2))

 100  DO 160  L=1,NL
       GL = G(L)                                      ! path (gram) thickness
       DG = D(L)                                      ! subslab thickness
       IF (G(L) .GT. 10.)   DG = 1.                   ! minimum thickness = 1
       NX = G(L)/DG + .9                              ! number of subslabs

       DO 105  J=1,NN
 105    FX(J) = F(J)                                  ! initialize FX(j)

 110   DO 140  N=1,NX                                 ! NX sub-slabs
        DO 130  I=1,NN                                ! primary isotope
         S2J = 0                                      !
         ZI = IZ(I)
         YI = IY(I)
         DO 120  J=1,NN                               ! initialize secondaries
          Z = IZ(J)                                   ! then to sum over
          Y = IY(J)                                   ! the I-secondary
          IF (Q(I,J) .EQ. 0.)   GO TO 120             ! from J-isotope
          S2J = S2J + FX(J)*(1.-0.5*(P(I)+P(J))*(DG/1673.))
     &          *Q(I,J)*(DG/1673.)/(1.+G(L)*(Z**2/Y)/RP/NX/2.)**(RI*1.5)
 120      CONTINUE
         F1(I,L) = FX(I)*EXP(-DG*P(I)/1673.)                              !I-pri
     &             /(1.+G(L)*(ZI**2/YI)/RP)**(RI*1.5/NX)
         F2(I,L) = 0.955*S2J/(1.0 + G(L)*(ZI**2/YI)/RP/NX/2.)**(RI*1.5) !I-sec
C  * * * The term  0.955  is for energy loss due to collision * * * * *
         FX(I) = F1(I,L) + F2(I,L)                                        !I-sum
         FI(I) = F(I)*EXP(-GL*P(I)/1673.)                        ! I-primodial
     &              /(1.0+G(L)*(ZI**2/YI)/RP)**(RI*1.5)
```

```
130     CONTINUE
140    CONTINUE

       DO 145  I=1,NN
        SF(I) = F1(I,L) + F2(I,L)                                  ! I-pri & sec
145    CONTINUE

       DO 150  J=1,NN
        GM(J,1) = 1.                                          ! Velocity threshold
        GM(J,2) = ((.5*IY(J))/IZ(J))**1.5                     ! Rigidity threshold
        F1(J,L) = FI(J)                                       ! primodial primary
        F2(J,L) = SF(J) - F1(J,L)                             ! secondaries
        IF (J.EQ. 1 .OR. IZ(J).NE.IZ(J-1))   SZ(J) = SF(J)              sum over
        IF (J.NE. 1 .AND.IZ(J).EQ.IZ(J-1))   SZ(J) = SZ(J-1) + SF(J)    element
        SJ = SZ(J)/(SF(8)+SF(9))                                        relative
C       IF (J.NE.59 .AND.IZ(J).EQ.IZ(J+1))                              optional
C    1   WRITE(3,4) IX(J), IY(J), F1(J,L), F2(J,L), SF(J)               !listing
C4      FORMAT (1X,A2,I3,6X,2F10.4,3F10.4)                              !
C       IF (J.EQ.59 .OR. IZ(J).NE.IZ(J+1))                              !
C    1   WRITE(3,4) IX(J), IY(J), F1(J,L), F2(J,L), SF(J), SZ(J), SJ    !
150    CONTINUE
160   CONTINUE

      DO 240 M=1,1                                                    !Velocity threshold
       KW = 16
        SW = 0.
        DO 210  L=1,NL
         WX(L) = W(L)*EXP(-(KW/100.)*G(L))                             ! exponential
     &
210      SW = SW + WX(L)                                               ! < 50 g/cmsq
        DO 212  L=1,NL
212      WX(L) = WX(L)/SW
        DO 215 J=1,NN
         S1(J) = 0.
         S2(J) = 0.
215      GM(J,M)=(2-M)+(M-1)*(IY(J)/2./IZ(J))**1.5                 ! geom. factor = 1
        DO 220  L=1,NL
         DO 220   J=1,NN
          S1(J) = S1(J) + WX(L)*F1(J,L)*GM(J,M)                     ! primary
          S2(J) = S2(J) + WX(L)*F2(J,L)*GM(J,M)                     ! secondary
220      CONTINUE
        DO 225 J=1,NN
225      SF(J) = S1(J) + S2(J)

        WRITE(4,5)  ID(M), KW, ID(M)                                ! output heading
5       FORMAT (/4X,A4,4X,'SOURCE',4X,'ARR PR',4X,'AR SEC',4X,
     1            'AR TOT', 3X,'(1-EXP)E-.',I2,'X',3X,A1/)
        DO 230  J=1,NN
         FI(J)=F(J)*GM(J,M)                                                 geom. f.
         IF (J.EQ. 1 .OR. IZ(J).NE.IZ(J-1))   SZ(J) = SF(J)                 sum over
         IF (J.NE. 1 .AND.IZ(J).EQ.IZ(J-1))   SZ(J) = SZ(J-1) + SF(J)      element
         IF  (SF(8)+SF(9).GT.0.)  SJ = SZ(J)/(SF(8)+SF(9))*100.            rel/C
         IF (J.NE.59 .AND.IZ(J).EQ.IZ(J+1))
     1   WRITE(4,6) IZ(J),IX(J),IY(J),FI(J),S1(J),S2(J),SF(J)
6        FORMAT (I3, A2, I3, 5F10.3, F10.2)
         IF (J.EQ.59 .OR. IZ(J).NE.IZ(J+1))
     1   WRITE(4,6) IZ(J),IX(J),IY(J),FI(J),S1(J),S2(J),SF(J),SZ(J),SJ
230      CONTINUE
240    CONTINUE
       END
```

APPENDIX C: Calculated Cross Sections of Silberberg and Tsao

3LI	6											0.000
0.00	0.00	0.00	0.00	0.00	0.00	0.00	0.00	0.00	0.00	0.00	0.00	
0.00	0.00	0.00	0.00	0.00	0.00	0.00	0.00	0.00	0.00	0.00	0.00	
0.00	0.00	0.00	0.00	0.00	0.00	0.00	0.00	0.00	0.00	0.00	0.00	
0.00	0.00	0.00	0.00	0.00	0.00	0.00	0.00	0.00	0.00	0.00	0.00	
0.00	0.00	0.00	0.00	0.00	0.00	0.00	0.00	0.00	0.00	0.00		
3LI	7											0.000
36.18	0.00	0.00	0.00	0.00	0.00	0.00	0.00	0.00	0.00	0.00	0.00	
0.00	0.00	0.00	0.00	0.00	0.00	0.00	0.00	0.00	0.00	0.00	0.00	
0.00	0.00	0.00	0.00	0.00	0.00	0.00	0.00	0.00	0.00	0.00	0.00	
0.00	0.00	0.00	0.00	0.00	0.00	0.00	0.00	0.00	0.00	0.00	0.00	
0.00	0.00	0.00	0.00	0.00	0.00	0.00	0.00	0.00	0.00	0.00		
4BE	7											0.000
21.00	0.00	0.00	0.00	0.00	0.00	0.00	0.00	0.00	0.00	0.00	0.00	
0.00	0.00	0.00	0.00	0.00	0.00	0.00	0.00	0.00	0.00	0.00	0.00	
0.00	0.00	0.00	0.00	0.00	0.00	0.00	0.00	0.00	0.00	0.00	0.00	
0.00	0.00	0.00	0.00	0.00	0.00	0.00	0.00	0.00	0.00	0.00	0.00	
0.00	0.00	0.00	0.00	0.00	0.00	0.00	0.00	0.00	0.00	0.00		
4BE	9											0.000
13.92	19.65	5.26	0.00	0.00	0.00	0.00	0.00	0.00	0.00	0.00	0.00	
0.00	0.00	0.00	0.00	0.00	0.00	0.00	0.00	0.00	0.00	0.00	0.00	
0.00	0.00	0.00	0.00	0.00	0.00	0.00	0.00	0.00	0.00	0.00	0.00	
0.00	0.00	0.00	0.00	0.00	0.00	0.00	0.00	0.00	0.00	0.00	0.00	
0.00	0.00	0.00	0.00	0.00	0.00	0.00	0.00	0.00	0.00	0.00		
4BE	10											0.000
10.74	21.52	0.86	25.42	0.00	0.00	0.00	0.00	0.00	0.00	0.00	0.00	
0.00	0.00	0.00	0.00	0.00	0.00	0.00	0.00	0.00	0.00	0.00	0.00	
0.00	0.00	0.00	0.00	0.00	0.00	0.00	0.00	0.00	0.00	0.00	0.00	
0.00	0.00	0.00	0.00	0.00	0.00	0.00	0.00	0.00	0.00	0.00	0.00	
0.00	0.00	0.00	0.00	0.00	0.00	0.00	0.00	0.00	0.00	0.00		
5B	10											0.000
13.12	11.38	9.69	11.87	0.00	0.04	0.00	0.00	0.00	0.00	0.00	0.00	
0.00	0.00	0.00	0.00	0.00	0.00	0.00	0.00	0.00	0.00	0.00	0.00	
0.00	0.00	0.00	0.00	0.00	0.00	0.00	0.00	0.00	0.00	0.00	0.00	
0.00	0.00	0.00	0.00	0.00	0.00	0.00	0.00	0.00	0.00	0.00	0.00	
0.00	0.00	0.00	0.00	0.00	0.00	0.00	0.00	0.00	0.00	0.00		
5B	11											0.000
13.98	17.60	6.43	8.46	15.75	26.68	0.59	0.00	0.00	0.00	0.00	0.00	
0.00	0.00	0.00	0.00	0.00	0.00	0.00	0.00	0.00	0.00	0.00	0.00	
0.00	0.00	0.00	0.00	0.00	0.00	0.00	0.00	0.00	0.00	0.00	0.00	
0.00	0.00	0.00	0.00	0.00	0.00	0.00	0.00	0.00	0.00	0.00	0.00	
0.00	0.00	0.00	0.00	0.00	0.00	0.00	0.00	0.00	0.00	0.00		
6C	12											98.900
13.12	11.38	9.69	4.45	2.87	21.26	58.38	0.04	0.00	0.00	0.00	0.00	
0.00	0.00	0.00	0.00	0.00	0.00	0.00	0.00	0.00	0.00	0.00	0.00	
0.00	0.00	0.00	0.00	0.00	0.00	0.00	0.00	0.00	0.00	0.00	0.00	
0.00	0.00	0.00	0.00	0.00	0.00	0.00	0.00	0.00	0.00	0.00	0.00	
0.00	0.00	0.00	0.00	0.00	0.00	0.00	0.00	0.00	0.00	0.00		
6C	13											1.100
13.92	16.23	7.17	7.16	4.75	10.40	31.42	48.16	0.20	0.00	0.00	0.00	
0.00	0.00	0.00	0.00	0.00	0.00	0.00	0.00	0.00	0.00	0.00	0.00	
0.00	0.00	0.00	0.00	0.00	0.00	0.00	0.00	0.00	0.00	0.00	0.00	
0.00	0.00	0.00	0.00	0.00	0.00	0.00	0.00	0.00	0.00	0.00	0.00	
0.00	0.00	0.00	0.00	0.00	0.00	0.00	0.00	0.00	0.00	0.00		
7N	14											7.000
13.12	11.38	9.69	4.45	1.91	19.38	27.57	42.33	21.17	0.04	0.00	0.00	

```
 0.00  0.00  0.00  0.00  0.00  0.00  0.00  0.00  0.00  0.00  0.00  0.00
 0.00  0.00  0.00  0.00  0.00  0.00  0.00  0.00  0.00  0.00  0.00  0.00
 0.00  0.00  0.00  0.00  0.00  0.00  0.00  0.00  0.00  0.00  0.00  0.00
 0.00  0.00  0.00  0.00  0.00  0.00  0.00  0.00  0.00  0.00  0.00
 7N  15                                                              0.000
13.92 15.29  7.68  6.61  4.06  9.98 27.92 23.68 22.89 48.64  0.43  0.00
 0.00  0.00  0.00  0.00  0.00  0.00  0.00  0.00  0.00  0.00  0.00  0.00
 0.00  0.00  0.00  0.00  0.00  0.00  0.00  0.00  0.00  0.00  0.00  0.00
 0.00  0.00  0.00  0.00  0.00  0.00  0.00  0.00  0.00  0.00  0.00  0.00
 0.00  0.00  0.00  0.00  0.00  0.00  0.00  0.00  0.00  0.00  0.00
 8O  16                                                            109.800
13.22 11.38  9.69  4.45  1.91 11.13 24.71 37.18 18.22 31.98 59.34  0.04
 0.00  0.00  0.00  0.00  0.00  0.00  0.00  0.00  0.00  0.00  0.00  0.00
 0.00  0.00  0.00  0.00  0.00  0.00  0.00  0.00  0.00  0.00  0.00  0.00
 0.00  0.00  0.00  0.00  0.00  0.00  0.00  0.00  0.00  0.00  0.00  0.00
 0.00  0.00  0.00  0.00  0.00  0.00  0.00  0.00  0.00  0.00  0.00
 8O  17                                                              0.000
13.99 14.62  8.03  6.22  3.61  9.42 25.09 20.78 19.55 22.01 25.76 49.12
 0.38  0.00  0.00  0.00  0.00  0.00  0.00  0.00  0.00  0.00  0.00  0.00
 0.00  0.00  0.00  0.00  0.00  0.00  0.00  0.00  0.00  0.00  0.00  0.00
 0.00  0.00  0.00  0.00  0.00  0.00  0.00  0.00  0.00  0.00  0.00  0.00
 0.00  0.00  0.00  0.00  0.00  0.00  0.00  0.00  0.00  0.00  0.00
 8O  18                                                              0.200
14.47 19.65  5.26  9.38  8.08  6.62 25.64 18.68 20.73 21.52 23.87 22.49
49.64  0.67  0.00  0.00  0.00  0.00  0.00  0.00  0.00  0.00  0.00  0.00
 0.00  0.00  0.00  0.00  0.00  0.00  0.00  0.00  0.00  0.00  0.00  0.00
 0.00  0.00  0.00  0.00  0.00  0.00  0.00  0.00  0.00  0.00  0.00  0.00
 0.00  0.00  0.00  0.00  0.00  0.00  0.00  0.00  0.00  0.00  0.00
 9F  19                                                              0.000
14.06 14.12  8.29  5.94  3.30  8.82 22.60 18.23 16.61 18.91 23.27 24.27
26.93 49.58  0.33  0.00  0.00  0.00  0.00  0.00  0.00  0.00  0.00  0.00
 0.00  0.00  0.00  0.00  0.00  0.00  0.00  0.00  0.00  0.00  0.00  0.00
 0.00  0.00  0.00  0.00  0.00  0.00  0.00  0.00  0.00  0.00  0.00  0.00
 0.00  0.00  0.00  0.00  0.00  0.00  0.00  0.00  0.00  0.00  0.00
10NE 20                                                             11.400
13.43 11.38  9.69  4.45  1.91  9.25 20.06 17.12 13.69 17.33 22.55 32.33
24.40 21.66 38.28  0.04  0.00  0.00  0.00  0.00  0.00  0.00  0.00  0.00
 0.00  0.00  0.00  0.00  0.00  0.00  0.00  0.00  0.00  0.00  0.00  0.00
 0.00  0.00  0.00  0.00  0.00  0.00  0.00  0.00  0.00  0.00  0.00  0.00
 0.00  0.00  0.00  0.00  0.00  0.00  0.00  0.00  0.00  0.00  0.00
10NE 21                                                             0.000
14.12 13.74  8.49  5.72  3.08  8.22 20.40 15.98 14.18 16.29 20.21 21.11
23.73 22.28 22.09 50.05  0.29  0.00  0.00  0.00  0.00  0.00  0.00  0.00
 0.00  0.00  0.00  0.00  0.00  0.00  0.00  0.00  0.00  0.00  0.00  0.00
 0.00  0.00  0.00  0.00  0.00  0.00  0.00  0.00  0.00  0.00  0.00  0.00
 0.00  0.00  0.00  0.00  0.00  0.00  0.00  0.00  0.00  0.00  0.00
10NE 22                                                             4.600
14.86 17.60  6.43  8.00  5.91  6.57 21.32 14.93 15.05 15.72 18.02 18.06
22.39 21.77 22.67 22.55 50.53  0.00  0.00  0.00  0.00  0.00  0.00  0.00
 0.00  0.00  0.00  0.00  0.00  0.00  0.00  0.00  0.00  0.00  0.00  0.00
 0.00  0.00  0.00  0.00  0.00  0.00  0.00  0.00  0.00  0.00  0.00  0.00
 0.00  0.00  0.00  0.00  0.00  0.00  0.00  0.00  0.00  0.00  0.00
11NA 23                                                             0.900
14.18 13.44  8.65  5.56  2.91  7.63 18.46 14.02 12.16 14.08 17.57 18.36
20.47 19.22 19.42 24.17 24.40 21.01  0.26  0.00  0.00  0.00  0.00  0.00
 0.00  0.00  0.00  0.00  0.00  0.00  0.00  0.00  0.00  0.00  0.00  0.00
 0.00  0.00  0.00  0.00  0.00  0.00  0.00  0.00  0.00  0.00  0.00  0.00
 0.00  0.00  0.00  0.00  0.00  0.00  0.00  0.00  0.00  0.00  0.00
12MG 24                                                            19.100
13.63 11.38  9.69  4.45  1.91  7.76 16.47 13.06 10.29 12.98 16.90 17.47
18.48 17.58 17.16 23.41 21.99 10.34 50.76  0.04  0.00  0.00  0.00  0.00
 0.00  0.00  0.00  0.00  0.00  0.00  0.00  0.00  0.00  0.00  0.00  0.00
 0.00  0.00  0.00  0.00  0.00  0.00  0.00  0.00  0.00  0.00  0.00  0.00
```

```
 0.00  0.00  0.00  0.00  0.00  0.00  0.00  0.00  0.00  0.00  0.00
12MG 25                                                          2.300
14.25 13.20  8.77  5.43  2.78  7.08 16.73 12.31 10.46 12.18 15.29 15.96
17.69 16.62 16.74 21.07 21.18 11.89 26.13 51.01  0.24  0.00  0.00  0.00
 0.00  0.00  0.00  0.00  0.00  0.00  0.00  0.00  0.00  0.00  0.00  0.00
 0.00  0.00  0.00  0.00  0.00  0.00  0.00  0.00  0.00  0.00  0.00  0.00
 0.00  0.00  0.00  0.00  0.00  0.00  0.00  0.00  0.00  0.00  0.00
12MG 26                                                          2.600
15.05 16.23  7.17  7.16  4.75  6.05 17.57 11.73 10.98 11.63 13.70 14.04
16.85 16.08 16.62 17.96 19.75 16.51 23.97 22.45 51.42  0.51  0.00  0.00
 0.00  0.00  0.00  0.00  0.00  0.00  0.00  0.00  0.00  0.00  0.00  0.00
 0.00  0.00  0.00  0.00  0.00  0.00  0.00  0.00  0.00  0.00  0.00  0.00
 0.00  0.00  0.00  0.00  0.00  0.00  0.00  0.00  0.00  0.00  0.00
13AL 27                                                          2.300
14.33 13.01  8.87  5.32  2.68  6.56 15.20 10.82  9.03 10.56 13.30 13.89
15.31 14.39 14.46 18.36 18.36 10.01 22.24 24.01 29.63 51.49  0.22  0.00
 0.00  0.00  0.00  0.00  0.00  0.00  0.00  0.00  0.00  0.00  0.00  0.00
 0.00  0.00  0.00  0.00  0.00  0.00  0.00  0.00  0.00  0.00  0.00  0.00
 0.00  0.00  0.00  0.00  0.00  0.00  0.00  0.00  0.00  0.00  0.00
14SI 28                                                         19.300
13.84 11.38  9.69  4.45  1.91  6.55 13.63 10.03  7.77  9.77 12.72 13.15
13.91 13.23 12.92 17.62 16.89  7.47 20.91 23.44 25.26 29.23 51.72  0.00
 0.00  0.00  0.00  0.00  0.00  0.00  0.00  0.00  0.00  0.00  0.00  0.00
 0.00  0.00  0.00  0.00  0.00  0.00  0.00  0.00  0.00  0.00  0.00  0.00
 0.00  0.00  0.00  0.00  0.00  0.00  0.00  0.00  0.00  0.00  0.00
14SI 29                                                          1.000
14.40 12.84  8.95  5.23  2.59  5.86 13.35  9.10  7.48  8.83 11.23 11.80
13.04 12.34 12.45 16.04 16.07  8.62 19.76 21.58 25.68 24.50 29.99 51.96
 0.20  0.00  0.00  0.00  0.00  0.00  0.00  0.00  0.00  0.00  0.00  0.00
 0.00  0.00  0.00  0.00  0.00  0.00  0.00  0.00  0.00  0.00  0.00  0.00
 0.00  0.00  0.00  0.00  0.00  0.00  0.00  0.00  0.00  0.00  0.00
14SI 30                                                          0.700
15.19 15.29  7.68  6.61  4.06  5.24 14.15  8.86  7.83  8.43 10.17 10.59
12.46 11.84 12.22 13.94 14.97 11.22 18.22 18.09 23.36 23.27 25.28 27.09
52.28  0.43  0.00  0.00  0.00  0.00  0.00  0.00  0.00  0.00  0.00  0.00
 0.00  0.00  0.00  0.00  0.00  0.00  0.00  0.00  0.00  0.00  0.00  0.00
 0.00  0.00  0.00  0.00  0.00  0.00  0.00  0.00  0.00  0.00  0.00
15P  31                                                          0.300
14.48 12.71  9.02  5.15  2.52  5.51 12.36  8.17  6.59  7.78  9.89 10.35
11.35 10.71 10.75 13.89 13.81  7.25 16.88 18.45 21.76 20.65 23.00 24.32
33.18 52.44  0.19  0.00  0.00  0.00  0.00  0.00  0.00  0.00  0.00  0.00
 0.00  0.00  0.00  0.00  0.00  0.00  0.00  0.00  0.00  0.00  0.00  0.00
 0.00  0.00  0.00  0.00  0.00  0.00  0.00  0.00  0.00  0.00  0.00
16S  32                                                          2.900
14.05 11.38  9.69  4.45  1.91  5.50 11.24  7.64  5.82  7.29  9.50  9.84
10.42  9.93  9.70 13.25 12.73  5.63 15.80 17.73 19.79 18.61 21.32 23.13
25.67 36.80 65.85  0.00  0.00  0.00  0.00  0.00  0.00  0.00  0.00  0.00
 0.00  0.00  0.00  0.00  0.00  0.00  0.00  0.00  0.00  0.00  0.00  0.00
 0.00  0.00  0.00  0.00  0.00  0.00  0.00  0.00  0.00  0.00  0.00
16S  33                                                          0.000
14.56 12.59  9.08  5.09  2.47  5.21 11.51  7.39  5.86  6.91  8.78  9.16
 9.98  9.40  9.38 12.14 12.00  6.18 14.59 15.94 18.66 17.63 19.62 20.79
25.27 24.35 33.00 52.92  0.17  0.00  0.00  0.00  0.00  0.00  0.00  0.00
 0.00  0.00  0.00  0.00  0.00  0.00  0.00  0.00  0.00  0.00  0.00  0.00
 0.00  0.00  0.00  0.00  0.00  0.00  0.00  0.00  0.00  0.00  0.00
16S  34                                                          0.100
15.31 14.62  8.03  6.22  3.61  4.79 12.19  7.27  6.11  6.62  8.05  8.37
 9.61  9.04  9.23 10.82 11.32  7.72 13.57 13.80 17.34 16.95 18.29 18.50
22.77 24.09 24.82 28.41 53.20  0.38  0.00  0.00  0.00  0.00  0.00  0.00
 0.00  0.00  0.00  0.00  0.00  0.00  0.00  0.00  0.00  0.00  0.00  0.00
 0.00  0.00  0.00  0.00  0.00  0.00  0.00  0.00  0.00  0.00  0.00
17CL 35                                                          0.100
14.88 12.61  9.22  5.04  2.42  6.00  8.68  7.22  4.46  6.64  6.96  8.83
```

```
 7.87  8.91  9.36 11.58 10.50  5.75 12.59 15.04 14.00 16.35 16.89 19.32
18.66 22.27 22.51 29.62 26.17 51.56  0.00  0.00  0.00  0.00  0.00  0.00
 0.00  0.00  0.00  0.00  0.00  0.00  0.00  0.00  0.00  0.00  0.00  0.00
 0.00  0.00  0.00  0.00  0.00  0.00  0.00  0.00  0.00  0.00  0.00
17CL 37                                                              0.000
16.86 17.13  7.17  7.40  5.07  5.27  9.93  7.26  4.61  6.07  6.35  7.65
 7.04  8.16  8.44  9.72  9.29  6.92 11.16 12.17 12.26 14.88 14.60 16.01
16.16 20.82 18.91 20.75 21.61 21.11 10.33  0.00  0.00  0.00  0.00  0.00
 0.00  0.00  0.00  0.00  0.00  0.00  0.00  0.00  0.00  0.00  0.00  0.00
 0.00  0.00  0.00  0.00  0.00  0.00  0.00  0.00  0.00  0.00  0.00
18AR 36                                                              0.800
14.72 11.60  9.88  4.45  1.91  5.94  7.94  6.78  4.04  6.27  6.52  8.44
 7.44  8.34  8.72 11.10  9.86  4.69 11.68 14.50 13.08 14.94 15.63 18.33
17.35 19.55 20.86 23.93 36.20 34.91 33.70  0.00  0.00  0.00  0.00  0.00
 0.00  0.00  0.00  0.00  0.00  0.00  0.00  0.00  0.00  0.00  0.00  0.00
 0.00  0.00  0.00  0.00  0.00  0.00  0.00  0.00  0.00  0.00  0.00
18AR 37                                                              0.000
15.43 12.78  9.45  4.99  2.38  5.70  8.15  6.60  4.03  5.98  6.25  7.92
 7.04  7.94  8.32 10.29  9.29  5.03 11.08 13.22 12.26 14.26 14.71 16.81
16.17 19.19 19.41 21.64 21.38 36.09 17.92  0.00 52.06  0.15  0.00  0.00
 0.00  0.00  0.00  0.00  0.00  0.00  0.00  0.00  0.00  0.00  0.00  0.00
 0.00  0.00  0.00  0.00  0.00  0.00  0.00  0.00  0.00  0.00  0.00
18AR 38                                                              0.100
16.37 14.69  8.62  5.94  3.30  5.43  8.64  6.56  4.06  5.72  5.99  7.42
 6.67  7.60  7.93  9.49  8.76  5.49 10.49 12.00 11.51 13.66 13.78 15.36
15.10 18.71 17.94 19.66 19.93 25.50 34.46 31.50 23.23 33.14  0.33  0.00
 0.00  0.00  0.00  0.00  0.00  0.00  0.00  0.00  0.00  0.00  0.00  0.00
 0.00  0.00  0.00  0.00  0.00  0.00  0.00  0.00  0.00  0.00  0.00
19K  39                                                              0.100
15.98 12.94  9.68  4.95  2.34  5.43  7.69  6.06  3.66  5.41  5.64  7.15
 6.33  7.13  7.45  9.20  8.27  4.44  9.82 11.72 10.82 12.54 12.91 14.74
14.14 16.69 16.89 18.81 18.51 22.83 15.37  7.82 30.07 20.74 52.56  0.15
 0.00  0.00  0.00  0.00  0.00  0.00  0.00  0.00  0.00  0.00  0.00  0.00
 0.00  0.00  0.00  0.00  0.00  0.00  0.00  0.00  0.00  0.00  0.00
19K  40                                                              0.000
16.90 14.76  8.90  5.82  3.18  5.19  8.13  6.03  3.69  5.19  5.42  6.72
 6.02  6.83  7.12  8.53  7.83  4.82  9.33 10.70 10.19 12.05 12.15 13.54
13.25 16.32 15.70 17.17 17.33 22.06 12.76 10.37 19.23 17.83 26.25 54.62
 0.00  0.00  0.00  0.00  0.00  0.00  0.00  0.00  0.00  0.00  0.00  0.00
 0.00  0.00  0.00  0.00  0.00  0.00  0.00  0.00  0.00  0.00  0.00
19K  41                                                              0.000
17.89 16.99  7.88  6.95  4.48  4.89  8.72  6.12  3.77  4.99  5.21  6.30
 5.73  6.58  6.80  7.88  7.42  5.25  8.84  9.73  9.61 11.56 11.38 12.47
12.45 15.83 14.52 15.82 16.30 20.99 10.03 12.62 16.18  8.75 22.61 27.33
38.78  0.00  0.00  0.00  0.00  0.00  0.00  0.00  0.00  0.00  0.00  0.00
 0.00  0.00  0.00  0.00  0.00  0.00  0.00  0.00  0.00  0.00  0.00
20CA 41                                                              2.500
16.53 13.12  9.90  4.92  2.31  5.35  7.68  7.40  4.34  6.70  6.70  8.84
 7.45  8.48  8.80 10.94  9.73  4.97 12.11 13.89 13.31 14.36 16.14 16.87
17.59 18.65 21.16 21.01 22.45 25.45 19.19  7.07 24.34 19.74 44.71 28.62
28.61  0.00 22.01  0.00  0.00  0.00  0.00  0.00  0.00  0.00  0.00  0.00
 0.00  0.00  0.00  0.00  0.00  0.00  0.00  0.00  0.00  0.00  0.00
20CA 42                                                              0.000
17.43 14.84  9.17  5.72  3.08  5.14  8.04  7.23  4.37  6.37  6.51  8.23
 7.19  8.03  8.57 10.04  9.41  5.15 11.82 12.64 12.88 13.79 15.56 15.53
16.53 18.44 19.35 19.53 20.47 25.40 16.45  9.13 22.14 15.14 33.71 28.43
18.63 26.45 27.40  0.29  0.00  0.00  0.00  0.00  0.00  0.00  0.00  0.00
 0.00  0.00  0.00  0.00  0.00  0.00  0.00  0.00  0.00  0.00  0.00
20CA 43                                                              0.000
18.41 16.97  8.21  6.77  4.26  4.86  8.55  7.16  4.45  6.07  6.33  7.65
 6.96  7.65  8.34  9.21  9.10  5.58 11.47 11.54 12.33 13.36 14.48 14.48
15.21 18.34 17.50 18.45 18.72 25.25 13.04 11.29 20.97 11.11 32.64 25.13
17.01 18.90  3.75 54.62  0.46  0.00  0.00  0.00  0.00  0.00  0.00  0.00
```

```
 0.00  0.00  0.00  0.00  0.00  0.00  0.00  0.00  0.00  0.00  0.00
20CA 44                                                          0.000
19.41 19.36  7.07  8.00  5.91  4.49  9.18  7.18  4.59  5.79  6.16  7.12
 6.74  7.32  8.10  8.48  8.78  6.02 10.45 10.60 11.51 13.03 13.28 13.66
13.98 18.23 15.82 17.65 17.34 24.73 10.01 14.00 18.64  8.17 29.58 23.57
16.52 18.72  2.60 24.66 57.53  0.59  0.00  0.00  0.00  0.00  0.00  0.00
 0.00  0.00  0.00  0.00  0.00  0.00  0.00  0.00  0.00  0.00  0.00
21SC 45                                                          0.000
18.52 16.60  8.33  6.46  3.97  6.19  9.87  7.06  4.33  5.54  5.87  6.89
 6.43  6.95  7.70  8.22  8.36  5.34  9.96  9.84 11.00 12.29 12.76 13.08
13.38 17.04 15.27 16.82 16.49 23.39 10.60 11.75 18.69  9.18 29.88 22.37
16.73 19.53  9.37 25.10 26.46 57.76  0.43  0.00  0.00  0.00  0.00  0.00
 0.00  0.00  0.00  0.00  0.00  0.00  0.00  0.00  0.00  0.00  0.00
22TI 46                                                          0.000
18.02 14.65  9.43  5.41  2.83  6.65  9.14  7.73  4.99  7.23  7.27  9.24
 7.97  8.69  9.56 10.73 10.46  5.22 12.79 12.41 13.89 14.75 18.69 16.41
19.19 19.53 22.01 20.47 22.35 27.43 18.56  8.65 25.17 17.25 39.49 28.86
25.02 14.73 18.80 48.65 35.52 26.42 56.35  2.31  0.00  0.00  0.00  0.00
 0.00  0.00  0.00  0.00  0.00  0.00  0.00  0.00  0.00  0.00  0.00
22TI 47                                                          0.000
18.86 16.47  8.55  6.26  3.77  6.46  9.87  7.85  5.10  6.85  7.16  8.57
 7.83  8.22  9.47  9.84 10.33  5.61 12.62 11.38 13.37 14.45 17.25 15.55
17.45 19.89 19.65 19.99 20.12 28.39 14.87 10.70 24.52 13.14 40.09 26.60
26.03 17.89 13.40 42.19 31.97 27.76 23.89 60.00  0.41  0.00  0.00  0.00
 0.00  0.00  0.00  0.00  0.00  0.00  0.00  0.00  0.00  0.00  0.00
22TI 48                                                          0.100
19.72 18.53  7.52  7.27  5.07  6.16 10.71  8.04  4.82  6.51  7.06  7.95
 7.71  7.84  9.37  9.07 10.15  6.03 12.[illegible] 10.56 12.35 12.83 15.69 15.02
15.82 20.41 17.58 19.84 18.42 29.13 11.70 12.97 23.43  9.78 36.76 25.56
21.78 23.65  9.93 35.79 32.23 33.14 21.02 27.06 63.14  1.09  0.00  0.00
 0.00  0.00  0.00  0.00  0.00  0.00  0.00  0.00  0.00  0.00  0.00
23V  49                                                          0.000
19.19 16.37  8.75  6.08  3.59  6.57  9.68  7.96  4.35  5.75  6.47  8.16
 7.05  7.64  8.42  9.37  9.17  4.60 11.16 10.73 12.05 11.50 14.49 14.27
16.62 17.03 18.93 17.69 19.14 23.72 15.68  7.55 21.55 14.44 33.83 24.38
23.63 14.11 17.16 45.19 27.13 31.72 32.87 27.28 22.88 91.96  0.00  0.00
 0.00  0.00  0.00  0.00  0.00  0.00  0.00  0.00  0.00  0.00  0.00
23V  50                                                          0.000
20.03 18.32  7.78  7.01  4.76  6.30 10.45  8.12  4.64  5.68  5.60  7.59
 6.94  7.26  8.36  8.63  9.07  4.93 11.03  9.89 11.60 11.25 13.35 12.03
15.17 17.34 17.00 17.33 17.33 24.54 12.68  9.26 21.04 11.12 34.26 22.63
22.01 17.07 12.16 39.56 30.12 29.29 33.57 40.07 20.65 50.85 77.08  0.00
 0.00  0.00  0.00  0.00  0.00  0.00  0.00  0.00  0.00  0.00  0.00
23V  51                                                          0.000
20.86 20.40  6.71  8.05  6.29  5.94 11.30  8.34  4.98  5.62  5.75  6.11
 6.85  6.94  8.28  8.00  8.93  5.29 10.62  9.22 10.77 11.15 12.15 11.61
12.20 17.80 15.29 17.21 15.95 25.16 10.08 11.13 20.14  8.39 31.46 21.83
18.56 20.10  8.44 33.99 30.53 31.25 34.44 34.20 38.18 57.93 18.90 44.93
 0.00  0.00  0.00  0.00  0.00  0.00  0.00  0.00  0.00  0.00  0.00
24CR 50                                                          0.000
18.72 14.64  9.72  5.18  2.66  6.58  8.99  7.65  4.26  5.74  5.48  7.82
 6.79  7.33  8.11  8.95  8.81  4.45 10.71 10.22 11.54 10.99 13.79 12.08
15.83 16.35 17.99 16.90 18.16 22.75 14.73  7.34 20.54 13.49 32.33 23.06
22.53 13.65 15.89 42.57 28.92 29.81 31.11 44.79 43.99 53.56 51.30  0.00
 0.00  0.24  0.00  0.00  0.00  0.00  0.00  0.00  0.00  0.00  0.00
24CR 51                                                          0.000
19.52 16.27  8.94  5.92  3.44  6.42  9.63  7.75  4.49  5.68  5.61  6.30
 6.69  6.98  8.04  8.27  8.71  4.75 10.57  9.45 11.08 10.77 12.73 11.48
12.78 16.63 16.20 16.57 16.51 23.47 11.99  8.89 20.05 10.48 32.61 21.49
20.81 16.35 11.39 37.35 28.59 31.22 31.75 37.79 36.19 56.75 35.39 23.47
 0.00 39.69  0.38  0.00  0.00  0.00  0.00  0.00  0.00  0.00  0.00
24CR 52                                                          0.500
20.34 18.14  8.02  6.78  4.50  6.18 10.37  7.91  4.77  5.63  5.75  6.11
```

```
 6.59  6.68  7.96  7.68  8.57  5.07 10.18  8.83 10.30 10.67 11.62 11.09
11.65 17.03 14.62 16.45 15.23 24.01  9.61 10.60 19.19  7.99 29.93 20.75
17.63 19.08  8.02 32.24 28.95 29.60 36.95 32.25 35.97 54.57 34.00 17.00
21.00  9.76 46.12  0.51  0.00  0.00  0.00  0.00  0.00  0.00  0.00
24CR 53                                                          0.000
21.15 20.13  6.99  7.75  5.88  5.85 11.18  8.13  5.11  5.59  5.90  5.94
 5.73  6.43  7.86  7.18  8.30  5.42  9.50  8.34  9.51 10.67 10.57 10.85
10.67 15.29 13.33 16.40 14.34 23.91  7.64 12.39 16.78  5.99 26.37 20.66
14.33 21.64  5.55 27.99 29.45 29.20 36.64 32.40 32.27 53.94 53.31 17.00
16.74  2.34 14.84 71.44  0.00  0.00  0.00  0.00  0.00  0.00  0.00
24CR 54                                                          0.000
21.93 22.13  5.92  8.80  7.58  5.43 12.05  8.38  5.50  5.56  6.05  5.79
 5.87  5.41  7.69  6.75  7.82  5.78  8.79  7.96  8.78 10.72  9.64 10.72
 9.88 15.51 10.79 16.18 13.84 21.90  6.06 14.19 14.07  4.42 23.02 20.95
11.29 23.66  3.78 24.85 28.92 29.89 32.68 29.93 32.45 55.54 41.20 26.17
17.66  7.29  3.02 33.87 74.95  0.67  0.00  0.00  0.00  0.00  0.00
25MN 53                                                          0.000
19.85 16.20  9.12  5.76  3.30  6.52  9.48  7.87  4.36  5.76  5.51  6.50
 5.35  6.52  7.22  7.91  7.81  3.96  9.46  8.96 10.14  9.63 12.02 10.52
12.15 12.62 15.65 14.76 15.74 19.89 12.62  6.46 17.80 11.46 28.01 19.76
19.41 11.91 13.31 36.17 24.70 28.57 29.97 42.41 30.10 53.79 59.44 11.80
 4.32 17.48 21.33 62.45  0.00  0.00  0.36  0.00  0.00  0.00  0.00
25MN 55                                                          0.100
21.45 19.89  7.26  7.47  5.52  6.01 10.91  8.21  4.92  5.65  5.78  6.14
 5.62  5.39  6.08  6.84  7.62  4.50  9.01  7.80  9.09  9.39 10.20  9.72
10.19 13.07 11.20 12.58 13.32 20.96  8.38  9.20 16.69  6.93 25.92 17.94
15.21 16.42  6.90 27.70 24.81 25.39 31.55 31.10 34.78 51.73 55.18 17.31
 8.03 13.73 26.80 20.64 17.47 70.00 10.75  0.00  0.00  0.00  0.00
26FE 54                                                          1.300
19.41 14.64  9.99  4.99  2.51  6.53  8.87  7.61  4.28  5.76  5.52  6.49
 5.37  5.45  6.97  7.59  7.53  3.83  9.11  8.57  9.74  9.25 11.49 10.06
11.58 12.11 13.05 14.15 15.00 19.12 11.92  6.28 17.03 10.78 26.85 18.78
18.54 11.54 12.41 34.22 23.52 27.08 28.59 39.86 32.70 50.55 56.66 11.37
 4.19 24.56 47.81 44.85  0.00  0.00 63.42  0.00  0.00  0.00  0.00
26FE 55                                                          0.000
20.16 16.13  9.28  5.62  3.17  6.39  9.45  7.69  4.50  5.70  5.65  6.32
 5.50  5.41  5.91  7.06  7.45  4.07  8.99  7.98  9.34  9.08 10.65  9.62
10.63 12.28 11.81 12.13 13.74 19.66  9.83  7.48 16.63  8.52 26.93 17.66
16.94 13.58  9.11 30.22 23.34 25.33 29.27 34.02 33.14 52.04 58.57 13.83
 5.76 18.08 31.37 46.98  7.68 23.29 23.63  0.00 43.65  0.00  0.00
26FE 56                                                         20.700
20.95 17.83  8.45  6.37  4.06  6.19 10.10  7.83  4.75  5.66  5.79  6.15
 5.63  5.39  6.09  6.60  7.34  4.33  8.67  7.50  8.73  9.01  9.79  9.32
 9.76 12.52 10.72 12.03 12.72 19.88  7.23  7.94 14.58  6.63 24.53 17.06
14.50 15.65  6.58 26.38 23.62 24.15 29.99 29.55 32.96 48.46 50.48 10.93
 3.77 12.98 25.32 40.58 10.14 31.85 18.81 26.25 10.97 50.01  0.00
```

APPENDIX D: Elementary Particles in Cosmic Radiation

In addition to the nuclear components (including nuclei of hydrogen, i.e. protons) there are extraterrestrial sources of elementary particles. (The atmosphere of the Earth is a site of elementary particle production, e.g. pi- and K-mesons, muons, neutrinos, gamma rays, positrons, and hyperons.) In the discussion below, we shall discuss the extra-terrestrial sources of antiprotons, electrons, gamma rays, and neutrinos. The abundance of antiprotons ($\bar{p}/p \simeq 5X10^{-4}$) is higher than would be produced during cosmic-ray interactions in the interstellar gas. It has been proposed that some cosmic-ray sources are imbedded in dense clouds in which cosmic rays collide with nucleon-antinucleon pair production, while the heavy shielding by clouds breaks down heavier nuclei from such sources, and will hence not lead to an unduly high secondary-to-primary ratio of heavier nuclei.

Electrons are largely accelerated like the nuclear component by supernova shock-waves. However, electron-positron pairs, and also gamma rays, are produced at sites like pulsars, binary systems with an accreting compact stellar object like a neutron star or black hole, at ultra-massive black holes in the center of our Galaxy, at Active Galactic Nuclei and Quasars. Many of the positrons observed near Earth are produced by proton interactions in interstellar gas that generate pions, and subsequent pion-muon decays.

Gamma rays, already detected with the SAS-2 and COS-B gamma ray telescopes, are also produced by proton interactions in the

interstellar gas, with pion production, via neutral pion decay. Furthermore, lower energy (near 1 MeV) gamma-ray lines are produced by decay of radio-active nuclides (e.g. Co^{56}), which are generated in nucleosynthesis processes immediately before and during the supernova phase. The Co^{56} line was recently detected in SN1987 [51], the supernova in the large Magellanic cloud.

Neutrinos are produced during gravitational collapse of the core of the star to a neutron star during the supernova implosion-explosion. As protons become neutrons, via $p+e \rightarrow n+\nu$, the so-called neutronization neutrinos are formed. The gravitational collapse generates a huge amount of energy, a couple of percent of rest mass turns into energy, largely positron-electron pairs: $e^+ + e \rightarrow 2\ \gamma$ rays, but occasionally the $e^+ + e^-$ or 2 gamma rays yield $\nu + \bar{\nu}$ pairs, that escape and carry off the energy generated at the collapsing stellar core. These were recently observed from the supernova SN1987A [52,53] in the large Magellanic cloud. Neutrinos are also produced in proton interactions with pion production and decay. Experiments (DUMAND [54], GRANDE [55]) are under design to search for such neutrinos from (a) binary stellar systems with a beaming pulsar that strikes its companion star - Cyg X-3 is a likely source, (b) the Galactic disk, and (c) accretion disks about the ultra-massive black holes of Active Galactic Nuclei and Quasars.

REFERENCES

1. V.L. Ginzburg and V.S. Ptuskin, Astrophys. Space Phys. Rev. 4, 162 (1985).

2. M.M. Shapiro and J.P. Wefel, eds., Genesis and Propagation of Cosmic Rays (D.Reidel, Boston, 1988); pp. 1-70.

3. V.L. Ginzburg and S.I. Syrovatskii, The Origin of Cosmic Rays (Macmillan, New York, 1964); pp. 1-185.

4. R. Silberberg and C.H. Tsao, Bull. Am. Phys. Soc. II 15, 618 (1970).

5. M.D. DeCampli, F.D. Moore, and M.H. Phillips, "Radiation," NASA Report on Life Sciences Strategic Planning Study Committee, June, 1988, pp. 53-66.

6. J. Adams Jr. et al. "Cosmic Ray Effects on Microelectronics," NRL Memorandum Report 4506, August, 1981.

7. G.W. Cameron, "Elemental and Nuclidic Abundances in the Solar System," in Essays in Nuclear Astrophysics, ed., W.A. Fowler (Cambridge University Press, New York; 1982) pp.34-35.

8. R.Silberberg, C.H.Tsao, and J.R. Letaw, Astrophys. J. Suppl. 56, 369 (1984).

9. Websters New Collegiate Dictionary (8th ed. (1981), s.v. "Cosmic Rays."

10. A. Brozek and H. Pilkuhn, eds., Lectures on Space Physics (Germany, 1973); p.7.

11. H. Alfven, Phys. Rev. 75, 1732 (1949).

12. A. Unsold, Phys. Rev. 85, 857 (1951).

13. M. Casse, "Cosmic Ray Sources," in Composition and Origin of Cosmic Rays, ed. Maurice M. Shapiro (Boston: D. Reidel, 1983), pp. 193-230.

14. M.M. Shapiro, 20th ICRC (Moscow) 2, 260 (1987).

15. P.A. Ramana-Murthy and A.W. Wolfendale, Gamma-Ray Astronomy (Cambridge University, New York, 1986); pp. 203-204.

16. G. Burbidge, " Extragalactic Cosmic Rays, Active Galaxies and Quasi-Stellar Objects," in Composition and Origin of Cosmic Rays, ed. Maurice M. Shapiro (Boston: D.Reidel, 1983), pp. 245-250.

17. J. Bloemen et al., Astron. Astroph. 135, 12 (1984).

18. R. Silberberg, C.H. Tsao, and J.R. Letaw, Phys. Rev. Letters 26, 1217 (1983).

19. R. Cowsik et al., Phys. Rev. 158, 1238 (1967).

20. G. Gloeckler and J.R. Jokipii, Phys. Rev. Letters 22, 1448 (1969).

21. R. Cowsik and L.W. Wilson, 14th ICRC (Munich) 2, 659 (1975).

22. M. Simon, 15th ICRC (Plovdiv) 2, 125 (1977).

23. I.L. Rasmussen and B. Peters, Nature 258, 412 (1975).

24. B. Peters and N.J. Westergaard, Ap. Space Sci. 48, 2, (1977).

25. J.R. Jokipii, Astrophys. J. 208, 900 (1976).

26. S.A. Stephens, 17th ICRC (Paris) 13, 89 (1981).

27. R. Silberberg et al., 18th ICRC (Bangalore) 2, 179 (1983).

28. O. Havnes, Nature 229, 548 (1971).

29. M. Casse, P. Goret, and C.J. Cesarsky, 14th ICRC (Munich) 2, 646 (1975).

30. S.E. Woosley and T.A. Weaver, Ap. J. 243, 651 (1981).

31. J. Casse and A. Soutoul, Astrop. J. Letters 200, 75 (1975).

32. J.H. Adams Jr., K. Krombel, and A. Tylka, Bull. Am. Phys. Soc. 34, 1225 (1989).

33. J. Linsley, "Very High Energy Cosmic Rays" in Origin of Cosmic Rays, eds., G.Setti, A.W. Wolfendale, and G. Spada (D. Reidel, Boston, 1981); pp. 53-68.

34. B. Peters, Progr. Cosmic Ray Phys. 1, 191 (1952).

35. G. Rudstam, Zeitschrift Naturforschung 21a, 1027 (1966).

36. R. Silberberg and C.H. Tsao, Astroph. J. Suppl. 25, 315, (1973).

37. B. Edgardo et al., Table of Isotopes (Wiley, New York, 1978).

38. W.R. Webber, J.C. Kish, and D.A. Schrier, submitted to Phys. Rev. C. December, 1988.

39. J.A. Simpson, Ann. Rev. Nuc. Part. Sci. 33, 323 (1983).

40. M. Casse et al., 19th ICRC (La Jolla) 3, 167 (1985).

41. K. Kwiatkowski et al., Phys. Rev. Letters 50, 1648 (1983).

42. T.W. Armstrong, "The HETC Hadronic Cascade Code" in Computer Techniques in Radiation Transport and Dosimetry, eds., W.R. Nelson and T.M. Jenkins (Plenum Press, New York,1980): pp. 373-385.

43. J. Letaw, C.H. Tsao, and R. Silberberg, "Matrix Method of Cosmic Ray Propagation " in Composition and Origin of Cosmic Rays, ed., M.M. Shapiro (D. Reidel, Boston, 1983); pp. 337-342.

44. R. Silberberg et al., Radiation Research 98, 209 (1984).

45. R. Silberberg et al., Aerospace America, pp.38-41 (1987).

46. R. Silberberg, C.H.Tsao, and J.R. Letaw, " Natural Radiation Hazards on Manned Mars Mission ," NASA Report M002 Manned Mars Mission Workshop, Vol. 2, June, 1986, pp. 642-655.

47. J.R. Letaw, R. Silberberg, and C.H. Tsao, "Radiation Hazards on Space Missions Outside the Magnetosphere," 27th COSPAR Meeting, July, 1988.

48. J.F. Ziegler and W.A. Lanford, Science 206, 776 (1979).

49. R. Silberberg, C.H. Tsao, and J. Letaw, IEEE Trans. Nucl. Sci. 31, 1183 (1984).

50. R. Silberberg, C.H. Tsao, and J.R. Letaw, IEEE Trans. Nucl. Sci. 35, 1634 (1988).

51. S.M. Matz et al., Nature 331, 416 (1988).

52. K. Hirata et al., Phys. Rev. Letters 58, 1490 (1987).

53. R.M. Bionta et al., Phys. Rev. Letters 58, 1494 (1987).

54. A. Roberts, ed., Proc. DUMAND Summer Workshop, (Fermi National Accelerator Laboratory, Batavia, 1976).

55. M. Cherry et al., Bull. Am. Phys. Soc. 34, 1239 (1989).